INVESTIGATION OF ARGON PLASMA PROPERTIES AT HIGH PRESSURE

A THESIS

Presented to

The Faculty of the Division of Graduate

Studies and Research

by

Marvin Craig Wynn

In Partial Fulfillment

of the Requirements for the Degree

Master of Science in Mechanical Engineering

Georgia Institute of Technology

August, 1975

INVESTIGATION OF ARGON PLASMA PROPERTIES AT HIGH PRESSURE

Approved:

Dr. A. V. Larson

Dr. J. R. Williams

Dr. E. W. Thomas

Dr. J. C. Wu

Date approved by Chairman: 8/21/75

ACKNOWLEDGMENTS

I am deeply grateful to my thesis advisors, Drs. A. V. Larson and J. R. Williams, and to the other members of my reading committee, Drs. E. W. Thomas and J. C. Wu. My thanks are extended also to Mr. J. P. Tinkham, laboratory specialist, who, together with my advisors, has provided me with an unparalleled learning experience in the course of this study. I would also like to express my appreciation to the National Science Foundation, which, under project number ENG-7303919 A01, managed by Dr. Royal Rostenbach, and Dr. Jay Harris, has made this work possible.

Deserving of special thanks are my fellow students, Jeff Madill and Billy Newberry, whose support and companionship have served to make this effort more enjoyable and rewarding.

My appreciation is extended to Ms. Annette Plunkett for typing and editing assistance, Mr. Gene Clopton for his encouragement and aid in instrumentation, and Mr. George Halstead, who has been most helpful in part modification and machine fabrication of components.

To my parents, I express my deep appreciation for their guidance and support throughout my academic pursuits.

TABLE OF CONTENTS

Page

LIST OF TABLES

LIST OF ILLUSTRATIONS

NOMENCLATURE

I	arc current (amps)
E	field strength (volts/cm)
σ	electrical conductivity (mho/cm)
r	radius (mm)
P	pressure (atm)
T	temperature (°K)
EF	error factor used to fit trial function to experimental data
$B(\lambda,T)$	emissive power of a black body as a function of wavelength and temperature (watts/cm^2)
C_1	Planck's first constant 5.951×10^{-13} watt-cm^2/sr
λ	wavelength (Å)
C_2	Planck's second constant 1.4386 cm-°K
$\varepsilon(T)$	line emission coefficient as a function of temperature
h	Planck's constant 6.624×10^{-34} J s
c	speed of light 2.998×10^{8} m/s
A_{ki}	the atomic transition probability from electron state k to electron state i (s^{-1})
n_n	number desnity of neutral atoms (m^{-3})
g_k	statistical weight of the kth electron state
E_k	excitation energy of state k (J)
k	Boltzmann constant 1.3804×10^{-23} J/°K
ϕ	ratio of maximum intensity observed to black body intensity
n_e	number density of electrons (m^{-3})

NOMENCLATURE (Continued)

n_i	number density of ions (m^{-3})
n_t	total number density of the species (m^{-3})
$U_1(T)$	partition function for singly-ionized atom
m_e	electron mass 9.1086×10^{-31} kg
ϕ	ionization potential (eV)
J	current density (amp/m^2)
I(y)	intensity as a function of distance y ($watts/sr\text{-}m^2$)

SUMMARY

Measurements were made to determine the electrical conductivity of argon over the temperature range from 7000 °K to 11,500 °K at pressures of 1 to 100 atm. A steady, wall-stabilized, direct-current electric arc was operated at currents from 8 to 80 amperes in an argon atmosphere.

The arc column was observed by the use of side-on viewing ports covered with fused quartz windows. The intensity of the radiation from the arc was measured by a photomultiplier tube mounted on the exit slit of a spectrometer. Lateral intensity profiles at a given wavelength were measured by rotating a mirror such that the image of the arc moved across the entrance slit of the spectrometer.

The lateral intensity profiles were converted to radial emission coefficient profiles and then radial temperature profiles were calculated from data on the temperature dependence of line emission coefficients at the various pressures. This was calculated using data published by the National Bureau of Standards. It was necessary to have an optically thin plasma and local thermodynamic equilibrium in order to utilize this analysis.

Electrical measurements of the arc column were performed using the individual cascade plates as voltage probes for obtaining the voltage distribution along the cascade channel. Knowing then the temperature profiles and the total current in a cylindrically symmetric arc with constant axial field strength taken from the plate measurements, the

electrical conductivity as a function of temperature was deduced from the integral form of Ohm's law for the column using an iterative technique and a trial function for the electrical conductivity.

CHAPTER I

INTRODUCTION

The study of properties of high-pressure plasmas is of basic scientific as well as engineering interest. The applications of data on dense plasmas range from the development of arc-heated wind tunnels for re-entry simulation, studies of high-temperature gas core nuclear reactors, design of magnetohydrodynamic generators, and high-voltage switch design. The phenomena of the pressure broadening of spectral lines and the gray-body characteristics demonstrated by a self-absorbing plasma may also be better understood through high-pressure plasma experiments.

One experimental apparatus to study these high-density plasmas is the wall-stabilized, direct current, steady-state electric arc. Confinement of the arc in a columnar channel of suitable length-to-diameter ratio permits the experimenter to vary the type of gas, control accurately the ambient pressure, conveniently measure the arc voltage gradient, and determine the radial temperature profile from spectroscopic observations.

Devoto (1) has stated that argon is favored in experiments dealing with ionized gases for the following reasons: it is relatively cheap, it is monatomic and thereby free from the complexities introduced by the presence of molecules, it forms a stable electric discharge without problems in handling or oxidation of the electrodes, and most of its physical properties are reasonably well known.

This thesis deals with measurement of the electrical conductivity of argon up to 100 atm in a wall-stabilized electric arc of the type

first developed in Germany by Maecker (2). This apparatus has been used in studies on argon, hydrogen, and nitrogen by Maecker and Bauder (3) to measure electrical conductivity and radiative properties over a large pressure and temperature range.

Recent work by Bauder, Devoto, and Mukherjee (4) has been published on the electrical conductivity of argon up to 200 atm, but with no data points at 50 atm, and only a few experimental data points at 100 atm and 200 atm. Other work by Kopainsky (5) has been published for argon up to 20 atm (one experimental point at 20 atm) and by Morris, Rudis, and Yos (6) for argon at 2 atm. All this work has been performed in wall-stabilized, steady state arcs in apparatus similar to the Maecker cascade.

Data obtained in this project compares favorably with published experimental results (4,5,6) for argon at pressures of 1 and 10 atm, and provides additional and, in part, original experimental data in the temperature range 7000 °K to 12,000 °K for comparison with existing theories (4) concerning the electrical conductivity of argon at pressures up to 100 atm. The actual pressure and temperature ranges for this project are:

Pressure (atm)	Temperature Range (°K)
1	9000 - 11,000
10	8500 - 11,500
20	8000 - 11,000
50	7500 - 10,500
100	7500 - 10,000

CHAPTER II

THEORY

For an electric arc which may be modeled as possessing cylindrical symmetry, uniform cross-section, and lack of axial gradients except for voltage (field strength), Ohm's law may be written in integral form as,

$$I = 2\pi E \int_o^R \sigma(P,T) r dr \tag{1}$$

where I = current passing through the arc

E = field strength

R = arc radius

and $\sigma(P,T)$ = electrical conductivity of the arc medium as a function of pressure and temperature.

The above integral may be evaluated to predict the experimentally determined ratio I/E if the conductivity of the arc is known as function of arc radius, or

$$I/E = 2\pi \int_o^R \sigma(r) r dr \tag{2}$$

Holding pressure constant, the desired functionality may be achieved for electrical conductivity if $\sigma(T)$ is known and if the distribution of temperature, T(r), in the cylindrical model can be determined as a function of arc radius. In this study, a trial function must be assumed for $\sigma(T)$; thereafter, the experimentally determined T(r) allows the evaluation of the integral Ohm's law to predict the measured I/E,

$$I/E = 2\pi \int_{o}^{R} \sigma[T(r)]rdr \qquad (3)$$

Making measurements of T(r) at a given pressure for arcs with differing arc currents and hence different temperature ranges would allow better specification of the trial function used for electrical conductivity. Repeating this procedure at several different pressures would then allow evaluation of $\sigma(P,T)$ as a function of pressure.

The trial function used in this study was one shown by Devoto and Mukherjee (8) to successfully approximate the behavior of electrical conductivity of argon in the temperature range 8000-26,000 °K and at 1 atm pressure.

The measurement of T(r) was accomplished by spectrographic means. The intensity of an argon line, I(y), of the arc was measured as a function of lateral distance, y, from the centerline of the arc. The feature of cylindrical symmetry then allowed the unfolding lateral line intensity profiles into absolute volume emission coefficients $\varepsilon(r)$ as a function of arc radius by means of a modified Abel Inversion technique as described in Appendix A. The use of this technique assumed local thermodynamic equilibrium and optical thinness within the arc. Knowledge of the line emission coefficient dependence upon temperature from atomic theory then allowed the deduction of T(r) from $\varepsilon(r)$ by direct comparison.

Measurements of arc current, I_j and field strength, E_j for the jth arc in a series of arcs at a given pressure would then allow the numerical evaluation of the integral Ohm's law

$$I_j = 2\pi E_j \int_o^R \sigma[T_j(r)]rdr \qquad (4)$$

and the determination of $\sigma(T)$ for that pressure.

The assumptions used in the above analysis were subjected to suitable tests in the experimental procedure in order to check their validity. A more detailed explanation appears in the Analysis section.

CHAPTER III

APPARATUS

There appears in Figure 1 a schematic of the facility used to generate steady state arc discharges in atmospheres of various gases at pressures up to 1000 atm (7). The main components of the arc facility were a closed-loop water cooling system for protection of components in contact with the plasma, a high-pressure gas delivery system, and pressure vessels which contained the arc confinement devices, or cascades. This facility allowed steady-state operation of the electric arc at power levels up to 300 kw.

Cascade and Instrumentation

The heart of the project was a wall-stabilized arc of the cascade type which was operated within a steel pressure vessel and was mounted vertically with the cathode on the bottom, as depicted in Figure 1. The cascade consisted of ten individually water-cooled plates constructed from high-purity, oxygen-free copper. As illustrated in Figure 2, a cascade plate was the combination of two copper plates whose combined thickness was 2 mm. Cooling-water channels were engraved on the lower plate and the upper plate diffusion-bonded upon it. Cooling water entered through a diagonally opposed pair of outer holes in the plate and left through the other pair of holes. The turning action of the cooling water and its high flow velocity at the curved section of the channel resulted in a high heat transfer coefficient and the removal of water vapor bubbles

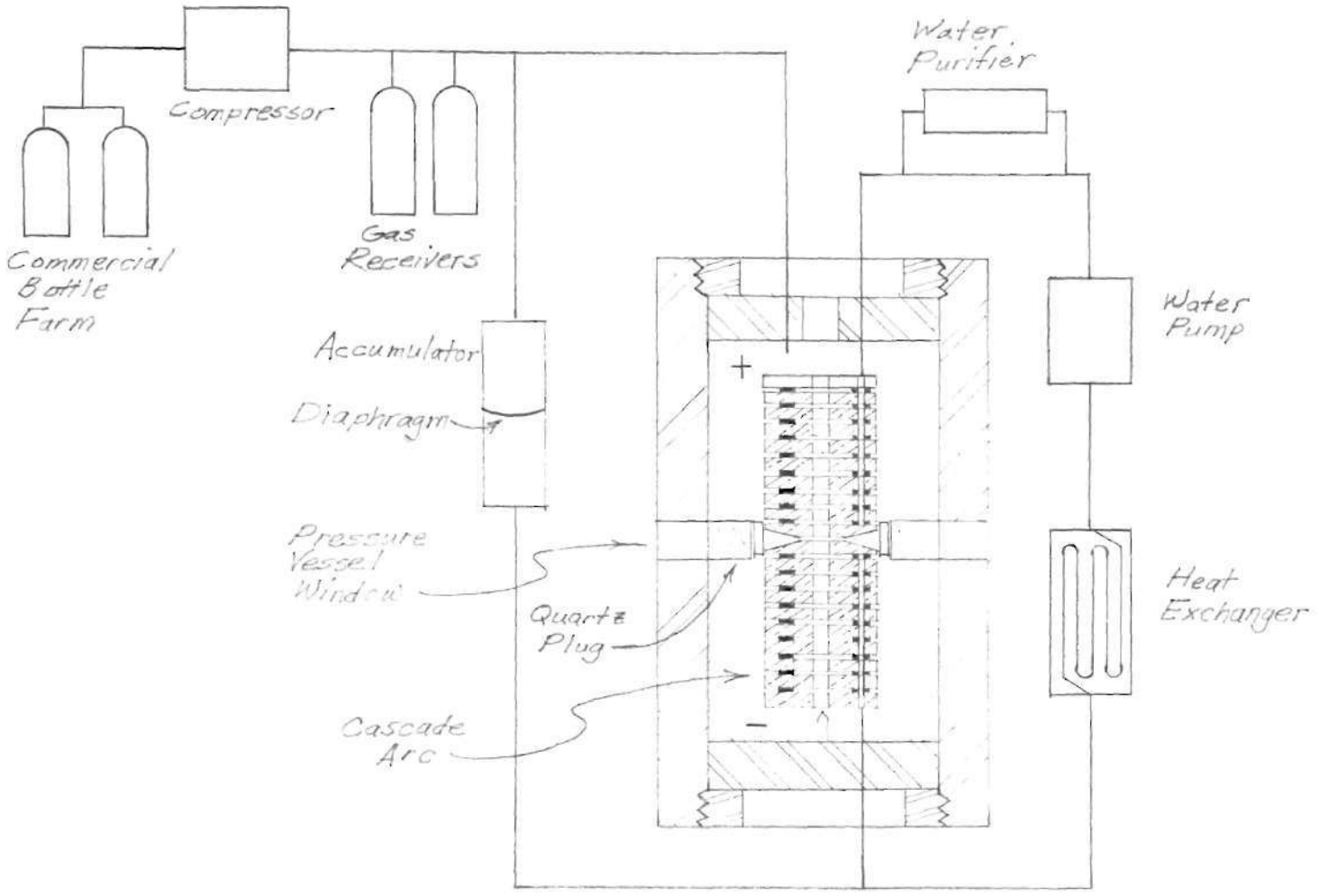

Figure 1. Arc Assembly Schematic Showing Gas and Cooling Water Flows

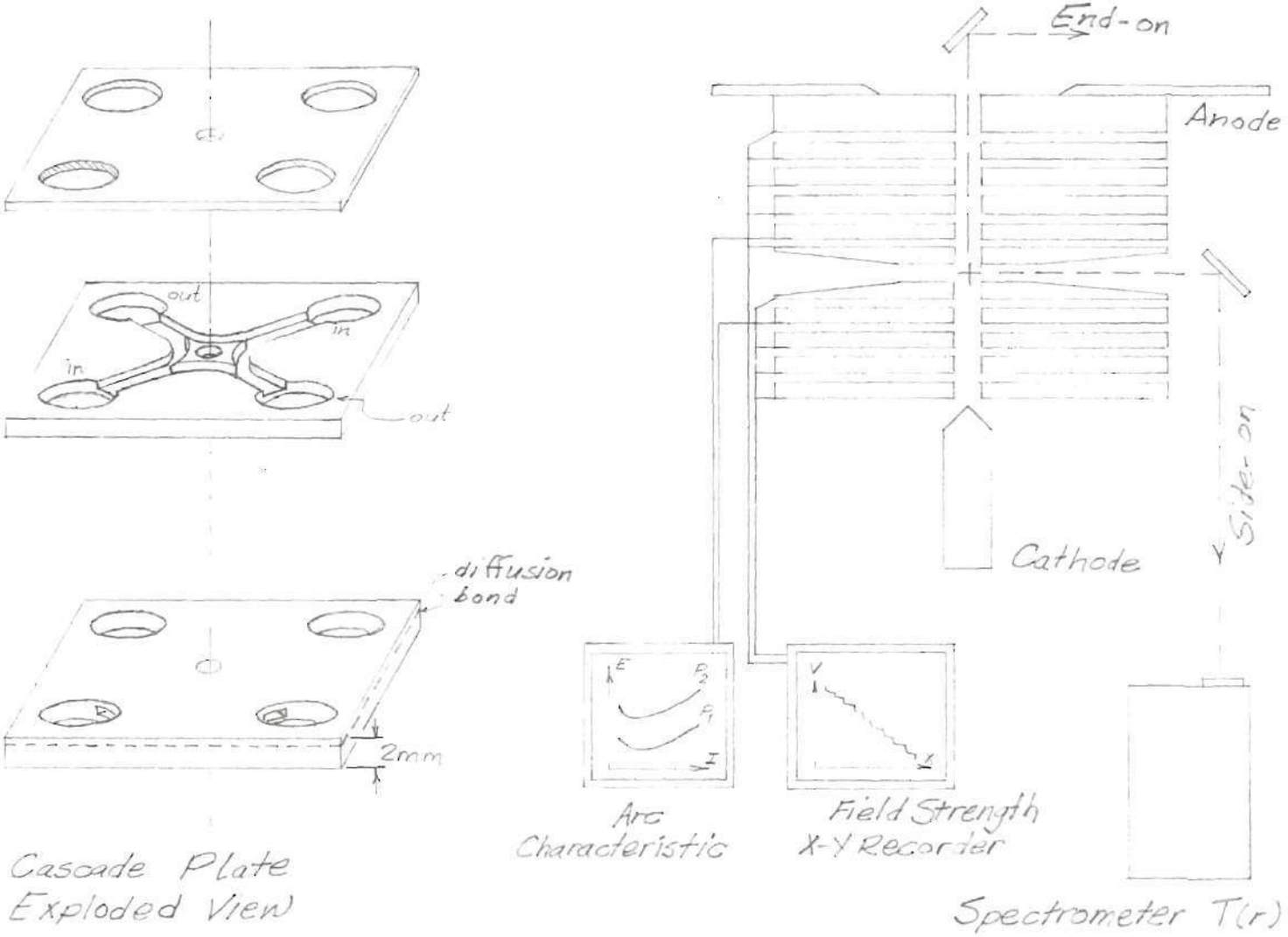

Figure 2. The Cascade Arc

produced by nucleate boiling. When stacked and carefully aligned, the arc channel formed by the central hole was capable of sustaining steady wall heat flux rates of up to 20 kw/cm (7).

The cascade plates were electrically insulated from each other by 0.54 mm silicone rubber washers and 0.356 mm lexan spacers. The cooling water was de-ionized in the water system to bring the resistance between neighboring cascade plates to values close to 0.2 MΩ (7). Each plate was at a floating potential so as not to short out the arc. The electrodes for the arc were a tapered thoriated tungsten cathode, 5 mm in diameter at the base and positioned on-axis with the arc channel, and a specially constructed 5 mm thick cascade plate with a central hole as the anode. The electrodes were also protected by the cooling water.

In order to make spectrographic measurements of the confined arc, it was necessary to view a horizontal segment of the arc at a space between plates. A window cavity was formed by the mating of two special cascade plates which were located at the center of the cascade. Ports were formed on two sides of the cascade by grooving the window plates on mating faces. Reflections were minimized by blackening the window plates in the grooved sections which formed the window ports. Visual access to the arc was protected by clamping a small (5 x 10 x 2 mm) optical quality quartz window over the aperture formed by the two modified window plates. End-on observation was allowed by the central hole in the anode plate. The end-on image of the arc was projected onto a screen and used as a visual monitor of the arc stability and purity.

The arc current was measured by way of a precision shunt in the power line. The current was supplied by a bank of voltage-regulated

A. O. Smith Model A2500-10 SP power supplies which had a total capacity of 1.5 MW. The operating point of the power supplies was controlled by external resistor banks which could be switched in or out with heavy-duty remote controlled motor contactors. These resistors allowed the argon arc to be sustained with currents as low as 8.4 amps, which proved valuable in investigations directed at conductivities in the lower temperature ranges (~7000 °K).

The electrical field strength was taken from the voltage gradient in the cascade plate stack. The voltage on each plate was plotted on the Y-axis of an HP 7004A X-Y recorder, while the X-axis was connected to an independent voltage source which provided voltages proportional to the distance of each plate from the cathode. The slope of the resulting plot corresponded to the field strength. The linearity of the slope graphically displayed the constant axial electrical field.

The temperature distribution as a function of radius was determined from spectroscopic observations (see Figure 3). The side-on image of the arc column was reflected off a front surface mirror which could be rotated remotely. The image was then focused on the entrance slit of a Czerny-Turner Model 1800 grating spectrometer by means of a movable lens between the mirror and the spectrometer. Radiation leaving the exit slit was received on a EMI Model 9558 photomultiplier tube, whose current was measured on a Keithley Model 416 piccoammeter and finally described graphically on a Clevite Brush Mark 250 strip chart recorder, as pictured in Figure 3.

The lateral intensity profiles were obtained by triggering the mirror motor and allowing the image of the arc to move across the entrance

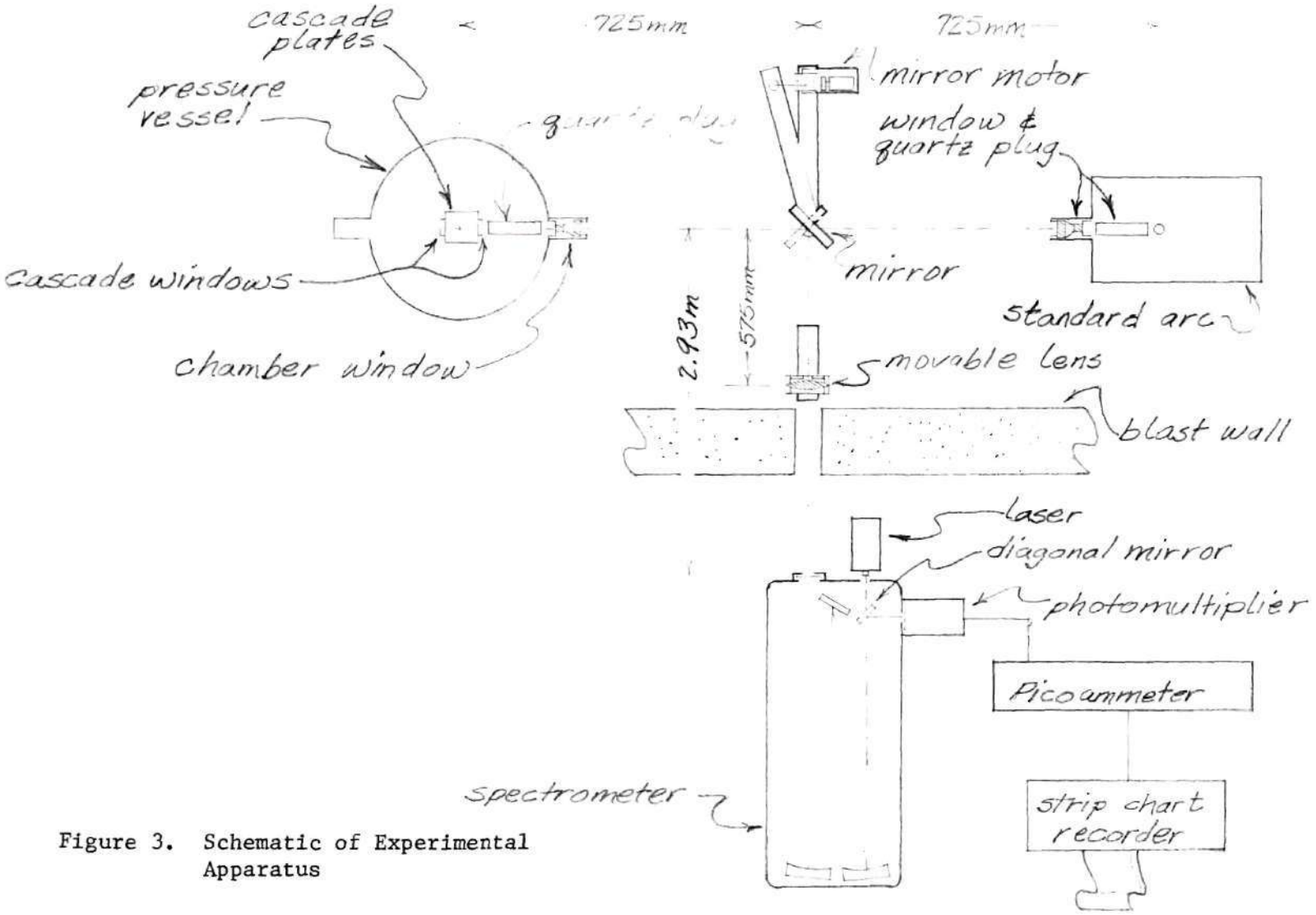

Figure 3. Schematic of Experimental Apparatus

slit of the spectrometer as the mirror rotated. The mirror was mounted on a pivoting arm which was moved by a reversible synchronous motor through a precision Gaertner reducer and slide. The axis of mirror rotation was in the plane of its mirrored surface. Measurements were made on the Mole Type 2371 standardized arc source simply by rotating the mirror through a right angle independently of the pivoting arm (see Figure 3).

Pressure Vessel

The steel pressure chamber had an inner diameter of 20 cm and had a maximum working pressure of 1000 atm. The vessel was made of 4340 steel and had a burst pressure computed in excess of 5000 atm (7). Access to the arc device for argon, water and electrical power was made through high-pressure feed-through fittings in the specially constructed end plugs of the chamber. The vessel was equipped with two high-pressure quartz windows for side-on observation and a port for similar windows in each end plug.

At higher pressures, visual observation of the arc was disturbed by schlieren effects in the free gas space between the cascade window and the chamber window. These effects were thought to be due to the gas flow fields and high temperature gradients which were created inside the steel pressure vessel. To reduce these effects, optical grade quartz cylinders were placed in this free space, thus filling the optical path as completely as possible with solid material.

Gas System

High pressure argon was delivered commercially at about 150 atm and entered the gas system from a bottle farm consisting of from one to

six bottles. This gas could be further compressed to 1000 atm by a gas compressor of the diaphragm type, thereby insuring the purity of the gas. This higher pressure gas could be stored in ten receivers (as depicted in Figure 1) until needed.

The argon was delivered to the pressure vessel through a pressure regulator and was monitored using a Celesco P3D differential pressure transducer.

Water Cooling System

The water cooling system consisted of three major components; a positive displacement pump, a water purification system, and a heat exchanger with a 300 kW capacity in steady-state operation.

The pump was a specially developed Petrodyne dual pump, model 64, which maintained a constant water flow of about 40 liters/min at a static pressure equal to the working pressure in the test gas. The pump was designed for operation at pressures up to 1050 atm. The delivery of the cooling water at the test gas pressure reduced the strain on the thin-walled cascade plates and other parts of the pressure vessel assembly which were structurally weak.

An accumulator was placed at the interface of the gas and cooling water systems in order to equalize the static water pressure and gas pressure. The high static pressure of the test gas was transmitted to the closed water loop by means of a flexible rubber bladder enclosed in a steel pressure vessel. The bladder separated the two fluids and allowed for tube expansion and water compression within the loop. The bladder had a small response time due to its small relative mass and could therefore provide effective equalization in the event of rapid pressure fluc-

tuations in the system.

The cooling water ran through a 300 kW heat exchanger before returning to the pump from the arc apparatus. The heat exchanger was a nine-passage coaxial unit in which the inner tube contained the high-pressure water.

The Millipore water purification system started with tap water and passed it through two filtering units and one de-ionizing unit, all on a low-pressure by pass line. The water in the system was run through these filters between high pressure operations.

Table 1
Experimental Apparatus and Instrumentation

Cascade Plates: 50.8 x 50.8 x 2 mm each

Mirror: 3.5" x 5", Front surface, pivoted on plane of reflecting surface

Standard Arc: Mole Type 2371 Pyrometric Molarc Lamp with Mole Type 2381 Power Supply
Calibrated by: National Bureau of Standards
Spectral range: 3000 to 43,000A

Motor and Reducer: DC reversible synchronous motor
50 rpm
Gaertner Scientific Corporation
Reducer and slide

Spectrometer: Czerny - Turner Model 1800 grating type, f/8

Phototube: EMI Model 9558

Picoammeter: Keithley Instruments Model 416
High-speed picoammeter
Response time ≈ 4 ms

Strip Chart Recorder: Clevite Brush
Model 250 Recorder

Measurement Instruments: Hewlett-Packard 7004A
X-Y Recorder
H-P 5050 B Digital Recorder
H-P 3480 Digital Voltmeter with H-P 3485 A scanning unit
Celesco P3D Differential Pressure Transducer
Preston Instruments Model 8300
Wideband Floating Differential Amplifier

Calibration Instruments: Keithley Instruments Model 261
Picoammeter Source
Keithley Instruments Model 241
Regulated High Voltage Supply
Pace Wiancko Model CD25
Pressure Transducer Indicator

CHAPTER IV

PROCEDURE

Before the first experiment could be conducted, a number of tasks had to be completed. These tasks were:

(1) construction of the cascade and placement in the pressure vessel;

(2) optical alignment of the spectrometer with the chamber; and

(3) determination of a spectral line to be used in experiment and measurement of the spectrometer inverse dispersion.

Once these steps were taken, it remained only to set up the experiments by properly de-aerating and de-ionizing the cooling water, calibration of measuring instruments, and finally, striking the arc itself.

An option that was made available for data acquisition during this period but never fully utilized was the cam operator. The implementation of this device and its use is explained in Appendix C.

Preliminary Steps

Cascade construction. The cascade construction was started by placing the base manifold on the special stand as in Figure 4. Four aluminum guide rods were then inserted in this base. These rods were removed before the cascade was water-tested. The lexan wafer was slid down over these rods. Next, four silicon rubber washers used as water gaskets were slid down on the tubes and positioned in the spacer holes cut to accomodate them. The central bore gasket was then placed in its

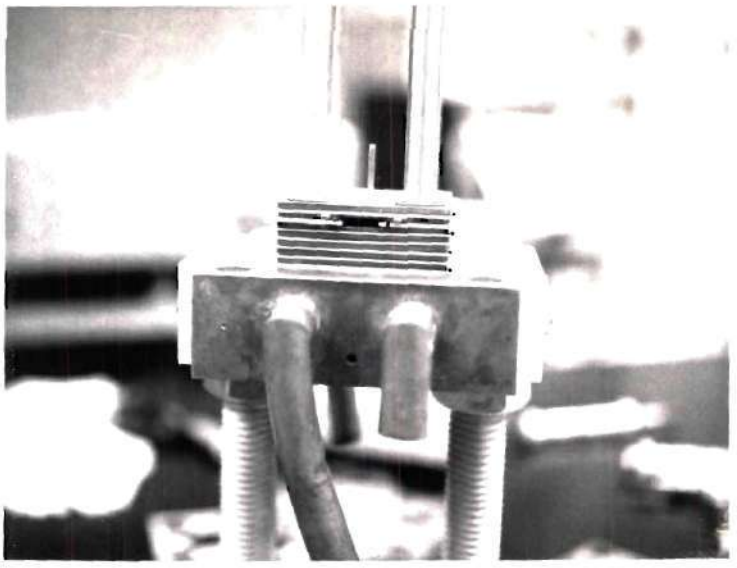

Side view of cascade during construction. Note four aluminum guide rods and centering pin. Window plates form access port as shown.

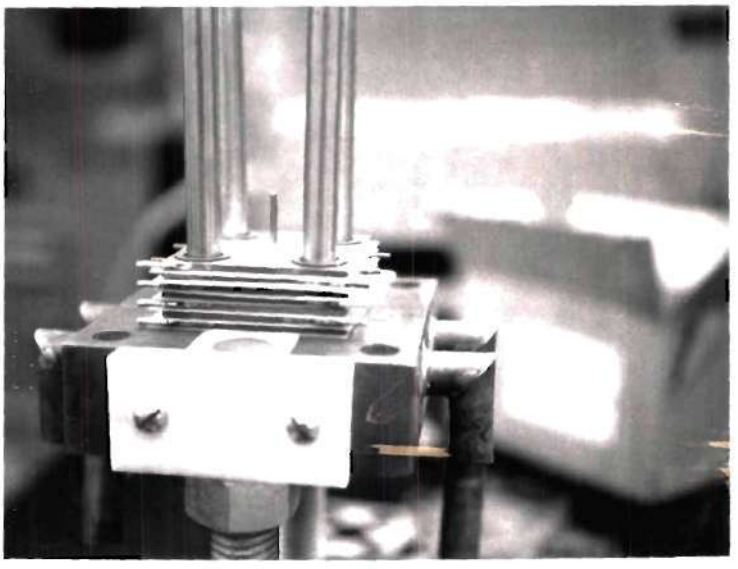

Electrical connections are visible in the above photograph. Note silicon rubber washers about guide rods and centering pin.

Figure 4. Cascade Construction

corresponding cutout in the spacer and centered on the arc channel. Care had to be taken to insure that the gaskets remained in their proper positions during this and subsequent motions of construction. Last, the copper plate was slid down on the gaskets.

The first plate and following plates were placed so that the electrical connections were all in the same plane face of the cascade once it was constructed but alternating in the directions of access in order to avoid shorts and cluttered connections (see Figure 5). A 2 mm diameter pin was inserted in the central bore to insure alignment of the arc channel during construction.

This sandwiching of a plate with a set of spacer and washers was repeated until the fifth plate was ready to be lowered. This fifth plate was the bottom half of the pair of so-called window plates which formed the window aperture of the arc. On top of this fifth plate, a special set of lexan spacers and silicon rubber washers had to be placed to allow proper clearance of 0.028 in. between these complementing plates. The mating window plate was then set in place.

This completed, three more plate-and-spacer combinations were lowered onto the assembly with the 5 mm anode plate last to complete the actual cascade. Another spacer with gaskets was laid atop the anode and the top manifold of the assembly was lowered on. The completed cascade is pictured in Figure 5.

Hold-down bolts secured the cascade assembly and the guide rods were withdrawn. Threaded plugs were used to seal off the water holes formerly occupied by the four aluminum guide rods.

The next step in cascade construction was a static water test.

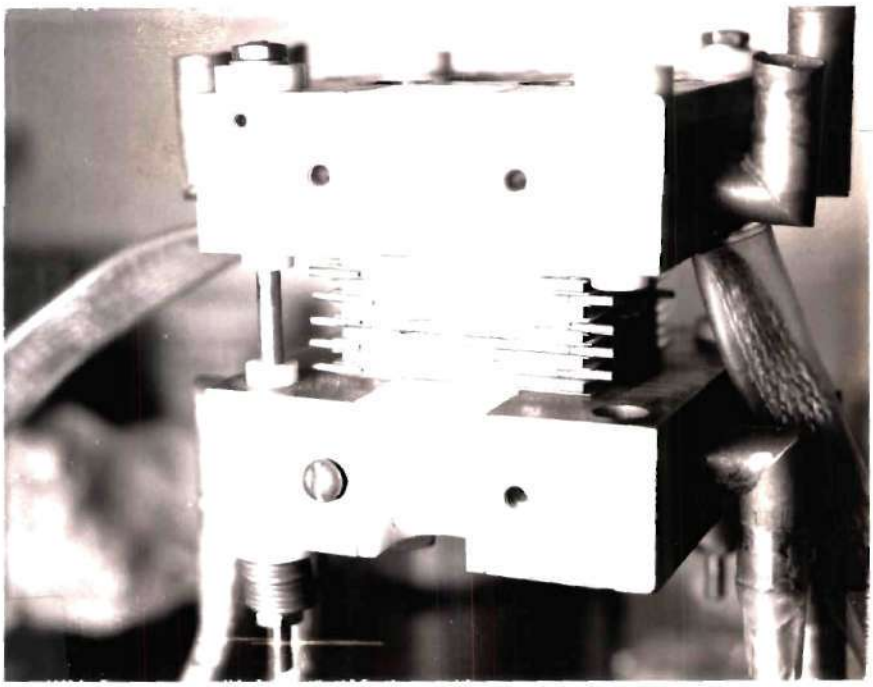

Note only two bolts secure top and bottom of cascade in this photograph. Anode leads fall off to left and right of completed cascade.

Figure 5. Completed Cascade

Hoses were connected to keep the water within the cascade cooling channels except for one inlet tube and an exit tube with a valve. After filling the assembly with water, the exit valve was closed off and the inlet hose left connected to an ordinary water faucet with line pressure of about 80 psi. The cascade was left in this test for a minimum of 1 hour and then checked for slow leaks. Upon passing this test, the cascade was disconnected from the hoses and the cathode and quartz windows attached to the assembly.

The cathode was inserted into its holder, a cylinder with four flanges at one end, each drilled and threaded for mounting on the base of the cascade. The cathode was secured in the holder by engaging the threads in the end of the holder with those in the end plug of the cathode. The cathode holder was mounted on the cascade and the cathode positioned in its holder until the tip of the cathode just entered the 2 mm hole in the bottom plate of the cascade. The end plug was then backed up one full turn, pulling the cathode tip away from the hole by approximately 2.5 mm. The cathode mounting was then complete.

The quartz windows were mounted on the cascade by means of screws made into one of the window plates. The lexan spacers were cut to provide clearance for the square windows on the face of the cascade. A rubber cushion was cut to surround the window aperture and provide a base for the quartz window. Hold-down straps of aluminum were drilled to allow them to slide down the screws on the window plate and extend from the quartz window to the edge of the window plate in an arched configuration. Screws tightened down on these aluminum straps compressed the quartz window down onto its rubber pad and thereby secured it in place.

Care had to be taken not to damage these delicate quartz windows since overzealous tightening always resulted in cracked windows.

The next step was mounting the cascade into the pressure vessel assembly. The cascade was lowered onto guide bars (visible in Figure 6) and secured to them by means of padded teflon plates at a height which insured proper visibility through the cascade once the water jacket was placed on the assembly. Then water hoses and electrical connections were made secure. The top plug of the pressure vessel assembly was made fast to the guide bars by a pin-and-hole type connection. The assembly was made complete by strapping on the copper water jacket. The entire assembly with water jacket open to reveal the cascade appears in Figure 6.

At this point the pressure vessel assembly was lowered into the pressure vessel and aligned through the vessel windows before tightening the end plugs. The high pressure water and gas connections were then made secure and double-checked.

Optical Alignment. The optical alignment was begun by leveling all optical components on their individual stands. A laser was placed in the position of the film holder on the spectrometer and the diagonal mirror removed from its position within the spectrometer (see Figure 3). The exit slit of the spectrometer was closed during this operation to protect the photomultiplier tube. The laser was turned on and adjusted so that the beam left the spectrometer through the entrance slit, after a correct traversal through the spectrometer.

The lens located before the mirror was raised or lowered until the laser beam was centered on it and then slid along the length of its track

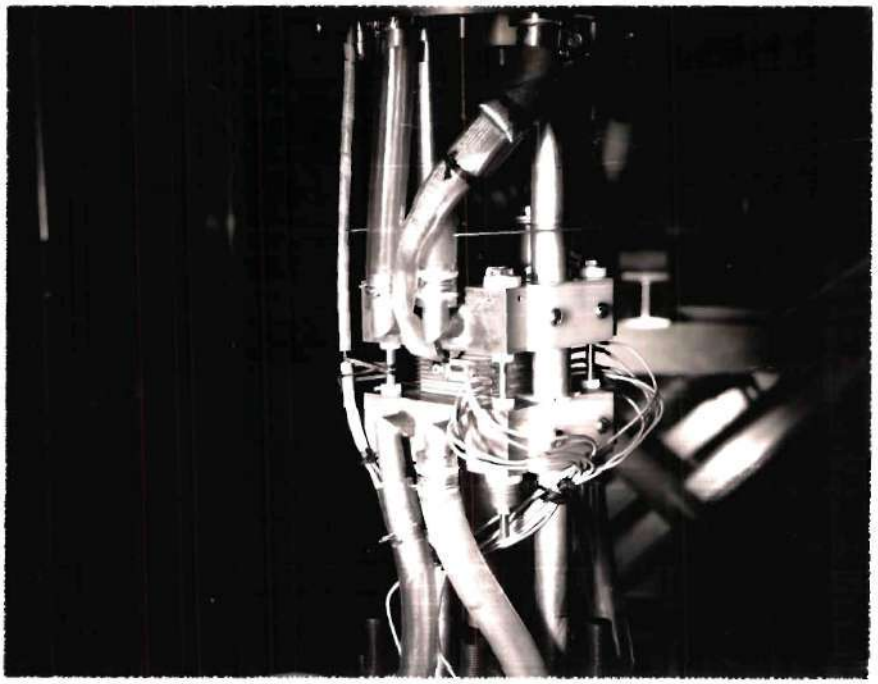

Cascade in place in pressure vessel assembly

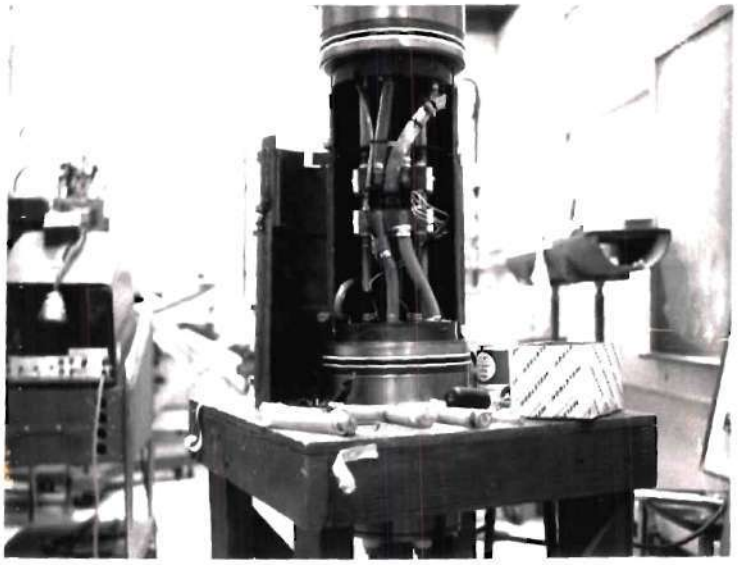

Figure 6. Pressure Vessel Assembly with Water Jacket Open

both ways. The lens stand was then adjusted so that the beam remained centered during the full extent of the travel of the focusing lens.

The mirror was next adjusted so that the laser beam was centered on the surface and was reflected back along its original path. The vertical perpendicularity of the mirror was checked in the following manner: the mirror was turned to face the chamber, which allowed the laser beam to graze the silvered surface and touch the further wall of the laboratory at the spot the beam would have touched with the mirror removed. This spot was marked. Then the mirror was rotated about ten degrees to get a reflection of the laser beam impinging on the wall about twenty feet away. This spot was also marked and the difference in height between this spot and the previous one revealed the degree of error in the mirror's vertical angle with respect to the laser. The height of the two spots was compared with a long, clear plastic hose filled almost entirely with water. One end of the hose was held to each mark and the distances from each meniscus were zeroed.

Next the mirror was turned to allow the laser beam to enter the window of the pressure vessel. The entire pressure vessel was raised or lowered by means of adjustable screws on the legs of its stand until the laser beam passed through the cascade and out the other side. The laser beam was made to travel through a horizontal space only 0.028 inch high after passing through three optical elements; diffusion enlarged the beam and made diffraction patterns inevitable. In correct alignment, the image emerging from the far side of the pressure vessel had to display a particular symmetry in its intensity pattern both horizontally and vertically from the central beam image. The leg screws on the pressure vessel

frame allowed attitude adjustments to be made until the proper beam pattern emerged, insuring that the beam was perpendicular to the quartz windows and that it passed directly through the cascade.

Finally, the mirror was turned 45 degrees to the beam in the direction away from the chamber. At the proper distance away (see Figure 3) the standard arc was set. This distance was measured from the face of the electrode in the arc mechanism to the mirror. All optical components in the pressure vessel assembly were duplicated in the standard arc optical path.

Determination of the Atomic Line for the Experiment and Measurement of the Spectrometer Inverse Diversion. Once the optical alignment was complete, the laser was removed and the diagonal mirror replaced in the spectrometer. The exit slit was opened to 1200μ and the entrance slit closed to 50μ.

The arc was struck at 20 amps and 1 atmosphere. The image of the arc was focused on the entrance slit of the spectrometer by adjusting the mirror and the focusing lens. The spectrometer was allowed to run automatically from 4000Å to 9000Å and the strip chart recorder was used to record the intensities of the lines. The printer output was compared against the tabulated values (10) of Ar I lines and the most significant lines were identified.

From these recordings, a line was chosen which best fit the purposes of the project. The 6965.4Å line was chosen because:

(1) it was a strong, isolated line in the higher wavelengths;

(2) the continuum was lower at these wavelengths due to the

emitting range of radiation from the arc; and

(3) the photomultiplier tube was well within its operating range in this wavelength area.

Next, the exit slit was closed and the diagonal mirror removed from the spectrometer. The entrance slit was closed to 30μ and a hand-operated shutter installed on the slit. The photographic plate was installed in the film holder. Two sets of exposures were made, one set centered at 7200Å and the other at 4200Å. It was known that the width of the plate would allow an exposure spectrum of about 800Å, so these two regions were chosen in order to identify several distinct lines in these wavelength ranges.

Exposures were 1/50, 1/10, 1, 5, and 25 seconds in length, and both sets of exposures were placed on the same photographic plate in narrow strips from top to bottom. This plate was developed and the significant lines identified. Distances from the 7270.65Å line to several other lines were measured and weighted towards the 6965.4Å line.

These measurements showed that the inverse dispersion of the spectrograph was 90.861Å per centimeter opening at the exit for λ = 6965.4Å. In the experiments run later, an exit slit width of 1200μ was used, giving a resolution of 10.903Å.

Preparation for Experiment

Preparing the system for a steady-state run of long duration consisted of:

(1) de-aeration and de-ionization of cooling water;

(2) calibration of instruments; and

(3) starting gas flows and initiating the arc.

Following these steps, the pressure vessel was taken to whatever pressure was desired and the current adjusted by switching resistor banks and adjustment of power supplies.

De-aeration and De-ionization. De-aeration was an involved process which required at least two people in order to refrain from damaging the sensitive accumulator. In a simplified explanation, the Petrodyne pump pressurized the water, dissolved most air bubbles in the water system and transported them to high points in the system. The air was then purged along with some water from the high points in the system; the spent water being replaced from the common University water system.

De-ionizing the cooling water was accomplished by pumping the cooling water through the Millipore filters with an auxiliary electric water pump. This process took at least four hours and was usually started the night before. The resistance between plates was measured before any run and typically was greater than 100 KΩ.

Calibration of Instruments. Four channels of a HP3480 DVM with an HP3485A scanning unit were used to display arc current, voltage, field strength, and pressure. An HP5050B digital recorder printed this information during the actual scan of the arc. In addition, an HP7004A X-Y recorder plotted the cascade plate voltage vs distance from the cathode. This plot was a check on arc stability and a visual verification of the lack of axial nonuniformities in the arc if the plot was linear.

The arc current was measured by means of a precision shunt in the lead to the cathode. The voltage across the shunt was taken to two

Preston Model 8300 wideband floating differential amplifiers, one of which amplified the signal to a voltmeter on the front console for quick visual reference, and the other supplied the scanning DVM and digital recorder. The signal to the DVM could also be used as an input to an oscilloscope for visual monitoring.

A Keithley Model 241 regulated voltage supply was placed in the circuit in the place of the shunt and had a parallel connection to a second HP3480 DVM on the front console. The voltage supply was turned on and adjusted with the second DVM. The correct calibrations for the voltmeter and DVM were then achieved by adjusting either of the two Preston amplifiers.

The voltage calibration was performed in a similar manner. The calibrated voltage supply was placed in the circuit in place of the cathode and anode by means of the second DVM, as before. The Preston amplifier carrying the signal to the scanning DVM was then adjusted until the readout on the scanning DVM was correct to within a multiplicative constant.

The field strength measurement was taken between plates on the cascade plate probes. The voltage supply was placed in the circuit on the plate leads and turned on as before. The output on the ranging DVM on this channel had to be multiplied by the inverse of the distance between the selected plates after the output was adjusted with its respective amplifier. The distance between plates was calculated from known dimensions of plates and spacers.

The pressure measurements were taken by means of a Celesco P3D differential pressure transducer which was calibrated with a Pace Wiancko

Transducer Indicator Model CD25.

The X-Y recorder was calibrated with the Keithley voltage supply and a series of adjustable potentiometers. The potentiometers were tuned to values of resistance analogous to the distance from a plate being measured at that moment by the stepper to the cathode. Ten potentiometers were used, one for each plate in the cascade. This calibrated the X-axis of the X-Y recorder.

The Y-axis was calibrated by placing the voltage supply in the circuit to the Y-axis amplifier. The voltages supplied to the recorder ranged up to +100 V and downwards in increments of 10 V until +20 V, whereupon the increments became 5 V. The position of the pen on the X-Y recorder was checked visually at each station and adjusted if necessary by means of the tuning controls on the amplifier.

Gas Flows and Striking the Arc. Before the arc could be struck, several checks had to be made. The Petrodyne pump had to be pumping the cooling water through the cascade; the electrical instruments had to be allowed to warm up, especially the photomultiplier tube; the calibrations had to be made after the warm up (30 minutes); the gas flow had to be started into the pressure vessel and the power supplies adjusted to the lowest voltage above the extinguish point of the arc.

Since the arc was struck by hand, a means of inserting a starting stick had to be provided. This was done by keeping the window port on the upper end plug out until steady operation had been achieved at 1 atm.

The arc was initiated by bringing a tungsten-tipped starting stick with insulating handle in contact with the cathode from above and then

closing the circuit. The stick was then carefully withdrawn by hand, stretching the arc to the anode plate. Since the stick was at anode potential, the arc attached itself to the anode plate instead of following the stick out the top of the cascade.

Striking the arc required three people; one to give a countdown and switch the power supplies on, one to break the circuit to the starting stick once the arc was established, and finally, the person actually holding the stick. Once the arc was started, the person who held the stick secured the top window port in place. At this point, a lens used to focus the longitudinal view of the arc was swung into place and adjusted to give the best image. Then, persons next to the pressure vessel retired to the other side of the blast wall and the experiment could begin.

Conducting the Experiment. Essentially, the procedure was to trigger the mirror scanning motor and allow the image of the arc to move across the entrance slit of the spectrometer. This image caused an increase in photomultiplier current which was recorded through a picoammeter to the strip chart recorder. The motor on the mirror was reversible and usually two scans were made of the same arc, forward and reverse. This procedure was done for the Ar I line at 6965.4Å. Since the absolute line intensity was desired, a similar scan was made at 7000Å in order to determine the intensity due to continuum emission, since there were no lines near this wavelength. During the same time period of the arc scans, the digital recorder was activated, recording arc current, field strength, voltage, and pressure for the scan.

The current and pressure were marked on each line-continuum set, along with pertinent instrument settings. The pressure range began at 1 atm and was held constant during each series of ascending current settings. After each series was completed, the pressure was increased to the next desired setting and the current series repeated until the entire range of pressure-current combinations was covered.

After a block of data had been taken, the arc was shut off, the chamber de-pressurized, and the window port in the bottom plug of the pressure vessel removed. If a water leak had developed during the run at some point, droplets would accumulate at the bottom of the chamber during de-pressurization and would drain out the open port. A clean run was characterized by the absence of water at this stage.

Next, the mirror was rotated 90 degrees to allow the standard arc image to fall on the spectrometer entrance slit. The standard arc was then turned on and a record of the intensity at the line wavelength was taken on the strip chart recorder. The amplitude of this signal was equated with the spectral radiancy of a black body at 3803 °K as described by Planck's equation. The result was used to convert signal amplitude in vertical divisions on the strip chart paper to intensity in watts/sr-m^2.

Finally, the mirror was turned back to place the image of an arc in the cascade on the spectrometer entrance slit. The starting stick was placed in the cascade in the position of striking the arc. An illuminating light source was placed behind the stick on the far window of the pressure vessel so that an image of the shadow of the starting stick appeared on the spectrometer entrance slit. This image was scanned across

the entrance slit several times and recorded on the strip chart. Since the diameter of the stick was known, this procedure allowed a conversion from horizontal divisions on the strip chart to distance at the arc in mm, giving a means to measure arc radius.

CHAPTER V

ANALYSIS

Introduction

Three measurements were necessary to determine the electrical conductivity of argon at a given pressure and in a certain temperature range. They were:

(1) electric current passing through the arc, I;

(2) electric field strength in the arc, E; and

(3) absolute line intensity I(y) as a function of lateral distance y from the arc center.

The last measurement enabled the determination of radially dependent temperature profiles, T(r), when compared with data concerning the temperature dependence of the line emission coefficient for the wavelength examined. The integral Ohm's law was then written for the cylindrical model of the arc

$$I = 2\pi E \int_{o}^{R} \sigma(T) r dr \qquad (5)$$

A trial function for $\sigma(T)$ was initially assumed. Knowledge of the temperature profile allowed conversion of the temperature dependence of electrical conductivity to a radial dependence, $\sigma(r)$. Knowing the experimental values of arc current, I, and field strength, E, an error factor could be defined by

$$EF \equiv \sum_{i=1}^{N} \left(\frac{I_i}{E_i} - 2\pi \int_o^R \sigma_i(r) r dr \right)^2 \qquad (6)$$

where N is the total number of arcs of different current at a given pressure, I_i is the current of the ith arc, E_i the corresponding field strength of the ith arc, and $\sigma_i(r)$ is the electrical conductivity as a function of radius for the ith arc using the measured temperature profile $T_i(r)$ for that arc.

A computer code, ELCON (14), was written to evaluate the integral in the above expression and to minimize the error factor, EF, by adjusting parameters in the assumed trial function until the "best" fit, i.e. minimum EF, was obtained to the experimental I/E values.

The first step toward the determination of the electrical conductivity was the measurement of the arc temperature as a function of radius.

Temperature Profiles

Radially dependent temperature profiles were determined using absolute line intensities. The intensity of plasma radiation over a narrow wavelength range, $d\lambda$, was observed by the spectrometer and recorded by the chart recorder. The width of the wavelength band was chosen to include all of the spectral line under examination even with pressure broadening effects. Absolute line intensity was obtained by recording the intensity from a continuum wavelength close to that of the spectral line and subtracting from the total intensity measured at the line wavelength in order to remove the effect of continuum emission.

The intensity profiles, both line and continuum, which were ob-

tained by sweeping the image of the arc across the entrance slit of the spectrometer were folded at the profile centerline and the two sides of the curve matched, to within a small noise level, to examine arc symmetry. At each pressure and current the line and its corresponding continuum scan were divided into zones of equal width starting from the arc center. The values of intensity for the continuum scan were then subtracted from the corresponding value of intensity for the line scan, starting from the arc centerline and progressing outwards until no discernible signal could be detected.

The intensity profiles were calibrated with the standard arc as described in the Procedure section. The standard arc approximated the emission of a black body at 3803 °K in the wavelength range 3000Å to 42,000Å. Using these data and knowing the spectral emission of a black body from Planck's equation

$$B(\lambda,T)d\lambda = \frac{2C_1}{\lambda^5}\left(\frac{1}{e^{C_2/\lambda T}-1}\right) d\lambda \qquad (7)$$

the amplitude in vertical divisions on the strip chart paper could be converted to intensity in watts/sr-m^2 for both line and continuum wavelengths.

Knowing the lateral profile of absolute line intensity, the radial profile of absolute volume emission coefficient was obtained by use of the Abel Inversion technique as described in Appendix A.

Next, a relationship between absolute line emission coefficients and temperature was required for the argon 6965.4Å line. The emission coefficient was calculated from

$$\varepsilon(T) = \frac{hc}{4\pi\lambda} A_{ki} n_n g_k e^{-E_k/kT} \tag{8}$$

where A_{ki} = atomic transition probability for an electron at state k falling to state i

n_n = number density of neutral atoms

g_k = statistical weight of upper level (k)

E_k = energy level of upper state

h = Planck's constant

c = speed of light

k = Boltzmann's constant

λ = wavelength of photon emitted during transition

The value of A_{ki} for the argon 6965.4Å line was found from the National Bureau of Standards (11), and values for g_k and E_k appear in Drawin and Felenbok (10). The value of n_n was obtained from the perfect gas law and the Saha equation. The perfect gas law, which was used as an approximation of argon behavior in the temperature and pressure range of this study, is

$$P = n_t kT \tag{9}$$

where P is gas pressure, n_t is the total number density of the gas, k is Boltzmann's constant, and T is gas temperature. The number density of free electrons was obtained from Saha's equation for a singly-ionized gas

$$\frac{n_e n_i}{n_n} = 2U_1(T) \frac{(2\pi m_e kT)^{3/2}}{h^3} \exp\left(\frac{\phi-\Delta\phi}{kT}\right) \tag{10}$$

where n_e is the electron number density, n_i is ion number density, n_n is the density of neutral species, m_e is electron rest mass, h is Planck's constant, ϕ is ionization potential for argon single ionization, $\Delta\phi$ is the lowering of the ionization potential, and $U_1(T)$ is the partition function for the singly-ionized argon atoms. Values for $U_1(T)$, $\Delta\phi$, and ϕ for argon were obtained from Drawin and Felenbok (10). For the pressure and temperature conditions encountered in this experiment, n_n is very nearly equal to n_t, since the gas is only slightly ionized. The Saha equation may be solved for n_e since the local charge equilibrium dictates that

$$n_e = n_i \tag{11}$$

Also, since

$$n_t = n_n + n_e + n_i \tag{12}$$

the values of n_t, n_n, n_e, and n_i may be calculated using equations 9-12. Using equation 8 , values for $\varepsilon(T)$ were compiled in a matrix library over a pressure range from 1 atm to 1000 atm and a temperature range from 6000 °K to 16,000 °K.

Having calculated the emission coefficient for a spectral line as a function of temperature and measured the emission coefficient as a function of arc radius, the temperature as a function of arc radius was then determined by comparison. Temperature profiles of arcs examined in this study appear in Appendix B.

Electrical Conductivity

Measurement of the experimental values of arc current and field strength and the determination of radial temperature profiles allowed a solution of the integral Ohm's law as stated in equation 1 if the temperature dependence of electrical conductivity was known. The trial expression for $\sigma(T)$ could then be converted into $\sigma[T_j(r)]$, the electrical conductivity based on the temperature profile of the j th arc at a given pressure. Equation 4 may then be re-written as

$$I_j/E_j = 2\pi \int_o^R \sigma[T_j(r)]rdr \tag{13}$$

The error factor defined in equation 5 may be minimized by adjusting the parameters involved in the assumed expression for $\sigma(T)$. A plot of electric field strength vs arc current for the various pressures examined in this study appears in Figure 13.

The trial function used in the fit of equation 4 was

$$\sigma(T) = BT^{-c}e^{-D/T} \tag{14}$$

where B, C and D were constants determined in minimizing the error function. It was desired to display a quantitative measure of how closely the final values of B, C, and D in equation 14 predicted the arc characteristic of I/E which was measured for each arc. The deviation of $2\int_o^R \sigma(T)rdr$ from the experimental values of $I/\pi E$ was called Δ and was defined as

$$\Delta \equiv \frac{2\int_o^R \sigma(T)rdr - I/\pi E}{I/\pi E} \tag{15}$$

Each arc has a Δ associated with it, the sign of Δ being an indication of whether the fitted curve lies above (+) or below (-) the experimental value of I/E for that arc. Listed in Table 2 are values of Δ for all arcs examined in this study. "Run code" indicates whether the information was taken from Run 1 or Run 2. "Pressure" gives the pressure in atmospheres for a series of arcs operated at different arc currents, as appears in the "Current" column. The temperature range of each arc is given in the next two columns, T_H being the highest, or centerline, temperature and T_L being the temperature at the 1.0 mm radius. The experimentally measured values of $I/\pi E$ appear in the next column in amp-cm/volt, and the Δ of each arc appears in the last column in terms of percent of deviation from the adjacent value in the $I/\pi E$ column. After each current series at a fixed pressure, the constants B, C, and D from equation 14 are listed. The values of these constants were used to determine $\sigma(T)$ and also the internal consistency between experimentally and analytically determined data indicated by the values of Δ in the last column. An example of the usefulness of a measure of internal consistency is the values of Δ for Run 2, 1 atm. The values of Δ for this pressure alternate with increasing temperature and are uniformly within 2.22% of the corresponding $I/\pi E$ values. This means that the expression for electrical conductivity arrived at in the ELCON program upon integration across the temperature range from 8689 °K to 11,393 °K predicted values of $I/\pi E$ which in no case varied more than 2.22% from the values arrived at by experimental measurements.

In order to fit a given function with n independent parameters well to experimental data, at least n +1 data points are required. For

Table 2
Arc Characteristics and Conductivity Coefficients

Coefficients for $\sigma = BT^{-c}e^{-d/T}$ are listed after each pressure

Run Code	Pressure (atm)	Current (amp)	T_H (°K)	T_L (°K)	$\frac{I/\pi E}{\frac{amp-cm}{v}}$	Δ (%)
1	1	15.8	10670	8298	0.2742	-5.05
(excluding 80 amps)		21.2	11334	8999	0.3389	-0.55
		33.3	11830	10027	0.4429	5.62
		60.2	12106	11288	0.6346	-1.89
$B = 1.217 \times 10^{12}$		$C = 1.937$	$D = 6.547 \times 10^4$			
2	1	8.85	9312	8689	0.1805	-0.57
		9.61	9452	8855	0.1923	-1.42
		10.64	9569	9072	0.2050	0.65
		11.76	9725	9238	0.2209	1.85
		12.54	9872	9314	0.2317	1.23
		14.73	10165	9566	0.2734	-2.18
		16.70	10434	9636	0.2881	-1.77
		17.12	10517	9649	0.2909	2.22
		23.40	11287	10049	0.3622	0.12
		25.53	11393	10050	0.3846	-1.85
$B = 1.092 \times 10^{12}$		$C = 1.966$	$D = 6.255 \times 10^4$			
1	10	15.5	10870	8497	0.2027	-0.04
		20.8	11095	8553	0.2505	-0.87
		31.6	11494	9279	0.3221	1.55
		59.1	12060	10092	0.4565	-1.25
		80.2	12279	10644	0.5198	0.53
$B = 9.814 \times 10^{12}$		$C = 1.911$	$D = 6.810 \times 10^4$			
2	10	8.6	10313	7800	0.1204	-6.62
		9.4	10385	8041	0.1280	1.00
		10.4	10492	8047	0.1388	3.80
		12.0	10672	8256	0.1585	4.61
		12.4	10715	8221	0.1628	2.14
		14.7	10874	8437	0.1886	5.00
		16.0	10882	8440	0.2084	-4.33
		18.7	11018	8415	0.2358	-6.28
		23.4	11250	9062	0.2753	-0.13
		25.6	11317	8943	0.2926	1.67
$B = 1.010 \times 10^{12}$		$C = 1.764$	$D = 8.279 \times 10^4$			
1	20	15.4	10495	7893	0.1716	13.62
		20.7	10742	7875	0.2493	-7.74
		31.6	11080	9193	0.2862	3.60
		58.1	11375	9793	0.4114	-10.04

Table 2 (Continued)

Run Code	Pressure (atm)	Current (amp)	T_H (°K)	T_L (°K)	$I/\pi E$ ($\frac{amp-cm}{v}$)	Δ (%)
		77.3	11579	10285	0.3841	7.60
$B = 1.013 \times 10^{12}$		$C = 1.995$	$D = 5.971 \times 10^4$			
1	50	15.0	10224	7808	0.1295	-11.47
		20.0	10217	7671	0.1632	-4.81
		30.7	10431	7959	0.2204	-0.37
		56.2	10793	8794	0.3186	10.36
		79.7	10973	9308	0.4904	-3.68
$B = 1.455 \times 10^{12}$		$C = 1.504$	$D = 1.088 \times 10^5$			
2	50	8.44	9834	7414	0.0779	-0.55
		9.14	9890	7490	0.0843	-1.02
		10.6	9971	7844	0.0978	-0.02
		11.9	10130	7675	0.1082	-1.93
		12.06	10102	7706	0.1094	0.40
		14.31	10199	7953	0.1271	1.00
		15.61	10255	8009	0.1371	-0.04
		16.61	10308	8073	0.1438	0.42
		18.2	10317	7959	0.1544	2.36
		22.47	10426	8115	0.1818	1.52
		23.8	10423	8095	0.1897	-3.23
		26.2	10435	8126	0.2037	0.12
$B = 1.117 \times 10^{12}$		$C = 1.656$	$D = 9.362 \times 10^4$			
1	100	15.0	9825	7238	0.0971	7.50
		19.0	9834	7243	0.1251	2.09
		30.0	9897	7481	0.1722	-8.35
		54.4	10495	9344	0.2597	9.62
		80.0	10325	9388	0.3163	-6.36
$B = 1.120 \times 10^{12}$		$C = 1.796$	$D = 7.963 \times 10^4$			
2	100	8.2	9458	7930	0.0610	30.65
		8.95	9500	7280	0.0614	-12.80
		10.0	9654	7306	0.0720	-10.25
		11.6	9670	7553	0.0795	-6.26
		14.0	9705	7583	0.0888	1.40
		15.8	9685	7455	0.1007	-6.83
		18.2	9847	7618	0.1133	1.07
		22.0	9843	7682	0.1302	9.96
		24.2	9945	7820	0.1417	-15.20
		25.2	9905	8082	0.1465	3.96
$B = 1.786 \times 10^{12}$		$C = 1.360$	$D = 1.232 \times 10^5$			

each pressure, then, at least four arcs were required to span the same temperature range in order to fit the trial function well in that temperature range. A graph of the electrical conductivity vs temperature for Run 2, 1 atm appears in Figure 7 with the arc current and temperature ranges which support the curve shown beneath. On the bar which spans the temperature range for each arc is the particular value of Δ for that arc. The electrical conductivity curve is presented in three segments; a central region which is well established due to the number of arcs which help specify its location and two dashed end regions which, due to the lack of a sufficient number of arcs, is presented with less confidence.

In a similar manner, the graphs of electrical conductivity vs temperature for pressures of 1, 10, 20, 50, and 100 atmospheres for Runs 1 and 2 are presented in Figures 8-12, excluding the arc temperature range data, which may be found in Table 2.

Experimental Error

Errors in the final results of the data analysis were due primarily to uncertainties in measurement of arc current, field strength, and in the determination of temperature profiles. Use of the error factor in equation 6 to fit conductivity curves to experimental data caused relative variations in $\sigma(T)$ identical to those in I/E, depending on the closeness of fit. The influence of errors in the temperature profiles was less obvious, and the extent of several error modes was investigated.

Current and Field Strength. Arc current was measured in the lead to the cascade anode using a calibrated shunt with accuracy in voltage

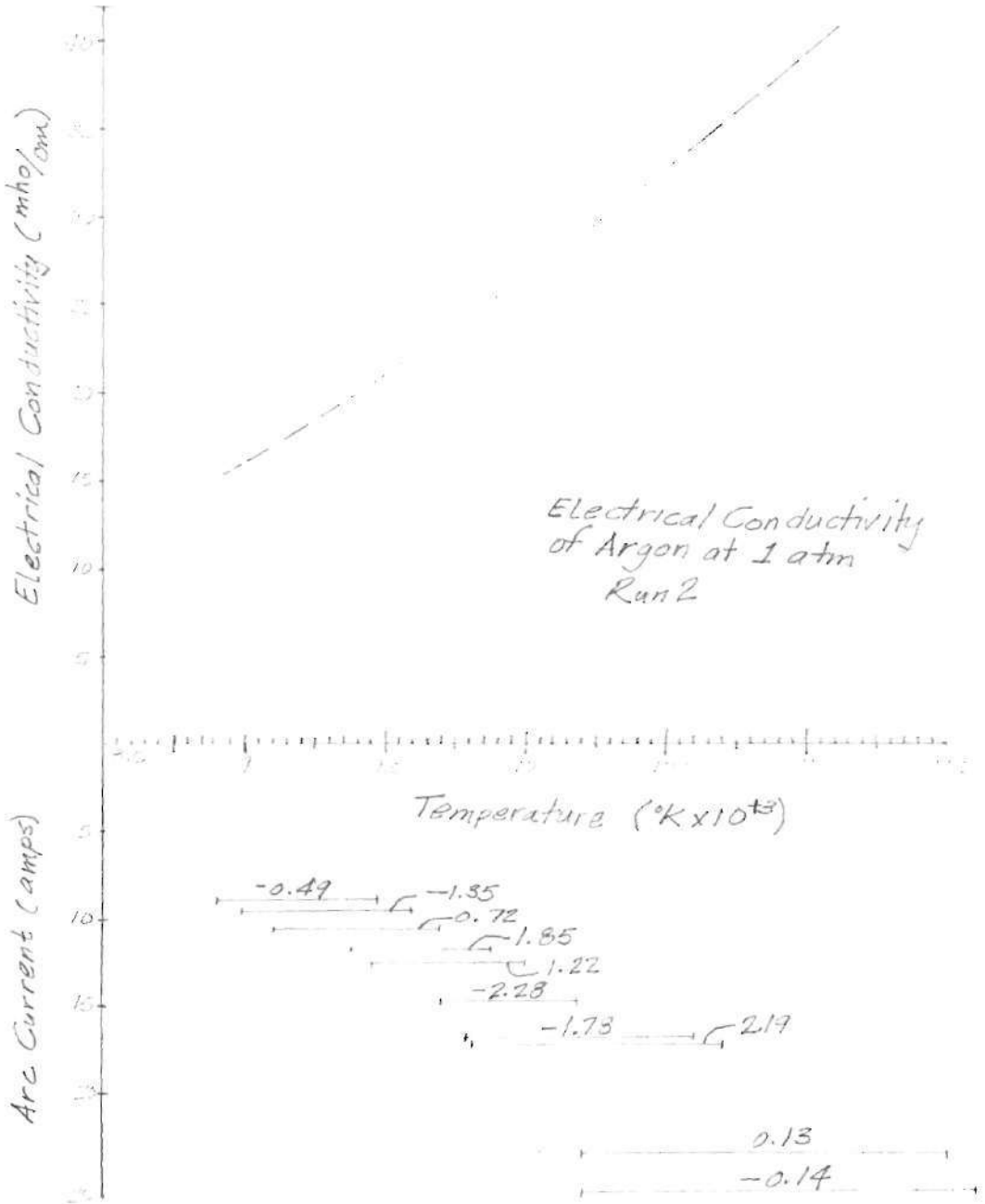

Figure 7. Electrical Conductivity of Argon at 1 atm with Temperature Ranges of Constitutive Arcs

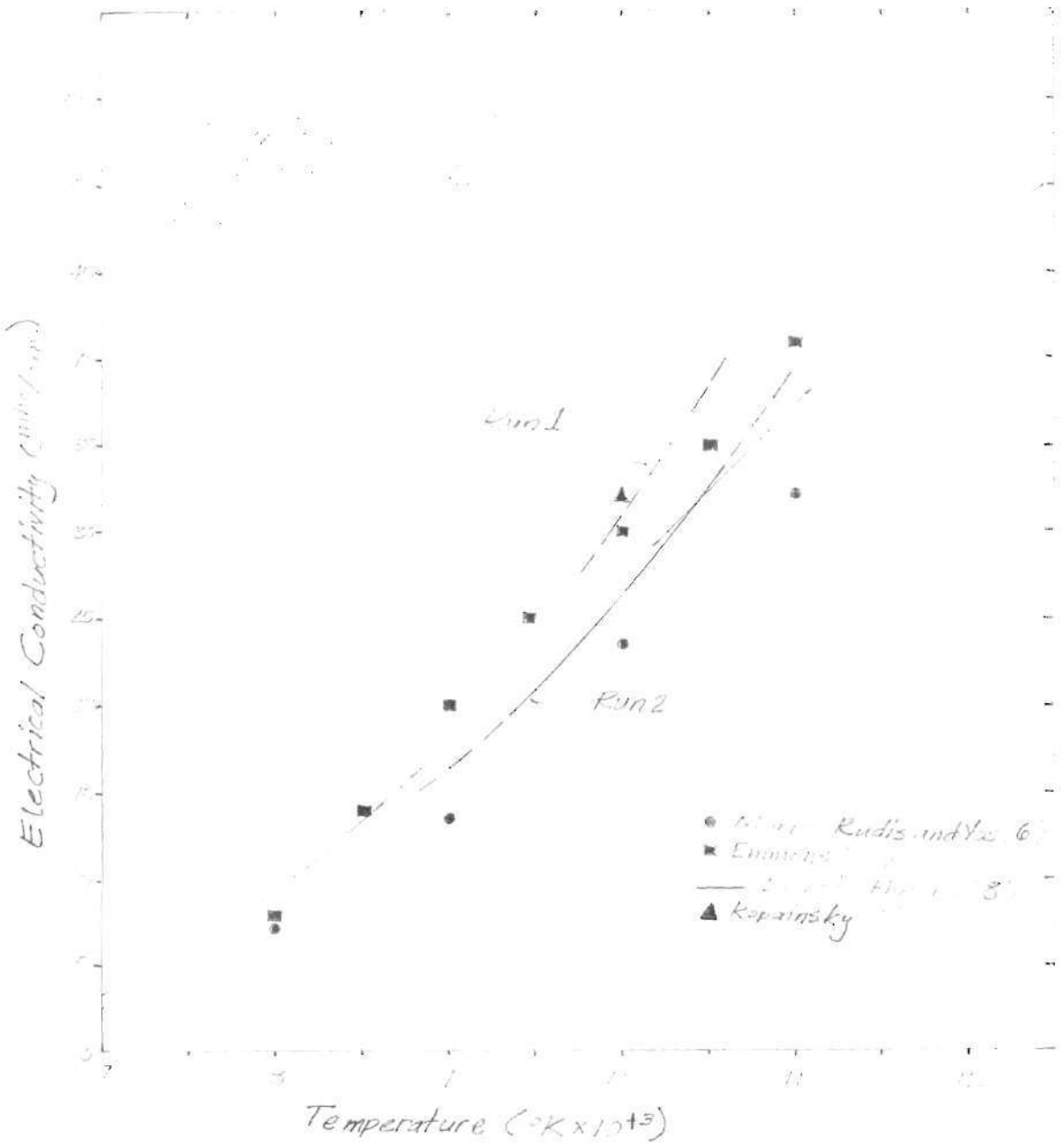

Figure 8. Electrical Conductivity of Argon at 1 atm

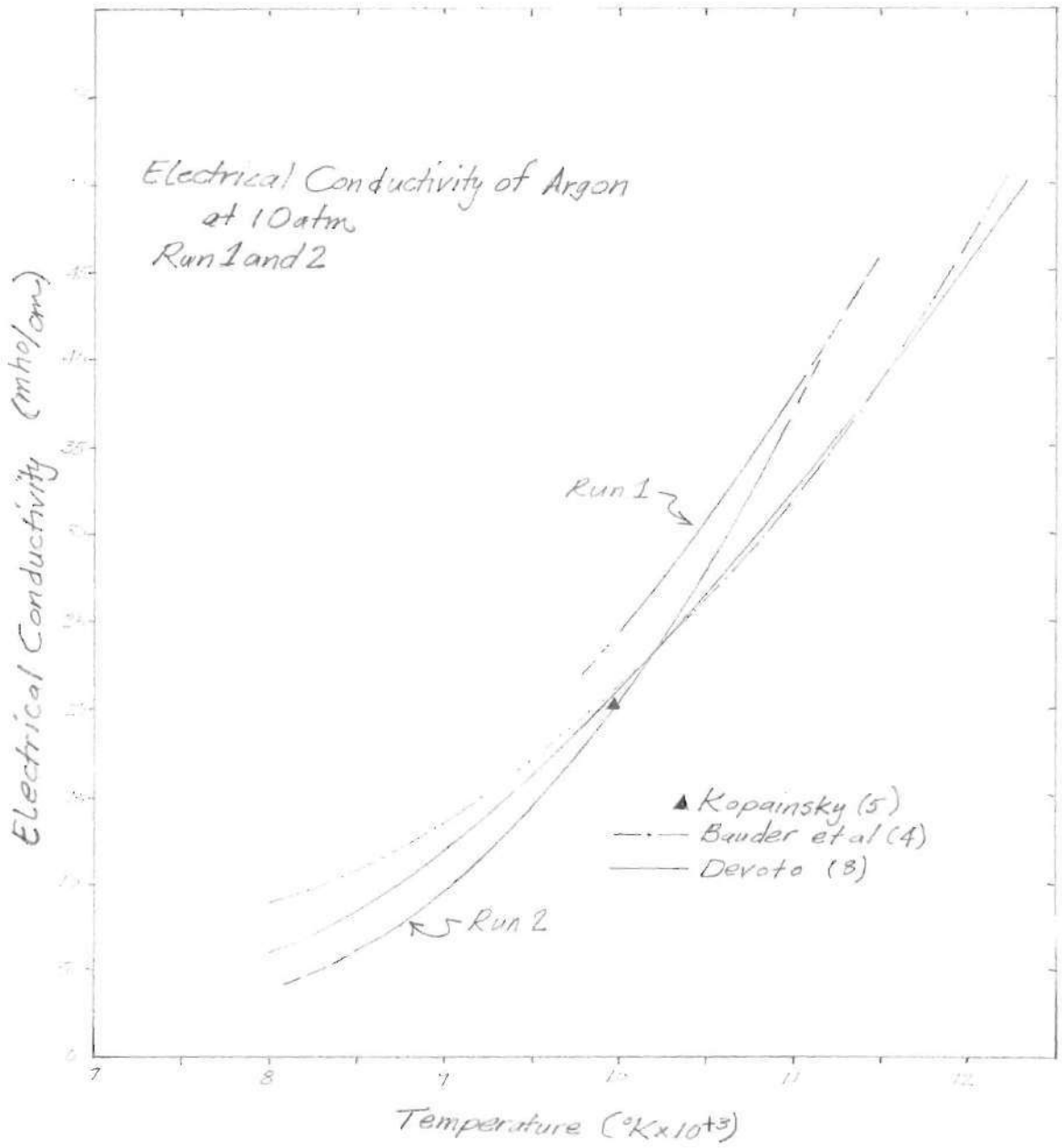

Figure 9. Electrical Conductivity of Argon at 10 atm

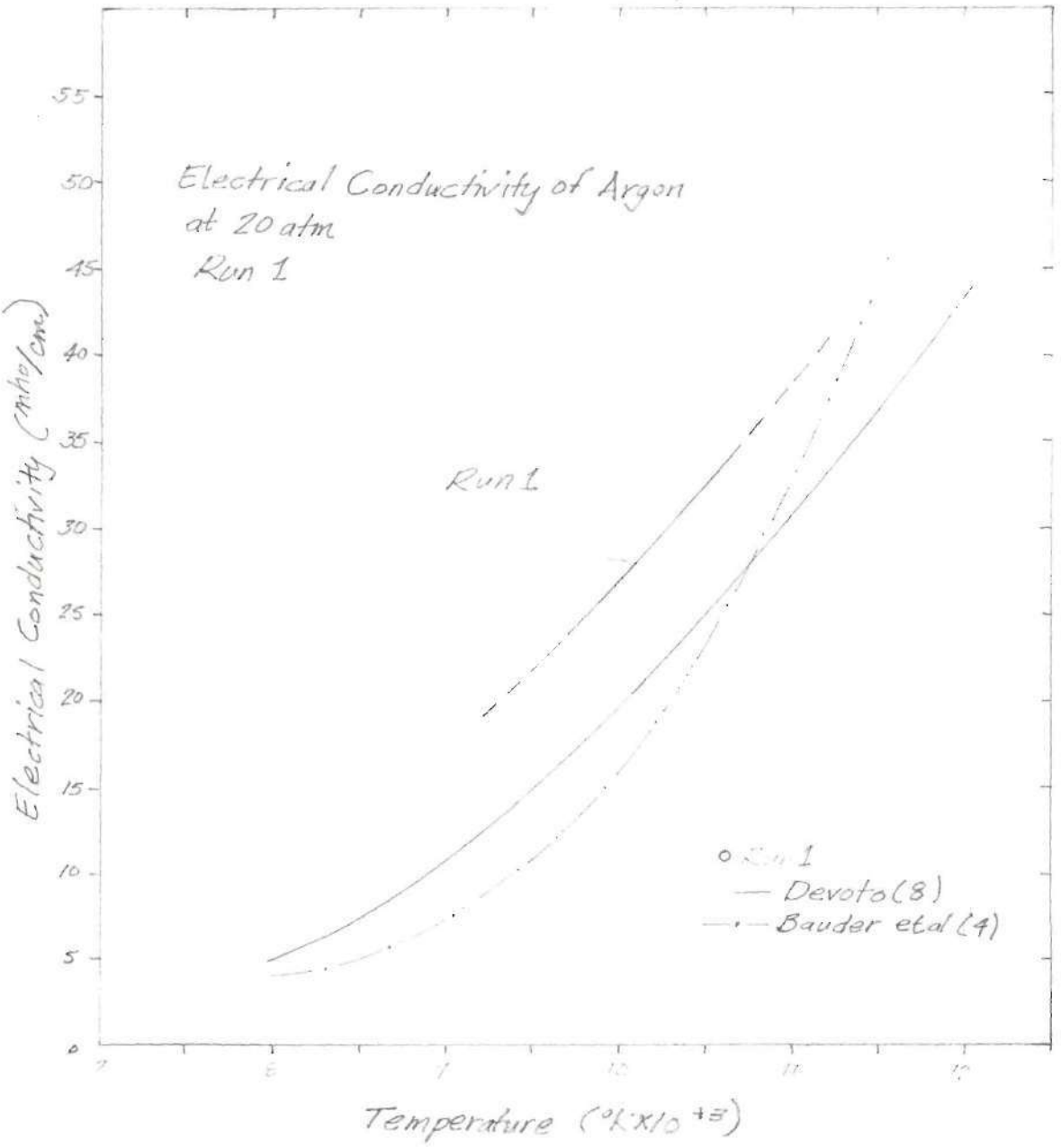

Figure 10. Electrical Conductivity of Argon at 20 atm

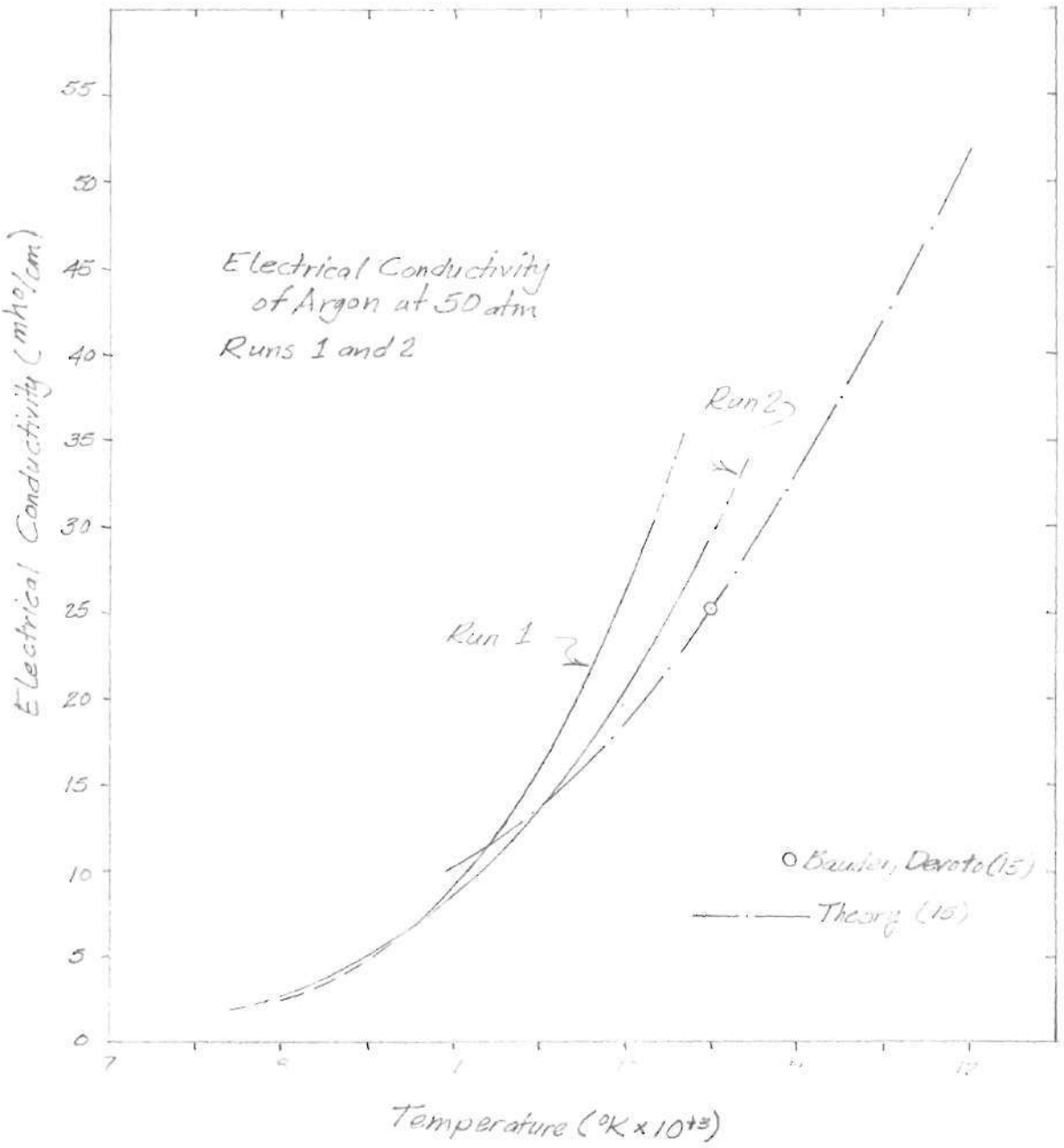

Figure 11. Electrical Conductivity of Argon at 50 atm

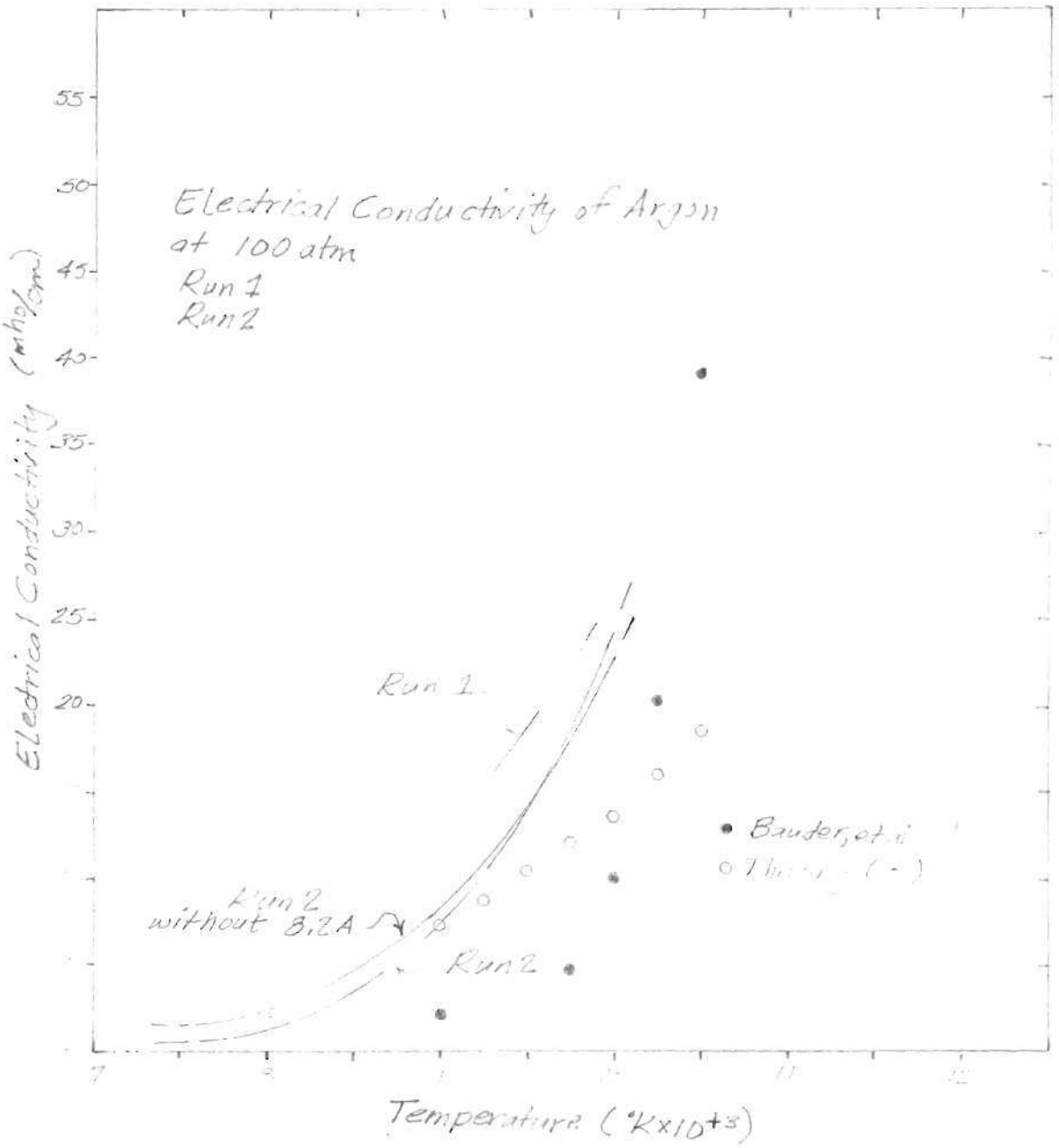

Figure 12. Electrical Conductivity of Argon at 100 atm

drop across it within 0.4% in the current range 0-500 amps. Field strength was measured using two cascade plates as potential probes, and was calculated by dividing their potential difference by the distance between them. Separation of the plates was calculated using known dimensions of cascade components. This measurement was estimated to be accurate to within 5%. Associated with field strength also was an error due to a finite resistance between cascade plates from using de-ionized cooling water. This error was estimated at 1%. Run 1, performed basically as a survey experiment, was conducted without de-ionized cooling water. The experience in this laboratory (12) suggested a correction factor between 5% and 10% to account for the untreated cooling water. A correction factor of 6% was chosen and the field strength values of Run 1 were uniformly increased by this amount. A comparison of corrected field strength values for Run 1 against those of Run 2, conducted with properly de-ionized cooling water, appears in the E vs I graph of Figure 13.

Both current and field strength were calibrated in a procedure where the accuracy of the calibration was dependent on a HP3480 DVM. This unit was reported reliable to ±0.01% of reading ±0.04% of range, giving an instrument error of 0.1% in values of I and E.

Uncertainty in values of I/E due to scatter of data points was typically less than 2.5%, with the uncertainty decreasing as pressure decreased and the arc operated more stably. Below 100 atm, no scatter was greater than 1% from the mean. Scatter was taken to be the deviation of data from the mean value of a rapid sampling of I and E values taken by the scanning DVM during the time period including a forward and reverse

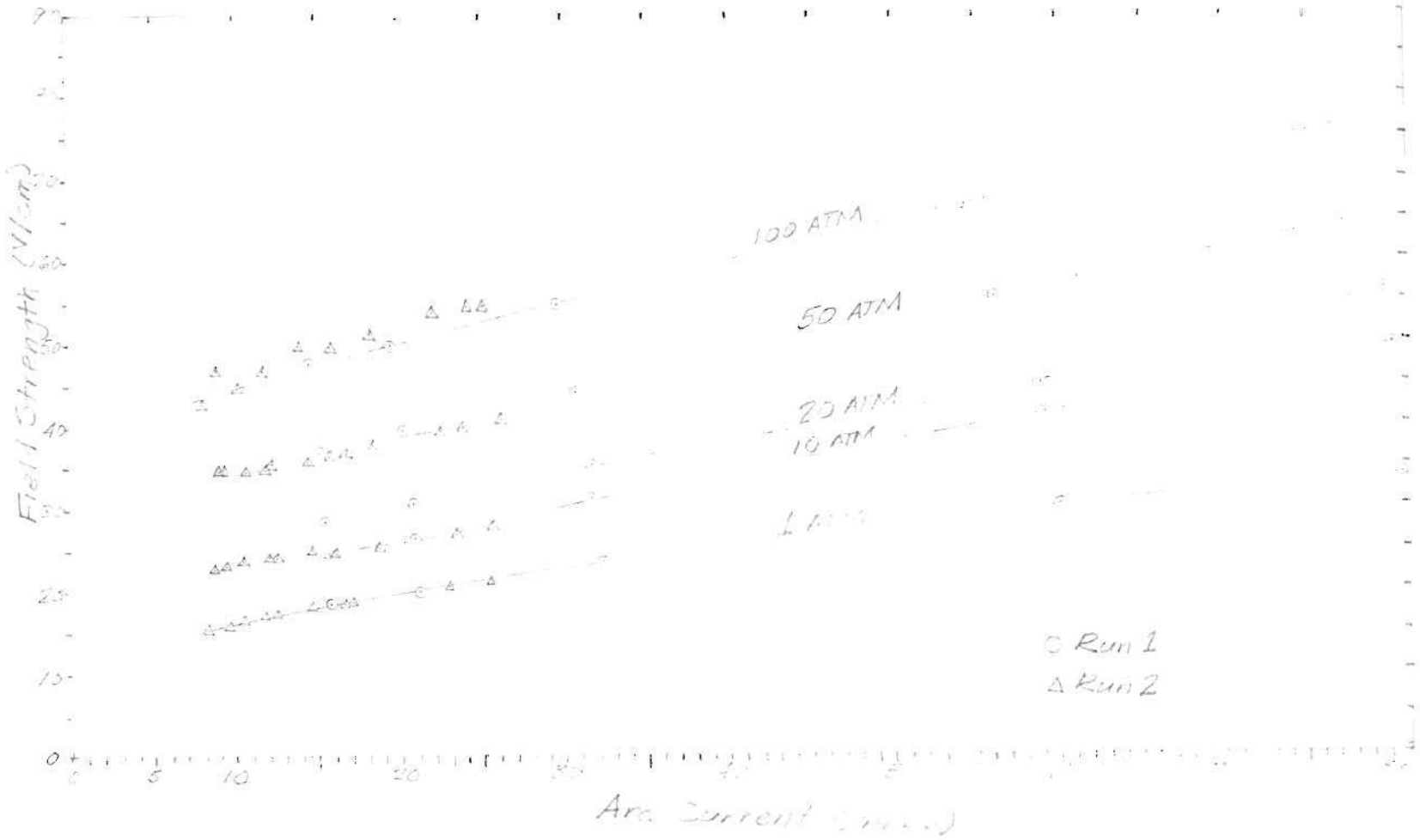

Figure 13. Confined 2 mm Arc Characteristics in Argon

scan of the arc.

Uncertainty in I/E values due to calibration and instrument error, measurement error, de-ionization error and scatter was about 5.7%, using the root of the sum of the errors squared as the means of calculation.

Intensity Profiles. The intensity profiles were evaluated using a relative measurement between the cascade arc and a standard arc of known intensity. Error introduced in evaluation of the known intensity was the primary source of intensity profile uncertainty.

The standard arc produced radiant energy equivalent to that of a black body at 3803 °K ±20 °K in the wavelength range from 3000Å to 42,000Å. This uncertainty allowed a 3.2% possible error in evaluating intensity profiles.

Equivalence of optical paths for the standard arc and the cascade arc to the spectrometer was required for the above evaluation. Calibration for Run 2 was performed, due to oversight, without the placement of a quartz cascade window in the standard arc optical path. Calibration at a later date with the proper optical path allowed an additional error to enter the analysis through differences in operating conditions; i.e. instrument warm-up, drift, slight differences in optical alignment, etc. A correction factor of 25% was calculated from the measurements made in order to account for the inclusion of the quartz window and the variation of experimental conditions. An uncertainty of 4% was estimated to be associated with the correction factor.

High frequency fluctuations of the trace of standard arc intensity were of the order of 15-20% of total signal amplitude. An average of the

fluctuations over a stable operating period was taken by eye to be the value of the signal amplitude. Error thought to be associated with this technique was 2.5%.

Small-amplitude fluctuations on intensity profiles were smoothed by hand and the value for each zone intensity was picked by eye from the smooth curve. Error associated with these techniques was smallest at centerline amplitudes, being typically less than 2.5% there. This uncertainty increased with radius as amplitude decreased, until they became equal close to the edge of the profile.

Error in intensity profiles due to calibration, correction, and reader error was about 6.2%, again using the root of the sum of the error squared as a means of calculation.

Temperature Profiles. Determination of temperature profiles required the use of intensity profiles and the line emission coefficient as a function of radius. Calculation of the latter from equation 8 required the atomic transition probability for the Ar I line at 6965.4Å, which was reported (11) with an associated uncertainty of 25%. In order to determine the effect of this uncertainty upon temperature profiles, a 25% upward shift of emission coefficients was introduced into the data stream at 1 atm, Run 1. Due to the logarithmic relation between $\varepsilon(T)$ and temperature, the resulting profiles were shifted upward unevenly from their previous positions; centerline temperatures were increased by about 2% and lesser temperatures were increased by values ranging down to 1%.

Self-absorption within the arc was a possible source of temperature error since the unfolding of intensity profiles by the Abel Inversion

assumed optical thinness of the arc at the wavelength of interest (6965.4Å). "Optical thinness" was taken to mean that the maximum intensity observed in the lateral intensity profile was less than 10% of the intensity which would be observed if the plasma were a black body radiating at the highest temperature in the plasma. The ratio of observed arc centerline intensity to the intensity of a black body at arc centerline was defined as Φ. Values of Φ were calculated for all arcs examined in this study and appear in tabulated form in Table 3. From this table, it may be seen that five arcs exceed the limit set by the meaning taken for optical thinness. These arcs were included in the analysis with the observation that their actual intensity profiles were probably higher in the region near the centerline by a factor close to $(1 + \Phi)$. No numerical correction was applied for these arcs.

Examination of intensity profiles revealed their extension beyond the 1.0 mm channel radius in the window port. Radiation from the free gas space between window plates and adjacent to the arc was thought to be due to gas heated by conduction from the arc near it. The influence of the "bulging" of the arc on values of electrical conductivity was not thought to be significant (see next section), but more study will be needed to determine its effect more exactly.

Uncertainty in centerline temperatures due to errors in intensity profiles and in determination of $\epsilon(T)$ was about 2.1%, using the root of the sum of the squares technique for evaluation.

Electrical Conductivity. Considering the error factor defined in equation 6

Table 3. Evaluation of Self-Absorption

Run Code	Pressure (atm)	Current (amps)	Max Temp (°K)	Maximum Observed Intensity (watts/sr-m^2)	Intensity of B.B @ 6965.4A (watts/sr-m^2)	Φ
1	1	15.8	10670.2	1.77×10^2	1.335×10^5	.00133
		21.2	11334.3	3.440×10^2	1.526×10^5	.00225
		33.3	11829.7	7.30×10^2	1.673×10^5	.00436
		60.2	12190.6	1.330×10^3	1.78×10^5	.00747
		80.8	12132.6	1.258×10^3	1.764×10^5	.00692
	10	15.5	10870.0	2.190×10^3	1.392×10^5	.01573
		20.8	11095.5	3.390×10^3	1.457×10^5	.02327
		31.6	11522.1	6.070×10^3	1.581×10^5	.03839
		59.1	12148.2	1.250×10^4	1.769×10^5	.07066
		80.2	12390.7	1.700×10^4	1.842×10^5	.09229
	20	15.4	10495.4	3.020×10^3	1.285×10^5	.02350
		20.7	10741.9	4.330×10^3	1.355×10^5	.03196
		31.6	11095.9	7.550×10^3	1.457×10^5	.05182
		58.1	11475	1.288×10^4	1.567×10^5	.08220
		77.3	11635.5	1.740×10^4	1.615×10^5	.10774
	50	15.0	10223.5	4.940×10^3	1.210×10^5	.04083
		20.0	10367	6.60×10^3	1.250×10^5	.05280
		30.0	10465	9.210×10^3	1.277×10^5	.07212
		57.0	10810	1.564×10^4	1.374×10^5	.11383
		79.7	11077	2.212×10^4	1.451×10^5	.15245
	100	15.0	9825.3	5.870×10^3	1.101×10^5	.05332
		19.0	9889.7	7.450×10^3	1.119×10^5	.06658
		30.0	10002.2	9.430×10^3	1.149×10^5	.08207
		54.4	10495.1	2.310×10^4	1.285×10^5	.17977
		80.0	10567.9	2.410×10^4	1.306×10^5	.18453
2	1	8.9	9354.8	4.221×10^1	9.772×10^4	.00043
		9.6	9451.8	5.018×10^1	1.002×10^5	.00050
		10.6	9568.6	6.578×10^1	1.033×10^5	.00064
		11.8	9752.7	8.577×10^1	1.081×10^5	.00079
		12.5	9884.3	9.969×10^1	1.117×10^5	.00087
		14.7	10249.9	1.552×10^2	1.217×10^5	.00128
		16.7	10461.1	1.963×10^2	1.276×10^5	.00154
		17.1	10590.4	2.309×10^2	1.312×10^5	.00176
		23.4	11294.8	4.720×10^2	1.514×10^5	.00312
		25.5	11551.3	5.723×10^2	1.590×10^5	.00360
	10	8.6	10313.4	9.794×10^2	1.235×10^5	.00793
		9.4	10429.9	1.217×10^3	1.267×10^5	.00961

Table 3 (Continued)

Run Code	Pressure (atm)	Current (amps)	Max Temp (°K)	Maximum Observed Intensity (watts/sr-m^2)	Intensity o B.B @ 6965.4A (watts/sr-m^2)	Φ
2	10	10.4	10568.5	1.459×10^3	1.306×10^5	.01117
		12.0	10725.5	1.880×10^3	1.350×10^5	.01393
		12.4	10786.7	1.956×10^3	1.368×10^5	.01430
		14.7	10978.8	2.570×10^3	1.423×10^5	.01806
		16.0	10945.3	2.579×10^3	1.413×10^5	.01812
		18.7	11067.0	3.170×10^3	1.448×10^5	.02189
		23.4	11282.2	4.331×10^3	1.511×10^5	.02866
		25.6	11348.8	4.892×10^3	1.530×10^5	.03197
	50	8.4	9862.6	2.90×10^3	1.111×10^5	.02610
		9.1	9904.7	3.128×10^3	1.123×10^5	.02785
		10.6	9970.7	3.635×10^3	1.141×10^5	.03186
		11.9	10141.1	4.553×10^3	1.187×10^5	.03836
		12.1	10144.9	4.645×10^3	1.188×10^5	.03910
		14.3	10225.9	5.463×10^3	1.210×10^5	.04515
		15.6	10269.3	6.012×10^3	1.222×10^5	.04920
		16.6	10316.8	6.600×10^3	1.236×10^5	.05340
		18.2	10356.1	7.226×10^3	1.247×10^5	.05795
		22.5	10446.1	8.818×10^3	1.272×10^5	.06932
		23.8	10442.8	8.727×10^3	1.271×10^5	.07653
		26.2	10502.4	9.919×10^3	1.287×10^5	.07707
	100	8.2	9458.3	4.221×10^3	1.004×10^5	.04204
		9.0	9535.9	3.591×10^3	1.024×10^5	.03507
		10.0	9650.8	4.503×10^3	1.055×10^5	.04268
		11.6	9669.9	4.872×10^3	1.060×10^5	.09596
		14.0	9772.5	5.856×10^3	1.087×10^5	.05396
		15.8	9713.4	5.943×10^3	1.071×10^5	.05549
		18.2	9847.2	7.321×10^3	1.107×10^5	.06613
		22.0	9980.4	9.284×10^3	1.143×10^5	.08122
		24.2	10031.9	8.854×10^3	1.157×10^5	.07653
		25.2	9968.2	9.651×10^3	1.140×10^5	.08465

$$EF = \sum_{i=1}^{N} \left(I/E - 2\pi \int_{o}^{R} \sigma(T) r dr\right)_i^2 \qquad (6)$$

it can be seen that any systematic relative change in all values of I/E for the arcs will cause an identical relative change in the values predicted for $\sigma(T)$, provided the error factor can be minimized to the same degree after the change in I/E values as before the change. For example, a uniform increase of I/E by 10% for all arcs in a given pressure series will cause a uniform 10% increase in $\sigma(T)$ for that pressure.

The effect of a 10% error in one arc in a pressure series on the values of $\sigma(T)$ was examined by increasing the $I/\pi E$ value for the 11.76 amp arc of Run 2, 1 atm, and the analysis repeated. Results appear in Table 4 with altered data denoted by a superscript star and a comparison made to the unmodified results. The large relative value of Δ^* at 11.76 amps denotes a strong deviation of the curve for $\sigma(T)$ from the modified value of $I/\pi E$ for that arc. Deviations from experimental data on the order of 2% for other arcs in the pressure series indicate closer agreement of the conductivity curve. Variation of electrical conductivity values in the temperature range affected by the modified 11.76 amp arc are less than 2.5%. It may be said, then, that variations of experimental values of I/E on the order of 10% for one arc in a series affects electrical conductivity values only slightly due to the weighted influence of adjacent arcs in the series. The probability of an error of the above type seems greater than the case of a 5.7% variation of all I/E values (discussed in section on Current and Field Strength), which would cause a consequent 5.7% variation in values of $\sigma(T)$.

Table 4. Error Study I
Effect on Electrical Conductivity of a 10% Increase in One Experimental I/E Value

Run Code	Pressure (atm)	Current (amp)	T_H (°K)	T_L (°K)	I/πE	Δ (%)	(I/πE)*	Δ (%)*
2	1	8.85	9,312	8,689	0.1805	-0.57	0.1805	1.43
		9.61	9,452	8,855	0.1923	-1.42	0.1923	0.40
		10.64	9,569	9,072	0.2050	0.65	0.2050	2.29
		11.76	9,725	9,238	0.2209	1.85	0.2430	-6.13
		12.54	9.872	9,314	0.2317	1.23	0.2317	2.52
		14.73	10,165	9,566	0.2734	-2.18	0.2734	-1.29
		16.70	10,434	9,636	0.2881	-1.77	0.2881	-1.04
		17.12	10,517	9,649	0.2909	2.22	0.2909	2.85
		23.40	11,287	10,049	0.3622	0.12	0.3622	0.14
		25.53	11,393	10,050	0.3846	-1.85	0.3846	-0.34

Temperature (°K)	Electrical Conductivity (mho/cm)	Electrical Conductivity* (mho/cm)
9,000	17.535	17.900
9,500	22.729	23.043
10,000	28.560	28.773
10,500	34.950	35.010
11,000	41.813	41.668

Note: starred quantities are associated with analysis of data with I/πE of the 11.76 amp arc increased by 10%.

Errors introduced through determination of temperature profiles were investigated in a manner similar to that above. Temperature profiles were generated by increasing the experimental emission coefficients by 25%. The new profiles were about 2% higher at centerline values and 1% higher at end values from their former positions, as was discussed in the section on Temperature Profiles. These profiles were continued through the analysis and $\sigma(T)$ values were obtained. These values are plotted in Figure 14 along with $\sigma(T)$ for the same temperature profiles before their modification. From this figure it may be seen that the net effect on $\sigma(T)$ was to lower it by about 6% at all temperatures.

The effect on $\sigma(T)$ of a pair of anomalous temperature profiles in a series was also studied. The pressure series of Run 1, 1 atm was used for manipulation. First, temperature profiles of two arcs at the extremes of the current (and also temperature) range were replaced with the same profiles modified by a 25% increase in emission coefficients. The subsequent values of $\sigma(T)$ are graphed in Figure 15, along with values of $\sigma(T)$ obtained from the unmodified series, and the same results are tabulated in section 1 of Table 5.

The raised extreme profiles caused a rotation of the electrical conductivity values from the unmodified curve; the value of the high-temperature end of the curve was lowered 5%. It was observed that the values of conductivity in the central region of the temperature range were affected by less than 2%.

Next, profiles of the two arcs in the central part of the current range were replaced by modified profiles and the original extreme profiles were retained. The graph of the results are also in Figure 15 and

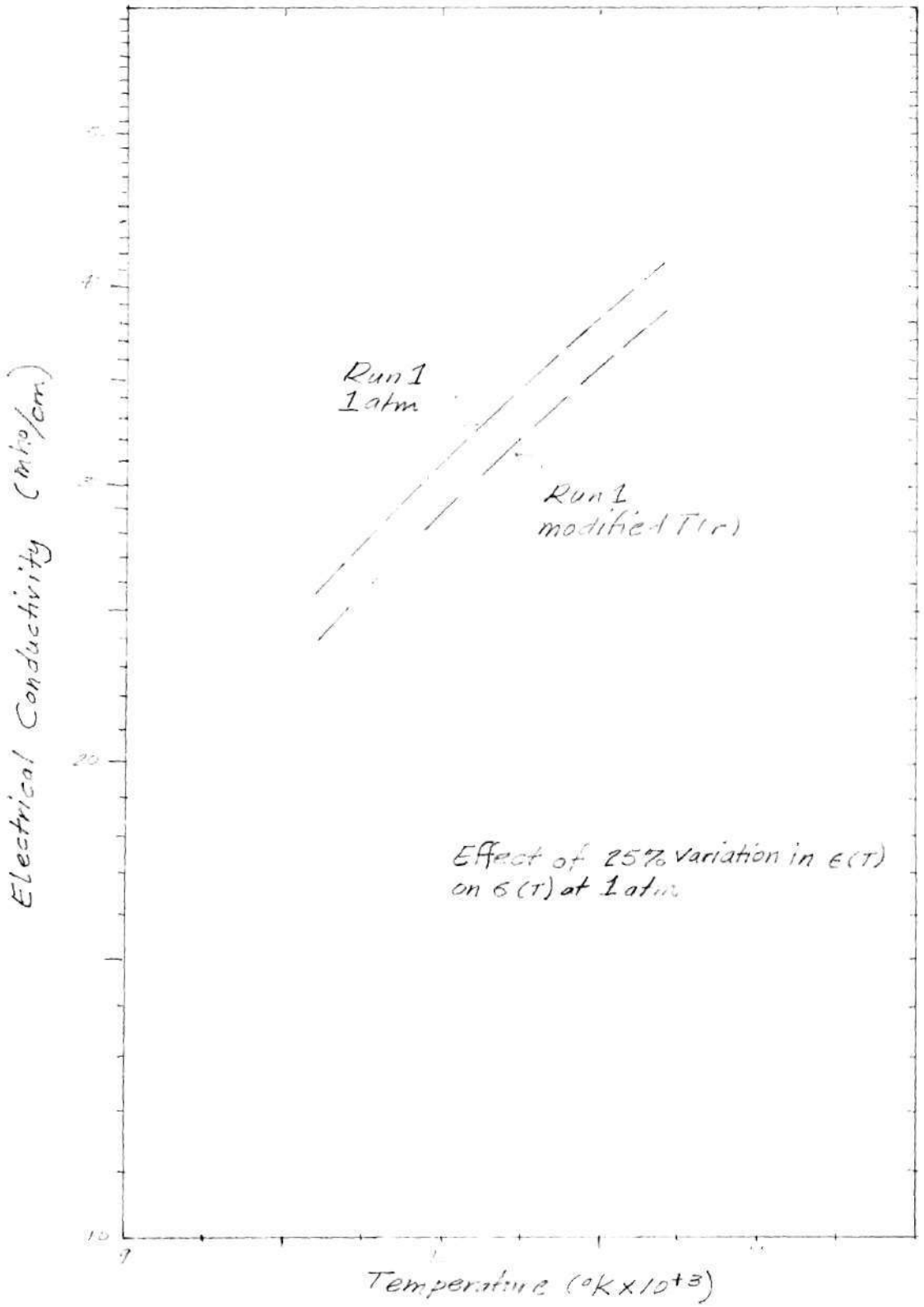

Figure 14. Error Study II - 1

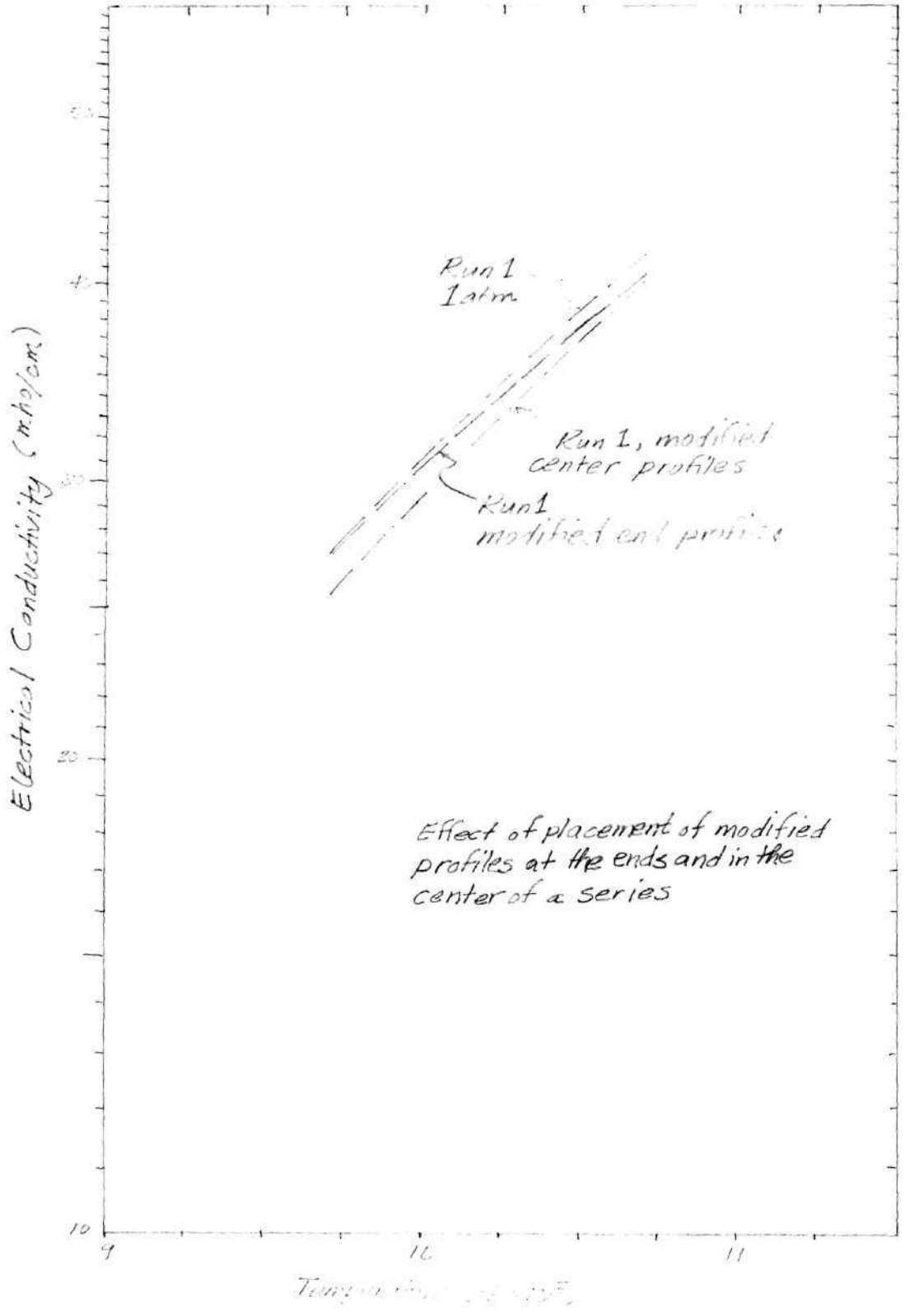

Figure 15. Error Study II - 2

Table 5. Error Study II
Effects of Modified Temperature Profiles on Argon at 1 atm

1. Lowest and Highest Current Arcs Affected by a 25% Increase in Emission Coefficient, Omitting 80A arc

Run Code	Pressure (atm)	Current (amp)	T_H (°K)	T_L (°K)	T_H*(°K)	T_L*(°K)	Δ (%)	Δ*(%)
1	1	15.8	10,670	8,298	10,860	8,395	-5.05	1.08
		21.2	11,334	8,999	11,334	8,999	-0.55	-2.42
		33.3	11,830	10,027	11,830	10,027	5.62	1.54
		60.2	12,160	11,288	12,399	11,511	-1.89	-0.31

2. Middle Current Arcs Affected by a 25% Increase in Emission Coefficient, Omitting 80A Arc.

Run Code	Pressure (atm)	Current (amp)	T_H (°K)	T_L (°K)	T_H*(°K)	T_L*(°K)	Δ (%)	Δ*(%)
1	1	15.8	10,670	8,298	10,670	8,298	-5.05	-10.39
		21.2	11,334	8,999	11,561	9,118	-0.55	2.11
		33.3	11,830	10,027	12,092	10,186	5.62	9.95
		60.2	12,160	11,288	12,106	11,288	-1.89	-4.41

Table 5 (Continued)

1. Modified End Arcs

Temp (°K)	(mho/cm) $\sigma(T)$	(mho/cm) $\sigma^*(T)$
9,000	18.424	18.823
9,500	24.332	24.436
10,000	31.094	30.748
10,500	38.639	37.675
11,000	46.880	45.127
11,500	55.716	53.004

2. Modified Middle Arcs

Temp (°K)	(mho/cm) $\sigma(T)$	(mho/cm) $\sigma^*(T)$
9,000	18.424	17.118
9,500	24.332	22.840
10,000	31.094	29.458
10,500	38.639	36.916
11,000	46.880	45.134
11,500	55.716	54.019

Note: Starred quantities are associated with analysis of data with modified temperature profiles.

tabulated in Table 5, section 2. The effect of this change was to uniformly shift the conductivity curve towards higher temperatures by about 110 °K, giving variations of 8% at the low-temperature end of the curve and 3% at the high temperature end.

From these studies, it may be said that the shape of the electrical conductivity curve was dominated by arcs in the central part of the temperature range. This observation was reassuring in that errors were expected to be greater at the extremes of the conductivity temperature range due to reader error at the low end and lack of sufficient numbers of arcs at the high end.

Suggested by the above studies, the effect on conductivity by arcs suspected of large variation within a series was examined by deleting the 80A arcs from Run 1, at pressures of 20, 50, and 100 atm. These arcs were suggested by the large relative values of Φ corresponding to them in Table 3. Comparison of conductivity for the three pressure-current series before and after deletion of the 80A arcs appears in Figures 16-18 and are tabulated in Table 6. Values of Δ and $\sigma(T)$ for the modified series appear starred.

From Table 6 it may be seen that the overall fit of the three curves was not worsened by the deletion of the 80A arcs, and in the case of 50 atm, the fit was materially improved. In each case the fit was improved at the high extreme of the temperature range of the curves. The effect of deleting the upper extreme arc was to allow the curve to be fit more closely to the next lower experimental I/E value. As may be seen from Table 6, the Δ of 20 atm, 58.1 amp was 10% low. The curve, then, was lowered at the upper extreme in order to come into better agreement with

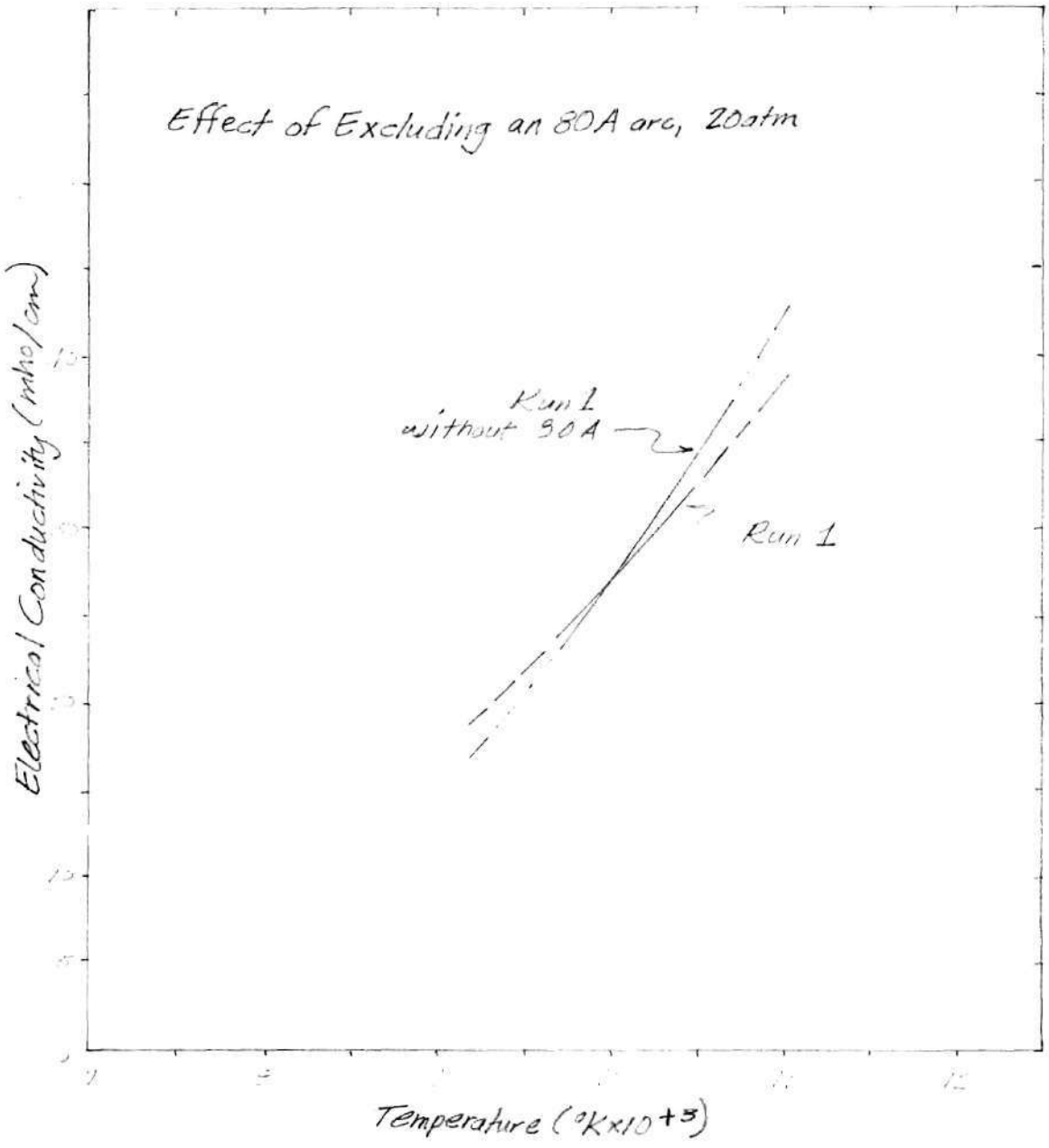

Figure 16. Error Study III - 1

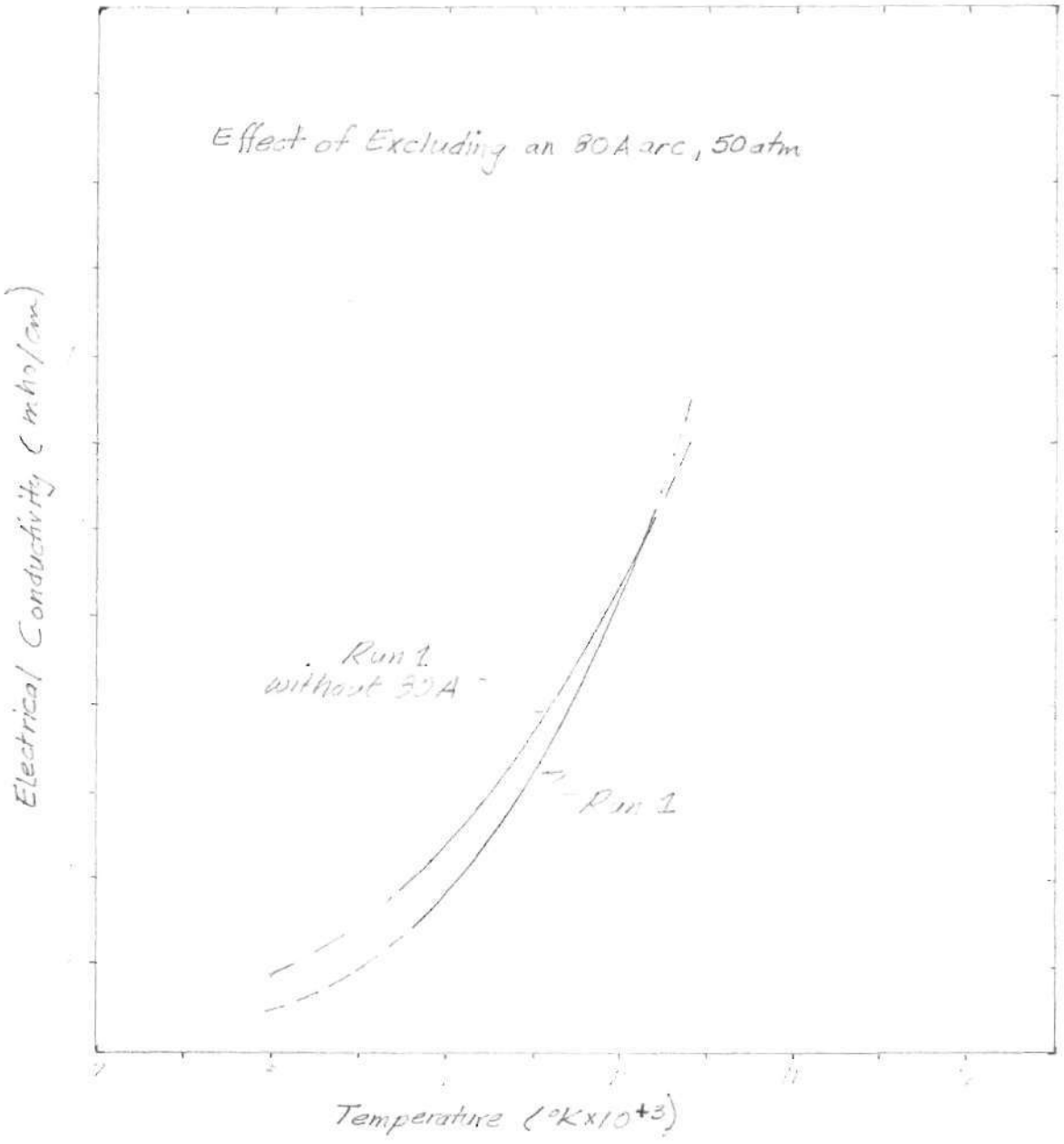

Figure 17. Error Study III - 2

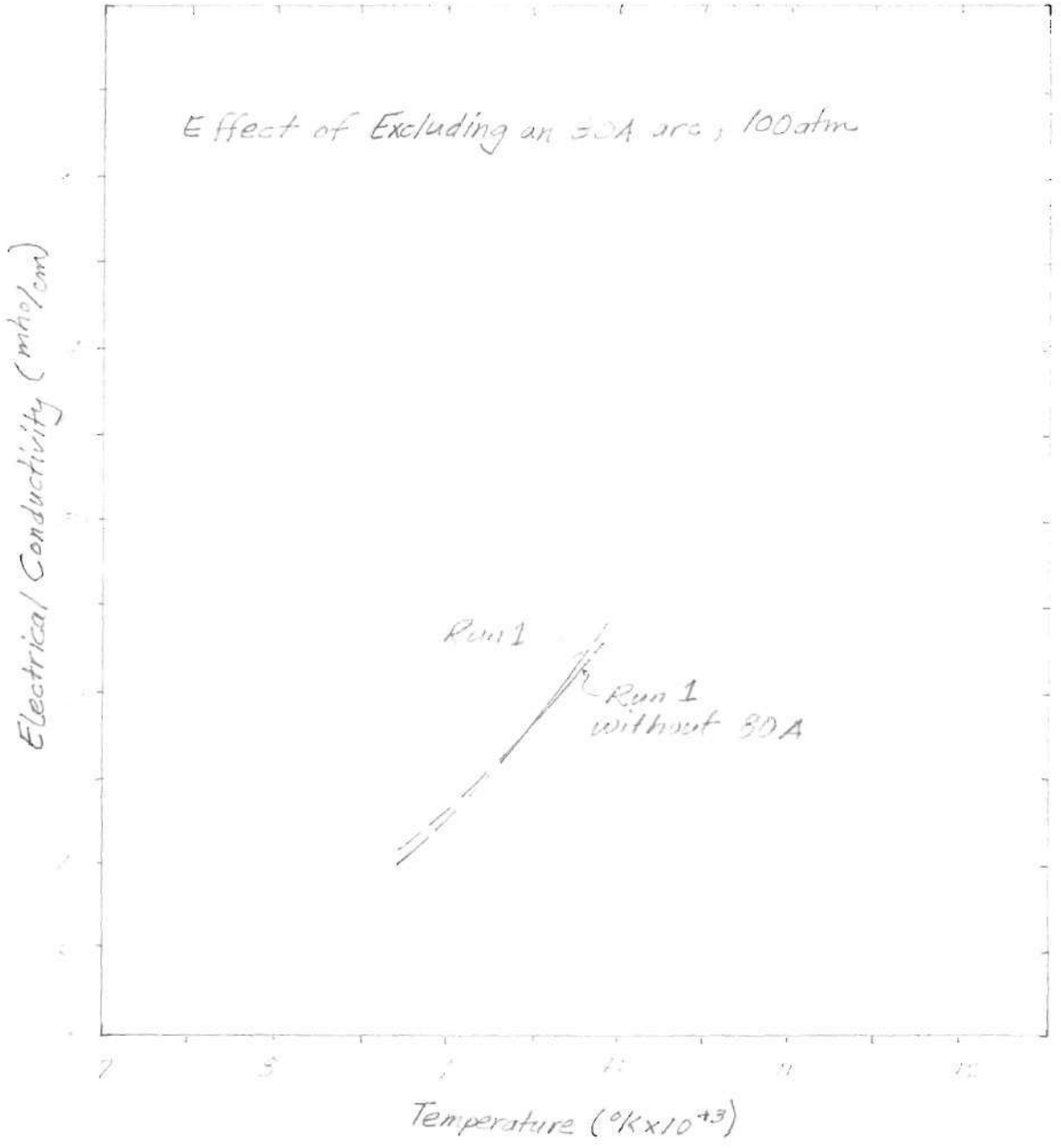

Figure 18. Error Study III - 3

Table 6. Error Study III
Effect on Electrical Conductivity of Deletion of 80A Arc for
20, 50, and 100 atm Series, Run 1

Run Code	Pressure (atm)	Current (amp)	T_H (°K)	T_L (°K)	T_H*(°K)	T_L*(°K)	Δ (%)	Δ*(%)
1	20	15.4	10,495	7,893	10,495	7,893	13.62	6.33
		20.7	10,742	7,875	10,742	7,875	-7.74	-10.26
		31.6	11,080	9,193	11,080	9,193	3.60	6.84
		58.1	11,375	9,763	11,375	9,763	-10.04	1.35
		77.3	11,579	10,285			7.60	
	50	15.0	10,224	7,808	10,224	7,808	-11.47	0.12
		20.0	10,217	7,671	10,217	7,671	-4.81	0.77
		30.7	10,431	7.959	10,431	7,959	-0.37	-0.85
		56.2	10,793	8,794	10,793	8,794	10.36	0.17
		79.7	10,973	9,308		9,308	-3.68	
	100	15.0	9,825	7,234	9,825	7,234	7.50	10.87
		19.0	9,834	7,243	9,834	7,342	2.09	3.14
		30.0	9,897	7,481	9,897	7,481	-8.35	-9.32
		54.4	10,495	9,344	10,495	9,344	9.62	1.23
		80.0	10,325	9,388			-6.36	

Table 6 (Continued)

Temp (°K)	σ(T) (mho/cm)	σ(T)* (mho/cm)	σ(T) (mho/cm)	σ(T)* (mho/cm)	σ(T) (mho/cm)	σ(T)* (mho/cm)
8,000			2.434	4.392		
8,500			44.945	7.518	8.404	9.313
9,000	17.220	14.998	9.239	12.055	12.763	13.317
9,500	21.920	20.431	16.092	18.300	18.451	18.239
10,000	27.095	26.851	26.421	26.524	25.587	24.087
10,500	32.667	34.227	41.202	36.958	34.249	30.840
11,000	38.554	42.503				
11,500	44.674	51.603				

Note: Starred quantities are associated with the analysis of pressure 50 series with the 80A arc deleted.

experimental data at the new end point. Similar reasoning may be applied to the curves of 50 and 100 atm.

Possible bulging of the arc in the window port next suggested examination of the effect of the selection of arc radius on electrical conductivity. The program which evaluated the integral in equation 6 was allowed to continue its evaluation out to 1.1 mm, or a 10% increase in arc radius, for the 1 atm series in Runs 1 and 2. Results are plotted in Figures 19 and 20 and appear tabulated in Table 7. As may be seen from Figures 19 and 20, the effect of a 10% increase in arc radius was to lower the values of $\sigma(T)$ uniformly by about 12%.

Bulging of the arc was not thought to be significant, however, due to agreement of results with experiments (4,6) where larger diameter arc channels were used and bulging would be far less and due to the following argument:

Consider current density, J, to be expressed as

$$J = \sigma(T)E \tag{16}$$

where E is the local field strength. Small current deformation in the window port would imply small J outside the arc channel radius of 1.0 mm. Higher resistance of the cooler gas in the free space between plates would make conditions unfavorable for current flow in this region. Similarly, constrictions placed on the arc at the top and bottom of the window port by the arc channel would discourage the movement of arc current into a longer, more resistive path between plates. In the case of current bulging, then, the $\sigma(T)$ falling rapidly with radius outside the arc channel radius and the decreasing local field strength due to longer effec-

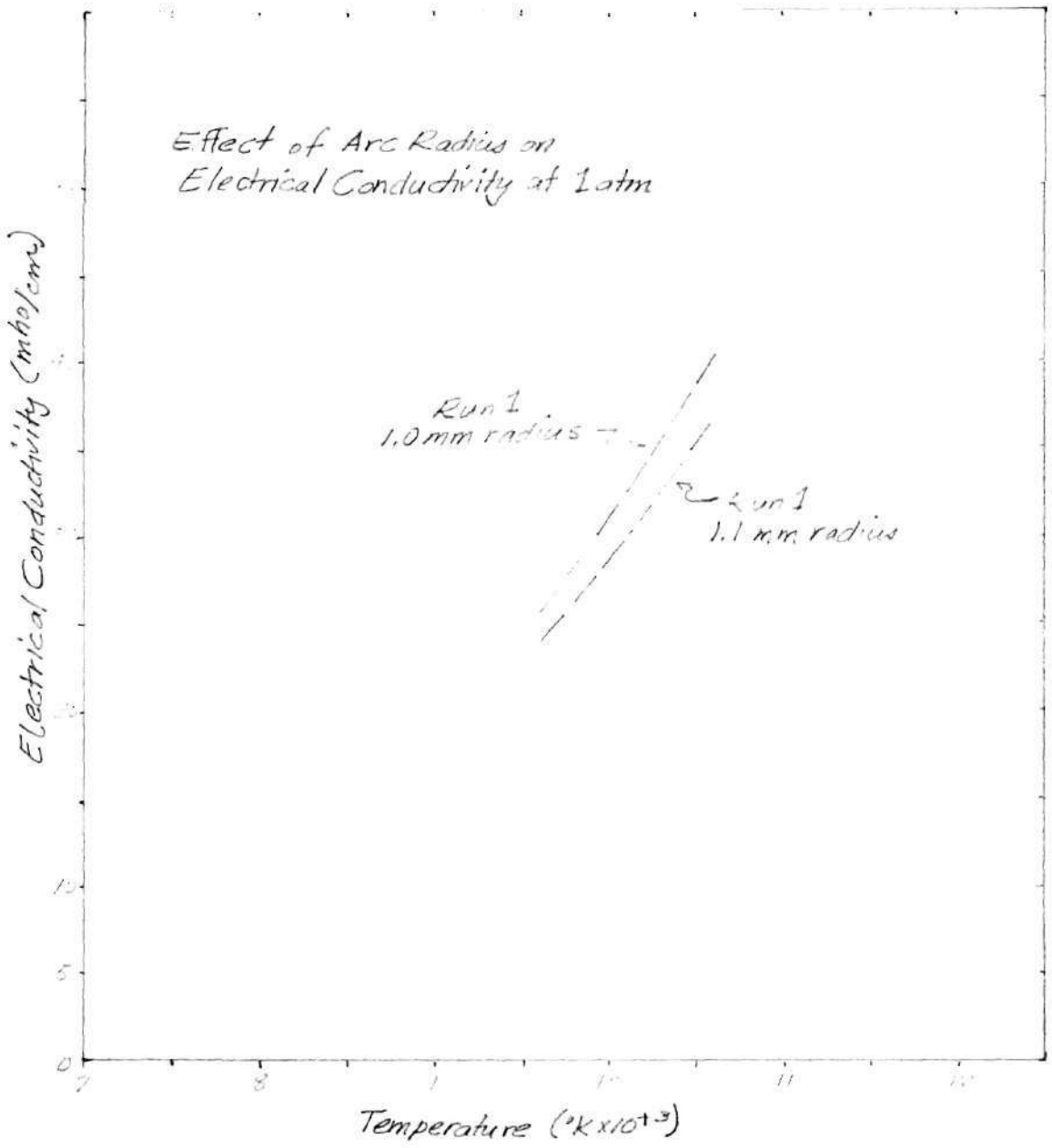

Figure 19. Error Study IV - 1

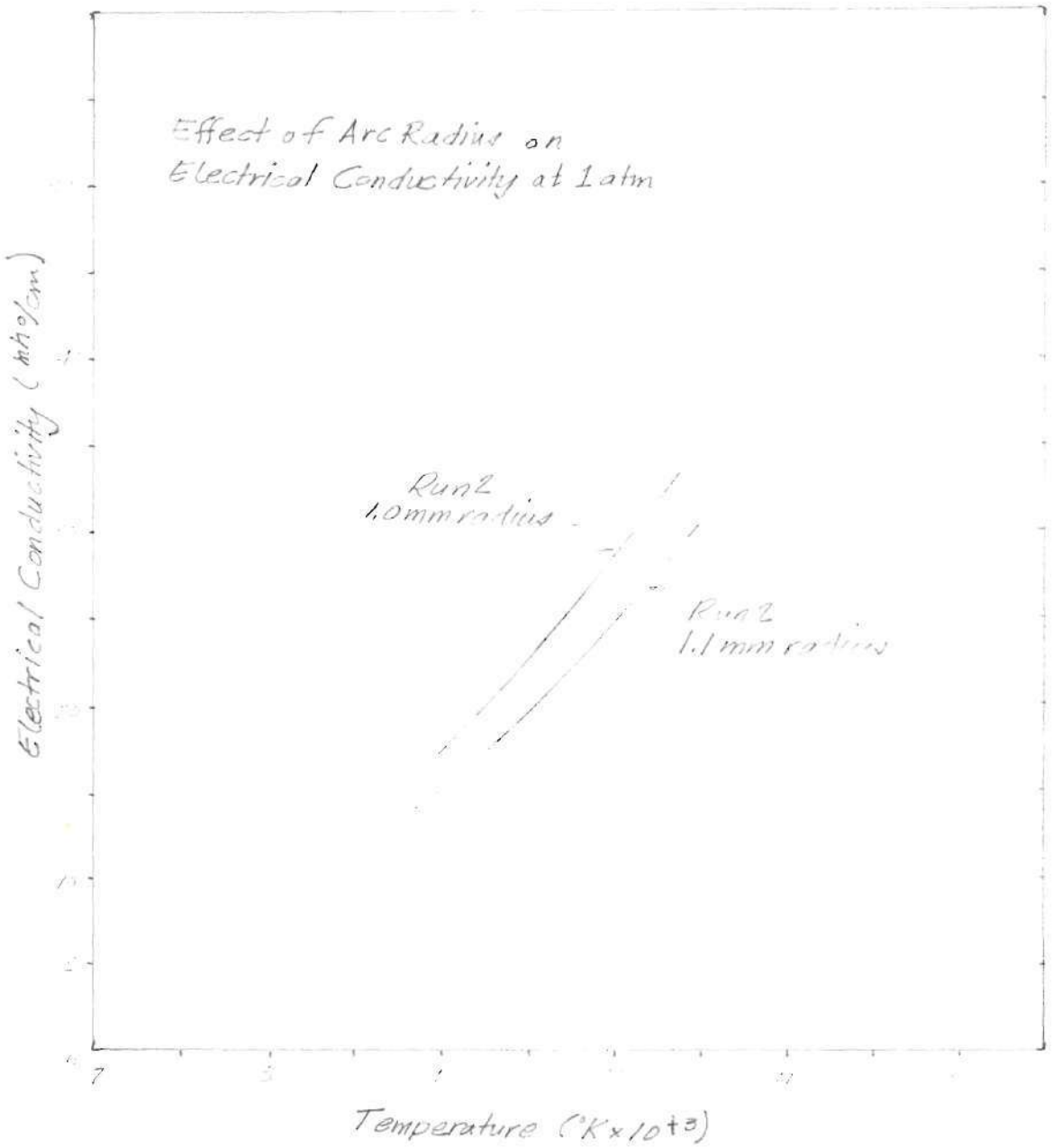

Figure 20. Error Study IV - 2

Table 7. Error Study IV
Effect on Electrical Conductivity of a 10% Increase in Arc Radius

Run Code	Pressure (atm)	Current (amp)	T_H (°K)	T_L (°K)	T_H*(°K)	T_L*(°K)	Δ (%)	Δ*(%)
1	1	15.8	10,670	8,298	10,670	8,046	-5.05	-4.04
		21.2	11,334	8,999	11,334	8,430	-5.45	-0.92
		33.3	11,830	10,027	11,830	9,402	5.62	4.98
		60.2	12,160	11,288	12,160	10,812	-1.89	-1.59
2	1	8.85	9,312	8,689	9,312	8,584	-0.57	-1.52
		9.61	9,452	8,855	9,452	8,584	-1.42	-2.71
		10.64	9,569	9,072	9,569	8,858	0.65	0.73
		11.76	9,725	9,238	9,725	8,974	1.85	1.93
		12.54	9,872	9,314	9,872	9,109	1.23	1.86
		14.73	10,165	9,566	10,165	9,252	-2.18	-2.11
		16.70	10,434	9,636	10,434	9,343	-1.77	-1.44
		17.12	10,517	9,649	10,517	9,533	2.22	3.04
		23.40	11,287	10,049	11,287	9,704	0.12	0.22
		25.53	11,393	10,050	11,393	9,751	-1.85	-0.92

	Run 1		Run 2	
Temp (°K)	σ(T) (mho/cm)	σ(T)* (mho/cm)	σ(T) (mho/cm)	σ(T)* (mho/cm)
8,500			13.037	11.006
9,000	18.424	17.672	17.535	14.937
9,500	24.332	22.842	22.729	19.518
10,000	31.094	28.627	28.560	24.705
10,500	38.639	34.949	34.950	30.433
11,000	46.880	41.722	41.813	43.217

Note: Starred quantities are associated with the analysis of the 1 atm series of Runs and 2 in which the assumption of a 1.1 mm arc radius is made.

tive path length combine to suggest small current flow (small J) in the region outside the arc channel radius of 1.0 mm.

The analysis program made a fit of a trial function to experimental data by altering the governing parameters of the trial function in a stepwise fashion. The fit of the curve to the data, then, was a choice among a number of fits each of which may have been considered equally "good". For this reason, an uncertainty of 4% was estimated to be associated with the values obtained with this analysis program.

In consideration, then, of the errors in measurements of arc current and field strength in the analysis and in the determination of radial temperature profiles, an error of 10-15% was found to be associated with the values of electrical conductivity found in this study for argon in a 2 mm diameter arc.

The oversight in calibration for the Run 2 intensity profiles which was mentioned previously was discovered too late to include in some parts of this report without extensive re-writing and consequent delay. Re-running the error analysis, it was felt, was not necessary because the relative nature of the statements made were directly applicable to the corrected data. Figures 7-19 were drawn using the corrected data and bear no unapplied correction factor save consideration of the experimental error of 10-15%. Tables 2-7 do not present corrected data. These tables are useful for illustration and may be used directly for the final results of electrical conductivity if a uniform correction of about 6.5% is applied to decrease the values of electrical conductivity presented in them. The discussions supported by the tables are not affected by the application of this correction factor. The temperature profiles presented

in Appendix B are from corrected data.

The exclusion of 80.8 amps, 1 atm, Run 1 in all phases of the analysis was due to the behavior of the intensity profile which suggested either an unrealistic physical interpretation or some sort of momentary instrument malfunction.

Values of electrical conductivity for 100 atm were presented in Figure 12 which excluded the arc at 8.2 amps for Run 2. This was suggested by the large relative value of Δ for this arc in Table 2 and the corresponding negative values of Δ in the 8.95, 10.0, and 11.6 amp arcs.

The resulting curve in Figure 12 shows increased values of electrical conductivity at the lower end of the temperature range (7500 °K - 9500 °K) as might be expected from the results of Error Study IV, which investigated the influence of arcs at the extremes of the $\sigma(T)$ temperature range. The fit of the curve to experimental data was improved by the exclusion of the 8.2 amp arc, giving values of Δ within 7% and typically 2% in the temperature range influenced previously by the 8.2 amp arc.

CHAPTER VI

CONCLUSIONS

Values of electrical conductivity presented at 1 atm in argon lie in the middle of experimental points from three independent sources (5, 6,9) and compare favorably with theory (8) in the temperature range 9000-11,000 °K, as depicted in Figure 8. At 10 atm pressure, more experimental data was provided to add to the previous point (5) while comparison with theory (8) showed agreement within experimental error for the temperature range 9500-11,000 °K. At lower temperatures, the experimental data falls below the theory, as shown in Figure 9. Data presented for 20 atm electrical conductivity differs strongly from theory (8) and experiment (4) in the temperature range (9700 °K - 10,700 °K) as shown in Figure 10. Confidence in the data from Run 1, however, is not as high as that from Run 2 and additional experiments in the 20 atm pressure range are needed.

Values for electrical conductivity at 50 atm compare favorably with theory (20) in the temperature range from 10,500 °K to 9000 °K and extend experimental information down to lower temperatures (8000 °K). A previous experimental point (20), determined by the examination of continuum radiation in the wavelength range 3600Å-4600Å is within the experimental error of values of electrical conductivity at 10,500 °K presented by Run 2.

The amount of experimental information on electrical conductivity of argon at 100 atm has been doubled by the addition of values presented

in Figure 12. These values differ strongly from previous experiments (4) except toward higher temperatures (10,000 °K), but agreement with theory (8) is superior in the temperature range in which data from this study is presented with the least uncertainty. Deviation from theory becomes about 50% at temperatures (>10,000 °K) for which less confidence is extended to the data from this study.

The method which was used to fit on electrical conductivity function to experimental arc characteristics in this study proved to be a powerful technique in determining an empirical expression for the electrical conductivity of argon in the temperature and pressure ranges examined. An exponential trial function of the type used in this study could be fitted to experimental data in argon with internal variation of between 2.2% and 16% in the best and worst cases, respectively.

Data provided by Run 2 tended to display more self-consistency than data from Run 1 due, it is thought, to several factors. Run 1 was intended as a survey experiment which would be used to explore system and arc sensitivities and to determine areas of procedure and analysis which needed more emphasis in subsequent experiments. Also, Run 1 was conducted without de-ionized cooling water in field strength ranges up to 70 v/cm, for which a small correction factor was applied. The uncertainty of this effect was directly related to conductivity error. Finally, since the trial function used was concerned with three variables, the five currents at each pressure in Run 1 allowed more of a margin in determining the electrical conductivity values than the ten currents at each pressure in Run 2.

Recommendations for further study include more high pressure

(>50 atm) experiments in order to determine repeatability and investigations into such physical phenomena as arc bulging and self-absorption within the arc. Argon is recommended as the working medium for the examination of these phenomena due to its stability and reduced wear characteristics at high pressure. Completion of system automation may also be considered as a means for pulse-type operation in higher temperature regimes than is now possible in steady-state operation.

APPENDIX A

MODIFIED ABEL DIAGNOSTIC PROGRAM (MAD)

The computer program, MAD (13), utilized the spatially observed surface radiation intensity as raw data fed in at N discrete points according to Figure 21. The program calculated the radially dependent temperature and emission coefficient for an optically thin plasma. The radius of the plasma was found from the radiation intensity profiles. It was assumed to be that position where the intensity dropped to zero.

The data fed in were first curve fitted with a third-order spline fit subroutine and interpolated to give observed intensity values for N zones. The program then calculated values of x(n,i) which was the thickness of zone i when observed at chordal position y_n, as shown in Figure 21. This distance was

$$x(n,i) = R\left[\left(1-\frac{i-1}{N}\right)^2 - \left(1-\frac{n}{N}\right)^2\right]^{1/2} - \sum_{j=i+1}^{n} x(n,j)$$

During the first iteration, the emission coefficients were calculated for each zone from the observed intensity I (y_n) and the values of x(n,i), assuming the plasma to be optically thin; i.e. the absorption coefficient k was set equal to zero for all zones. Starting from zone one and working toward the center, the emission coefficient of each zone was calculated using the emission coefficients of previously calculated zones from:

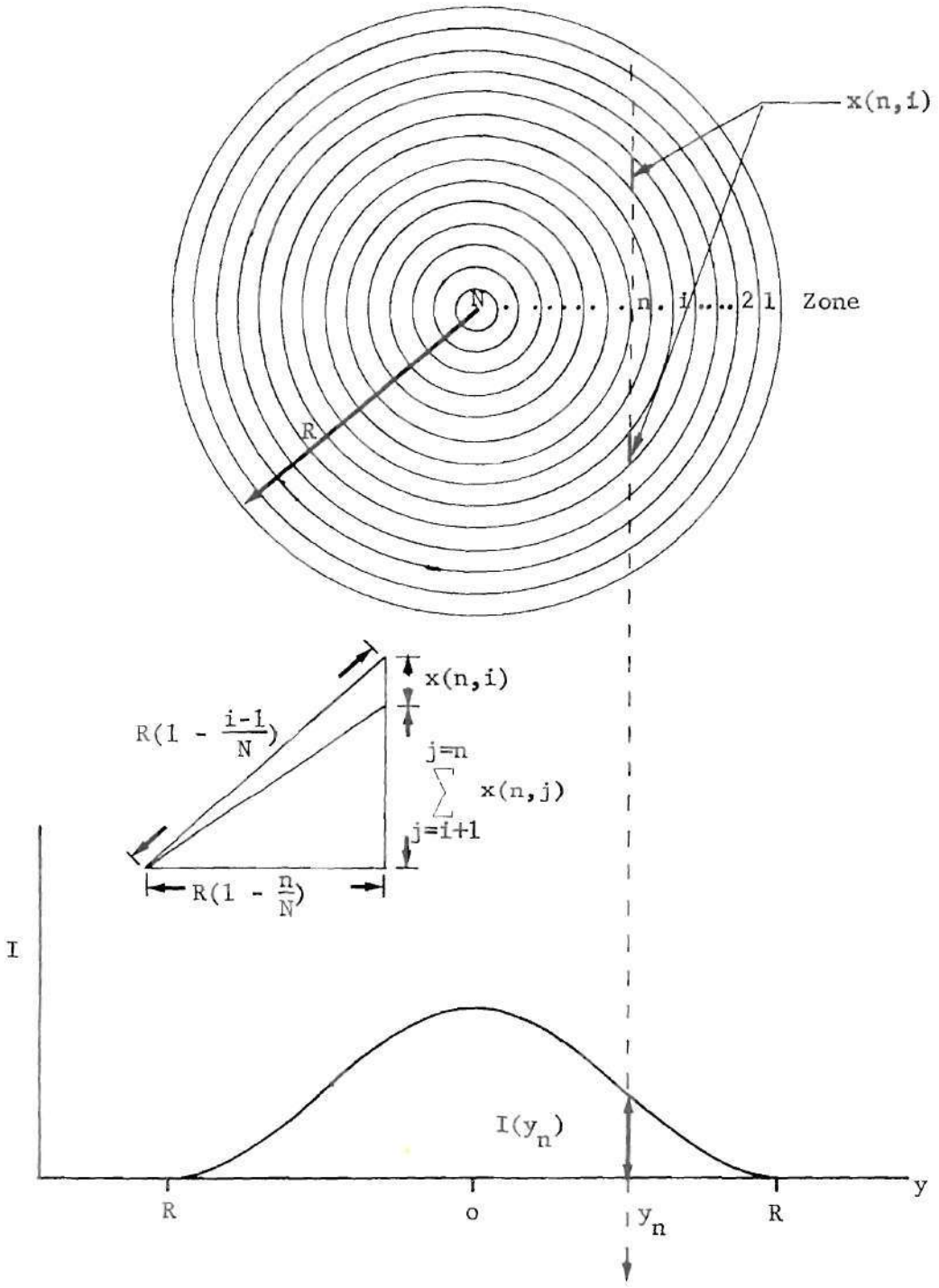

Figure 21. Plasma Geometry for Abel Inversion Program

$$I(y_n) = 2 \sum_{i=1}^{n} \varepsilon(i)x(n,i)$$

or

$$\varepsilon(n) = [I(y_n) - 2 \sum_{i=1}^{n-1} \varepsilon(i)x(n,i)] \frac{1}{2x(n,n)}$$

where $\varepsilon(i)$ for $i<n$ were calculated previously.

The temperature and number density for each zone would be calculated from the emission coefficient and the Saha, Boltzmann, and perfect gas relations as described in the Analysis section under Temperature Profiles. The correct temperature and number density for a given emission coefficients were then arrived at by binary search iterative procedure. After the first iteration, a new set of emission coefficients was calculated based on observed intensity data. These new emission coefficients were used to calculate new temperatures. The iteration terminated when the charges in emission coefficients and temperatures for all zones were less than one percent of the values in the previous iteration.

This analysis provided self-consistent radial distribution of temperature and emission coefficient for the distribution of the observed intensity for optically thin plasmas.

APPENDIX B

TEMPERATURE PROFILES

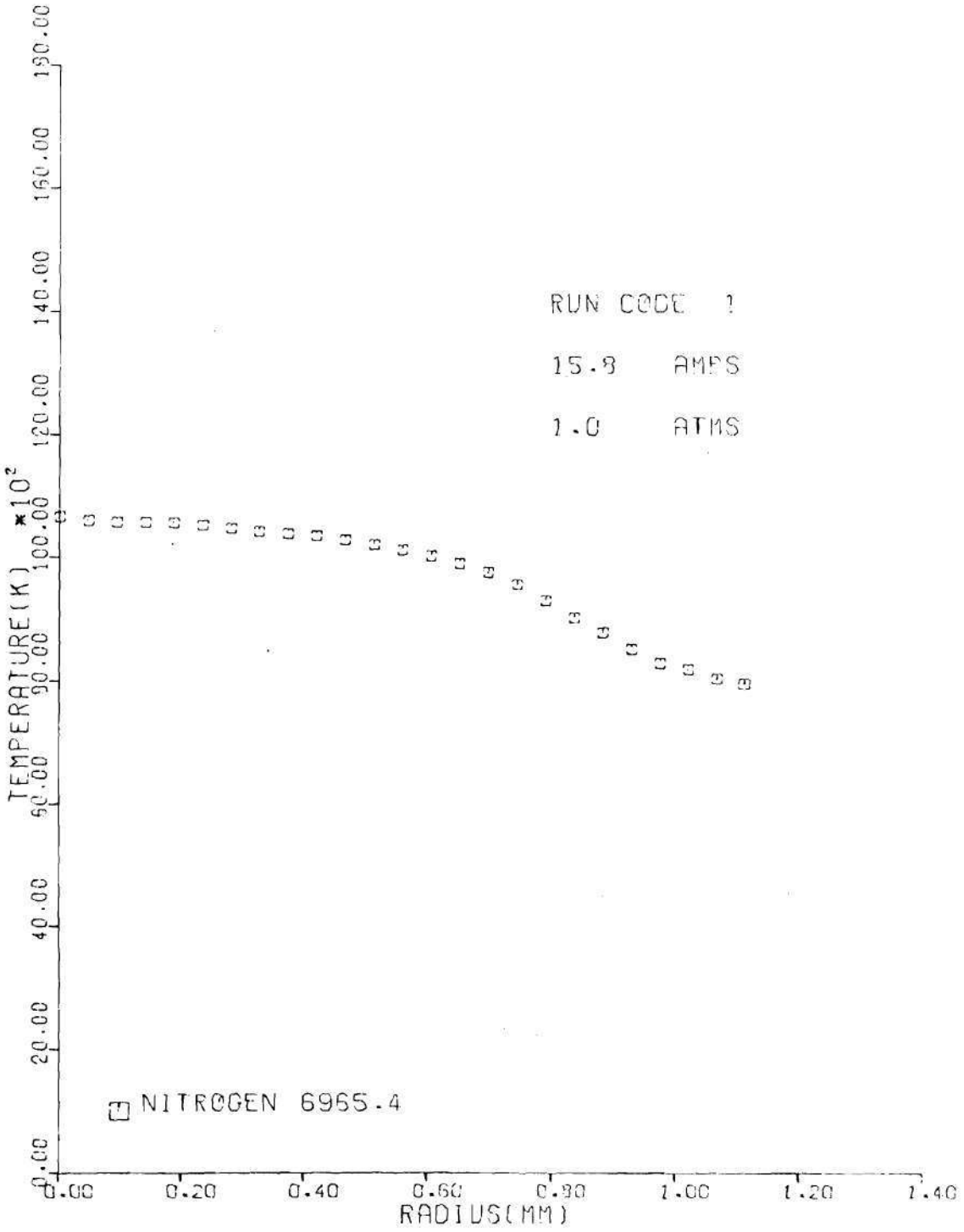
RUN CODE 1
15.8 AMPS
1.0 ATMS
TEMPERATURE(K) *10²
RADIUS(MM)
NITROGEN 6965.4
0.00
20.00
40.00
60.00
80.00
100.00
120.00
140.00
160.00
180.00
0.00
0.20
0.40
0.60
0.80
1.00
1.20
1.40

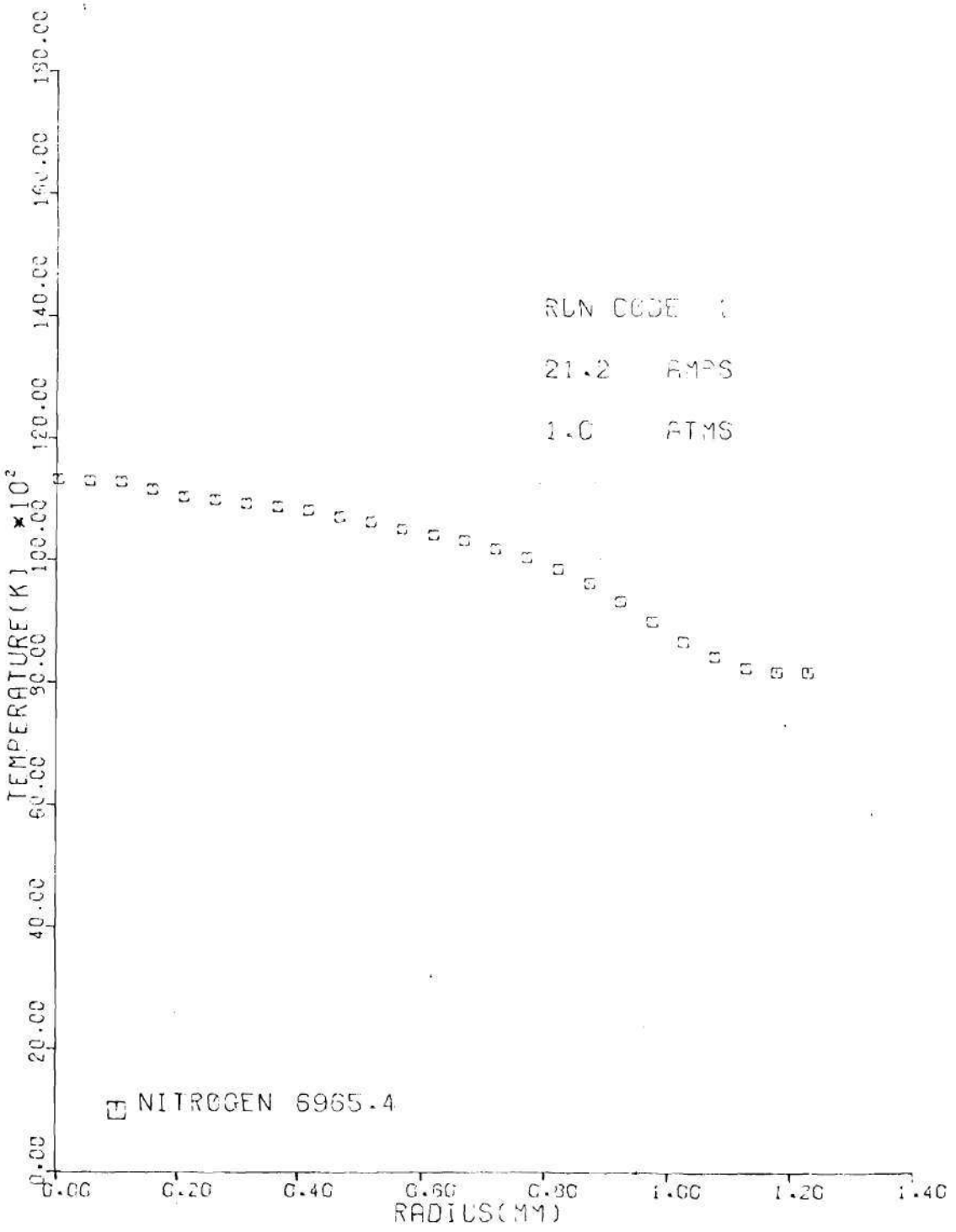
RUN CODE 1
21.2 AMPS
1.0 ATMS
TEMPERATURE(K) *10²
RADIUS(MM)
NITROGEN 6965.4

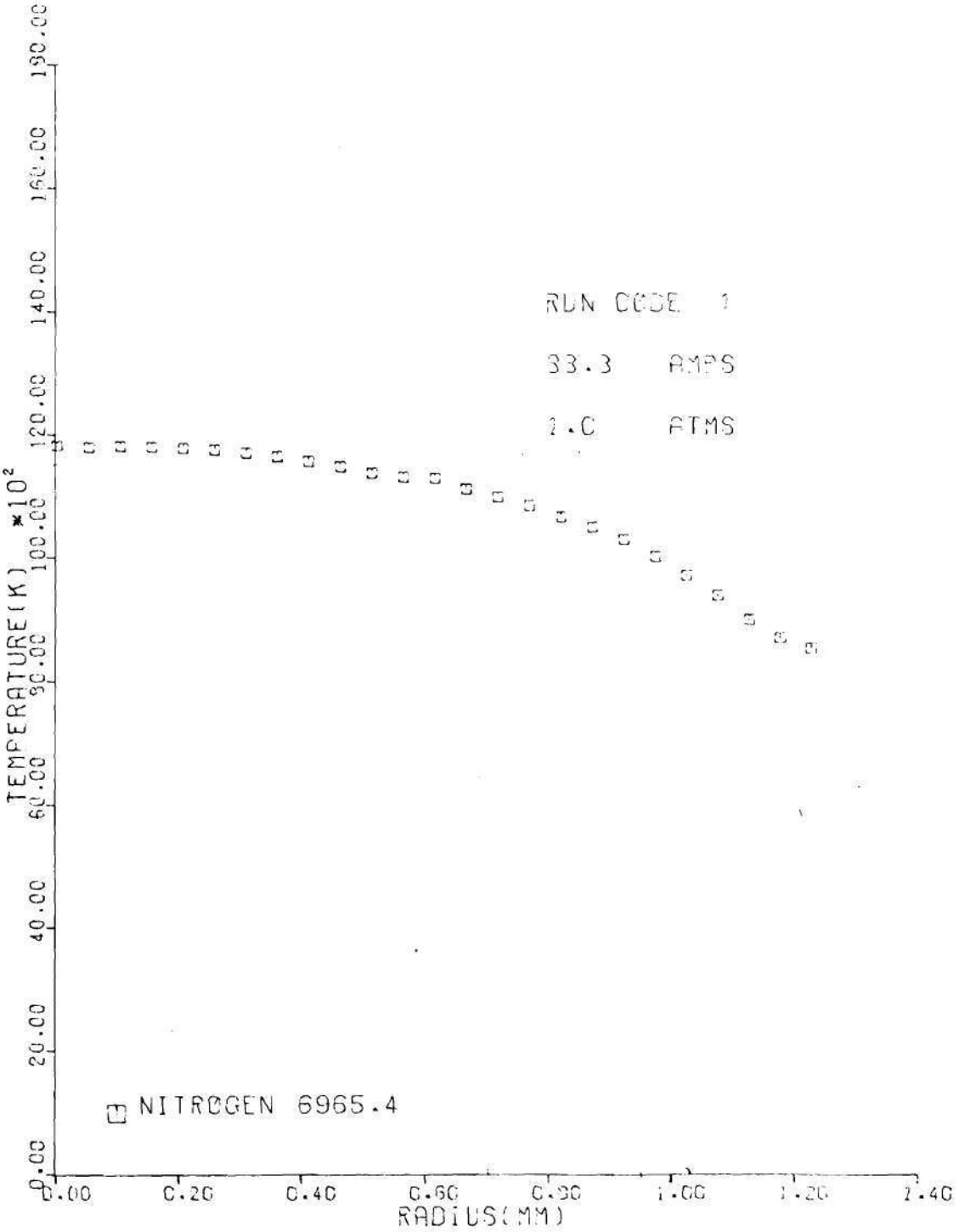
RUN CODE 1
33.3 AMPS
1.0 ATMS
TEMPERATURE(K) *10²
0.00
20.00
40.00
60.00
80.00
100.00
120.00
140.00
160.00
180.00
NITROGEN 6965.4
0.00
0.20
0.40
0.60
0.80
1.00
1.20
1.40
RADIUS(MM)

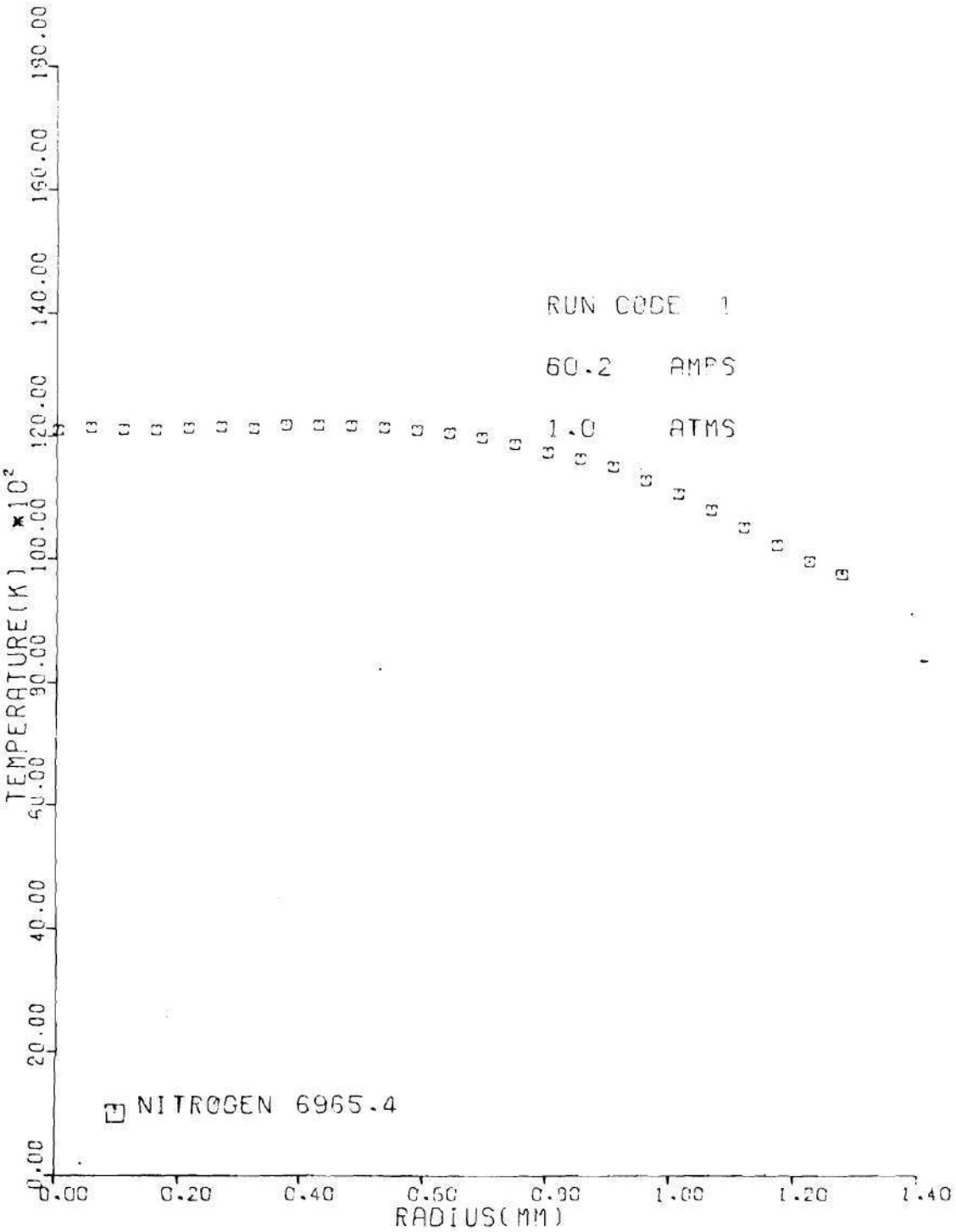
RUN CODE 1
60.2 AMPS
1.0 ATMS
NITROGEN 6965.4
TEMPERATURE(K) x10²
RADIUS(MM)
0.00
20.00
40.00
60.00
80.00
100.00
120.00
140.00
160.00
180.00
0.00
0.20
0.40
0.60
0.80
1.00
1.20
1.40

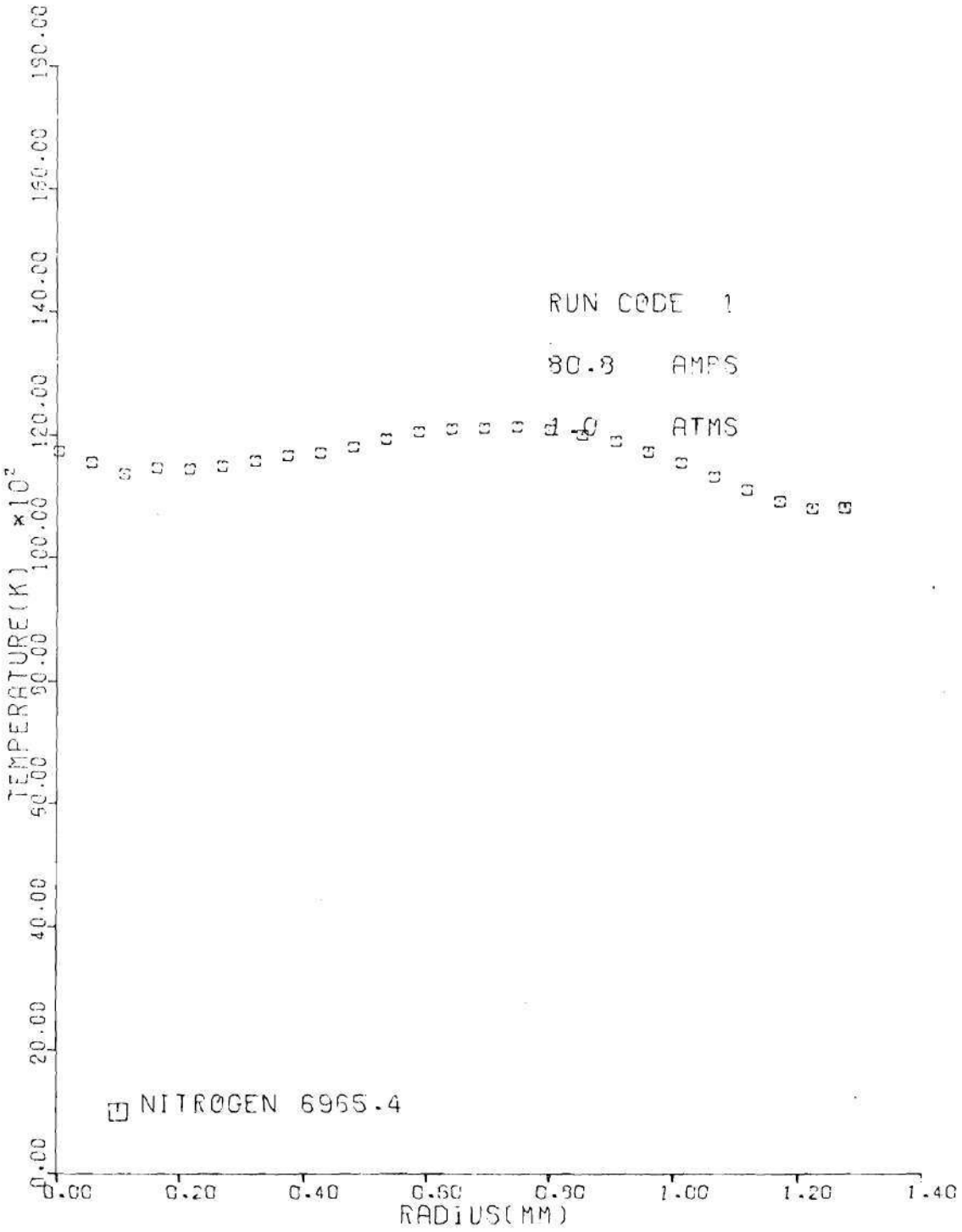
RUN CODE 1
80.8 AMPS
1.0 ATMS
NITROGEN 6965.4
TEMPERATURE(K) ×10²
0.00
20.00
40.00
60.00
80.00
100.00
120.00
140.00
160.00
180.00
0.00
0.20
0.40
0.60
0.80
1.00
1.20
1.40
RADIUS(MM)

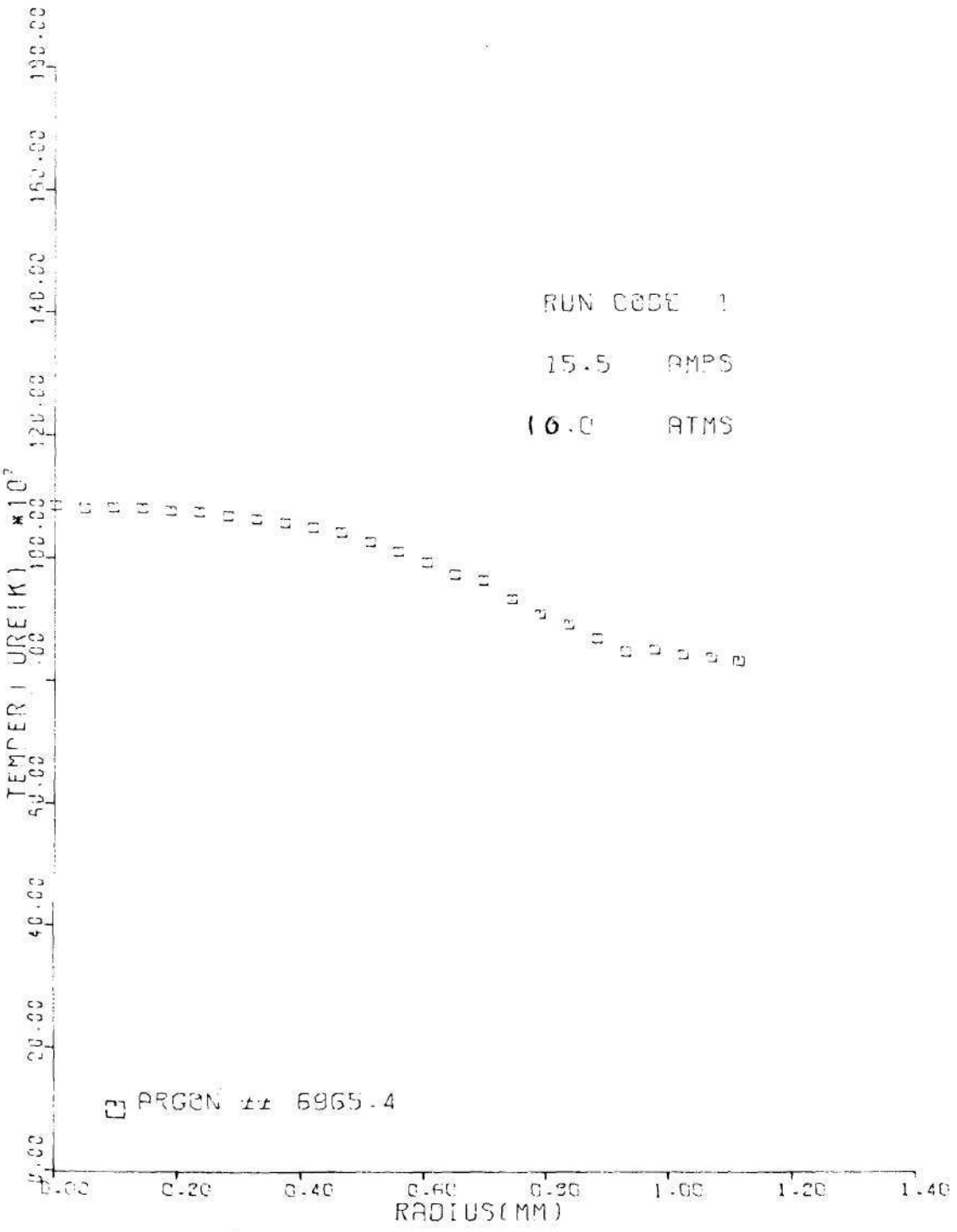
RUN CODE 1
15.5 AMPS
16.0 ATMS
TEMPERATURE(K) *10²
RADIUS(MM)
ARGON ** 6965.4

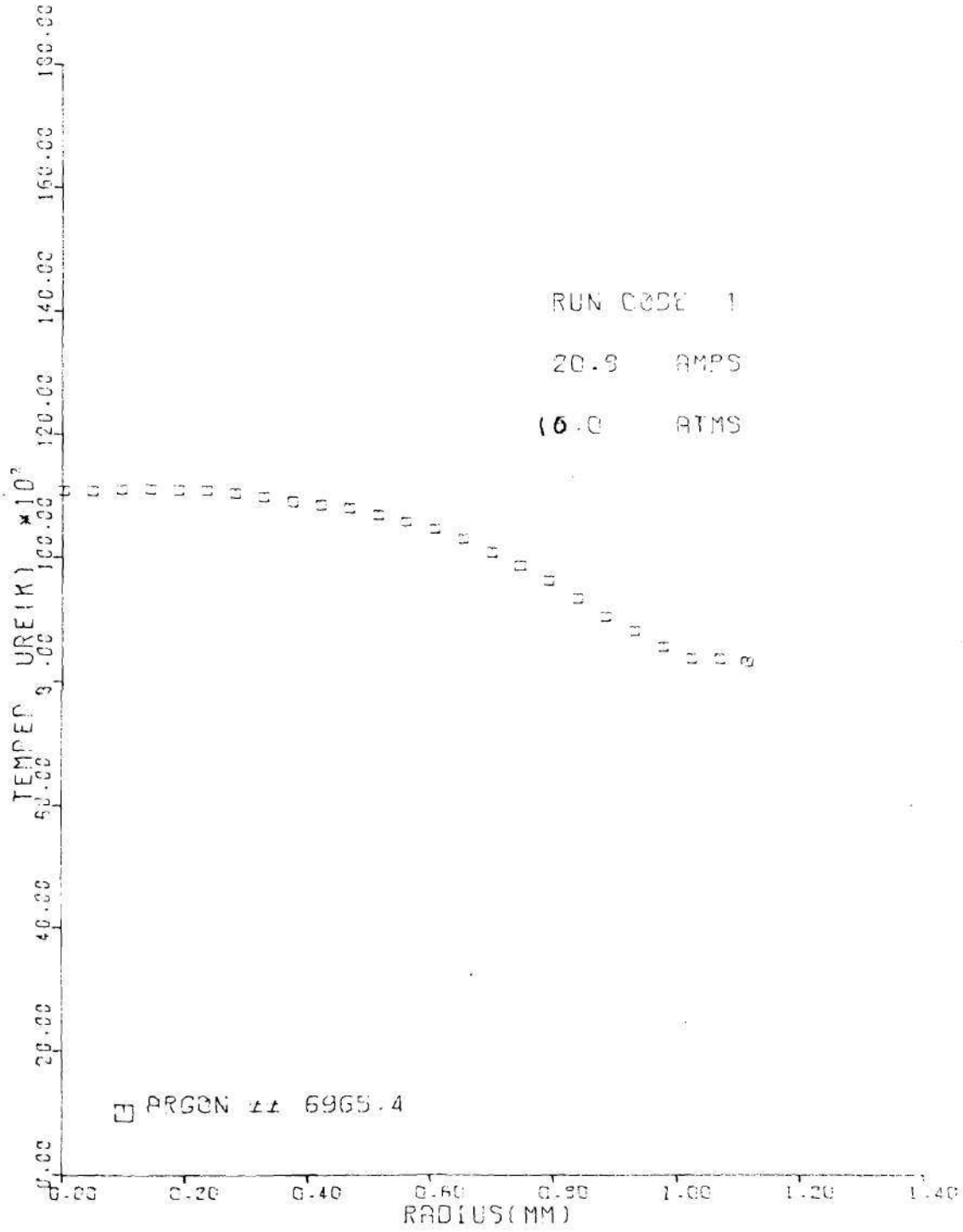
RUN CODE 1
20.9 AMPS
16.0 ATMS
TEMPER URE(K) ×10²
RADIUS(MM)
ARGON AT 6965.4

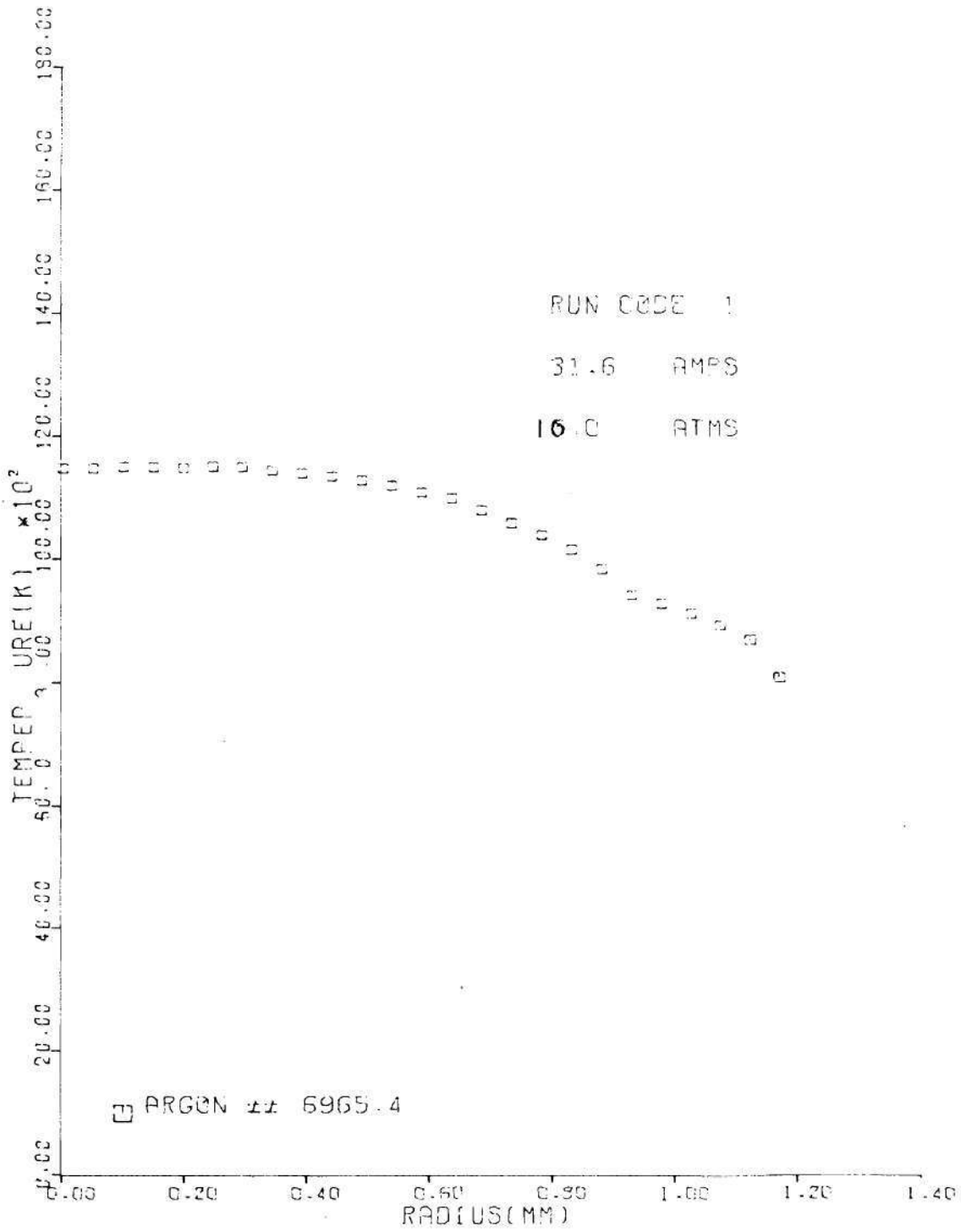
RUN CODE 1
31.6 AMPS
16.0 ATMS
ARGON ** 6965.4
TEMPER URE(K) *10²
RADIUS(MM)
0.00
0.20
0.40
0.60
0.80
1.00
1.20
1.40
20.00
40.00
60.00
120.00
140.00
160.00

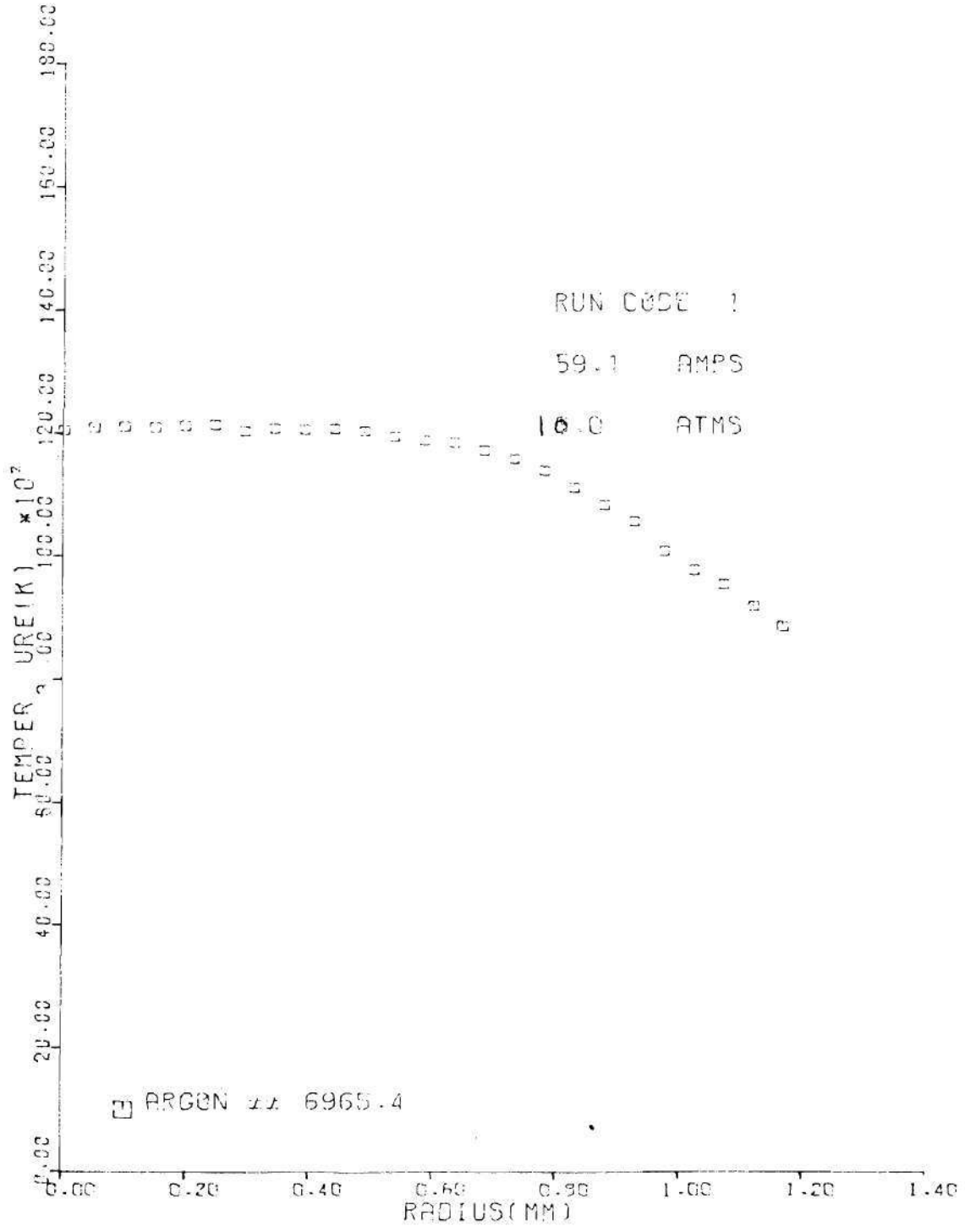
RUN CODE 1
59.1 AMPS
10.0 ATMS
TEMPER URE(K) *10²
ARGON ** 6965.4
RADIUS(MM)
0.00
0.20
0.40
0.60
0.80
1.00
1.20
1.40

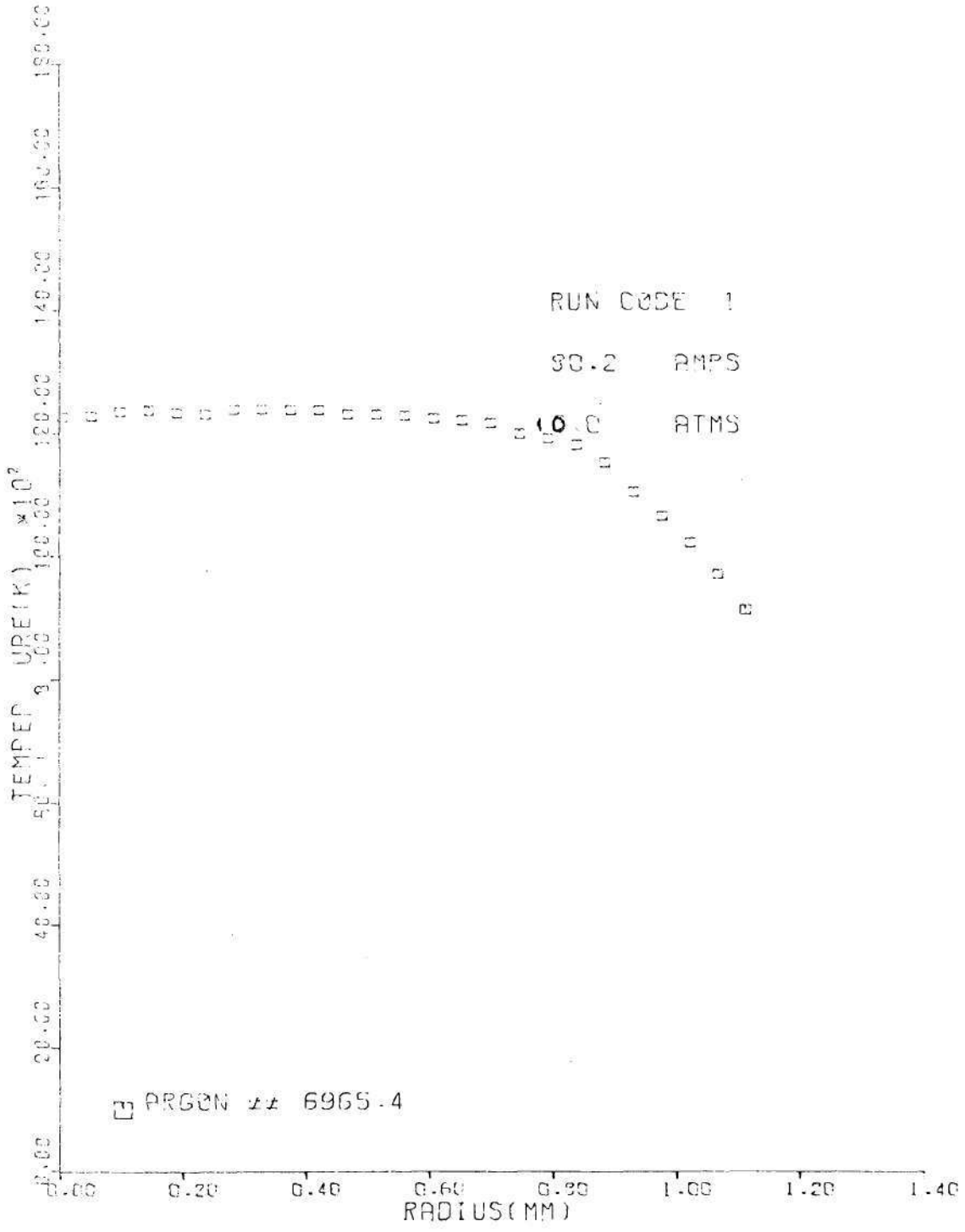
RUN CODE 1
90.2 AMPS
1.0 ATMS
PRGON ++ 6965.4
TEMPERATURE(K) ×10²
RADIUS(MM)
0.00
0.20
0.40
0.60
0.80
1.00
1.20
1.40

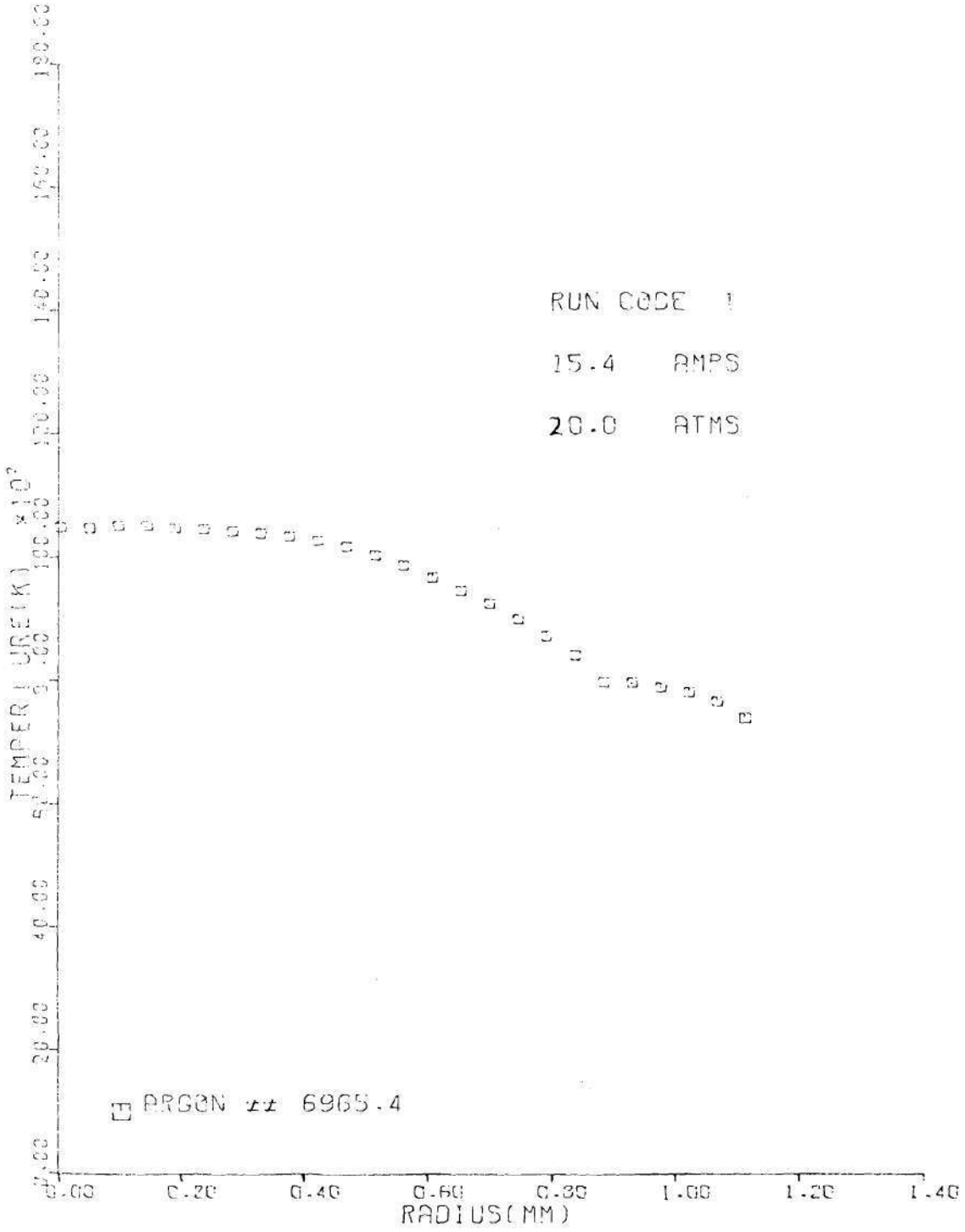
RUN CODE 1
15.4 AMPS
20.0 ATMS
TEMPERATURE(K) x10²
RADIUS(MM)
ARGON ** 6965.4

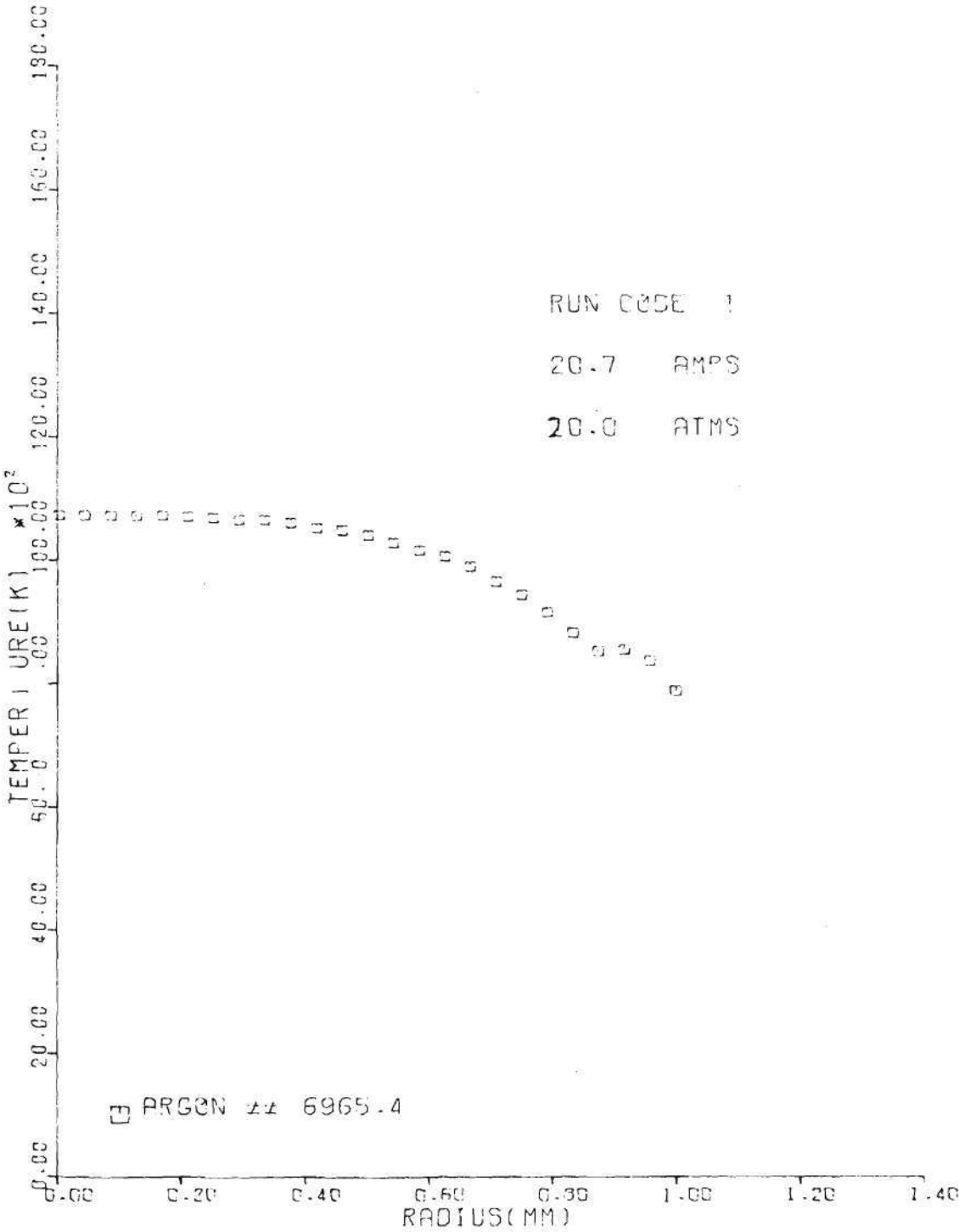
RUN CODE 1
20.7 AMPS
20.0 ATMS
TEMPERATURE(K) *10²
0.00
20.00
40.00
60.00
80.00
100.00
120.00
140.00
160.00
180.00
0.00
0.20
0.40
0.60
0.80
1.00
1.20
1.40
RADIUS(MM)
ARGON ** 6965.4

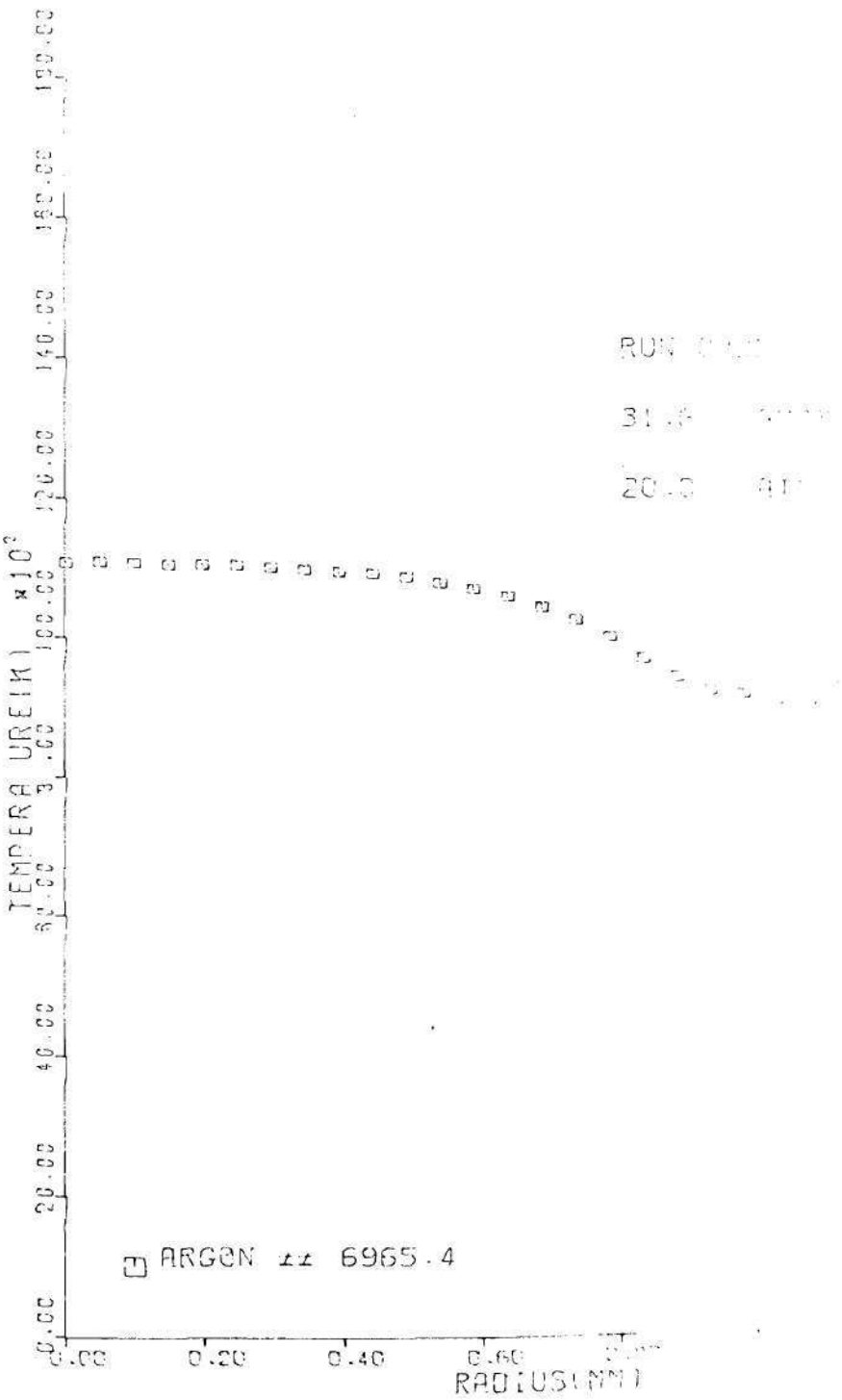
TEMPERATURE (K) x10³
RADIUS (MM)
ARGON AT 6965.4

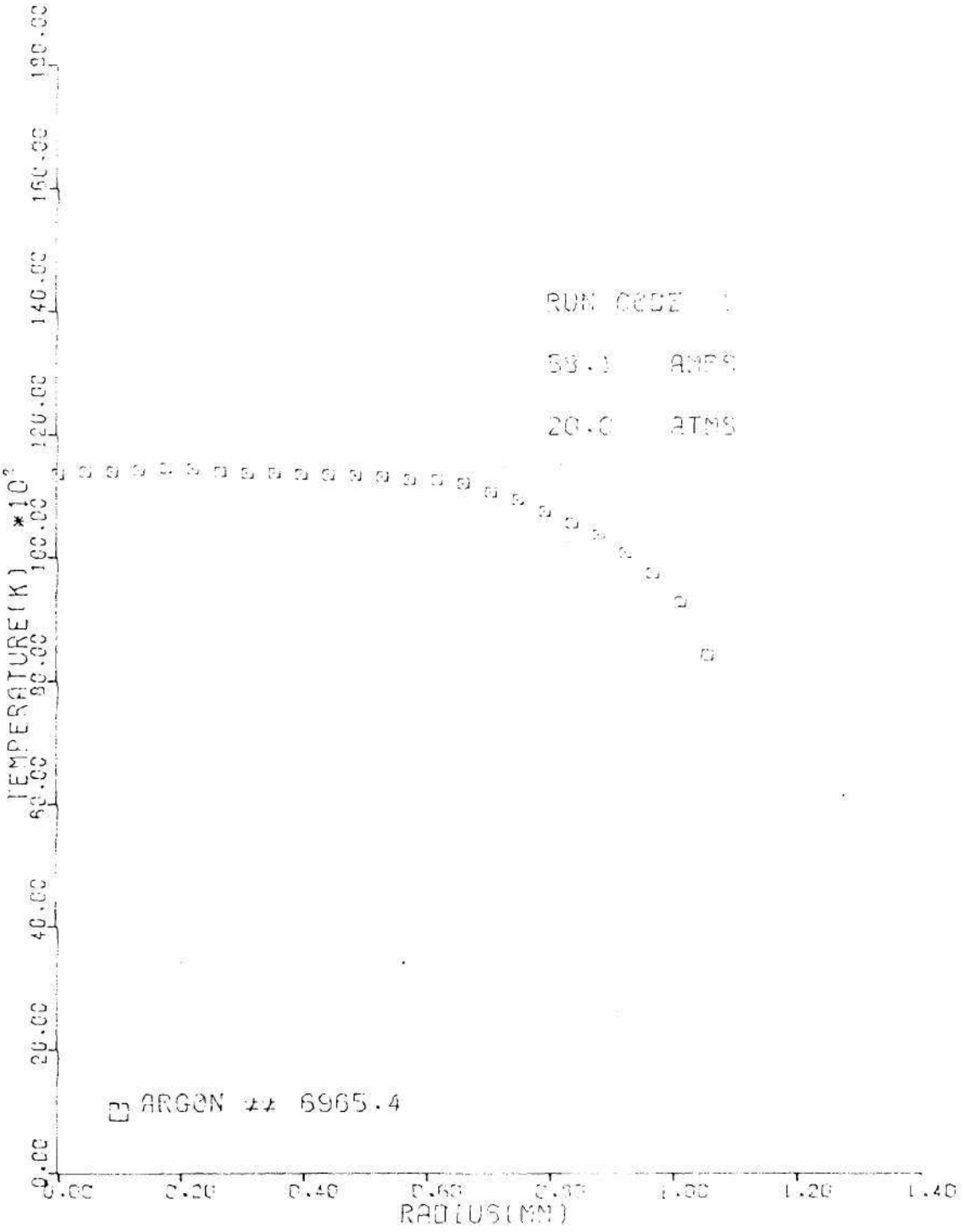
RUN CODE
50.1 AMPS
20.0 ATMS
TEMPERATURE(K) *10²
0.00
20.00
40.00
60.00
80.00
100.00
120.00
140.00
160.00
180.00
0.00
0.20
0.40
0.60
0.80
1.00
1.20
1.40
RADIUS(MM)
ARGON ** 6965.4

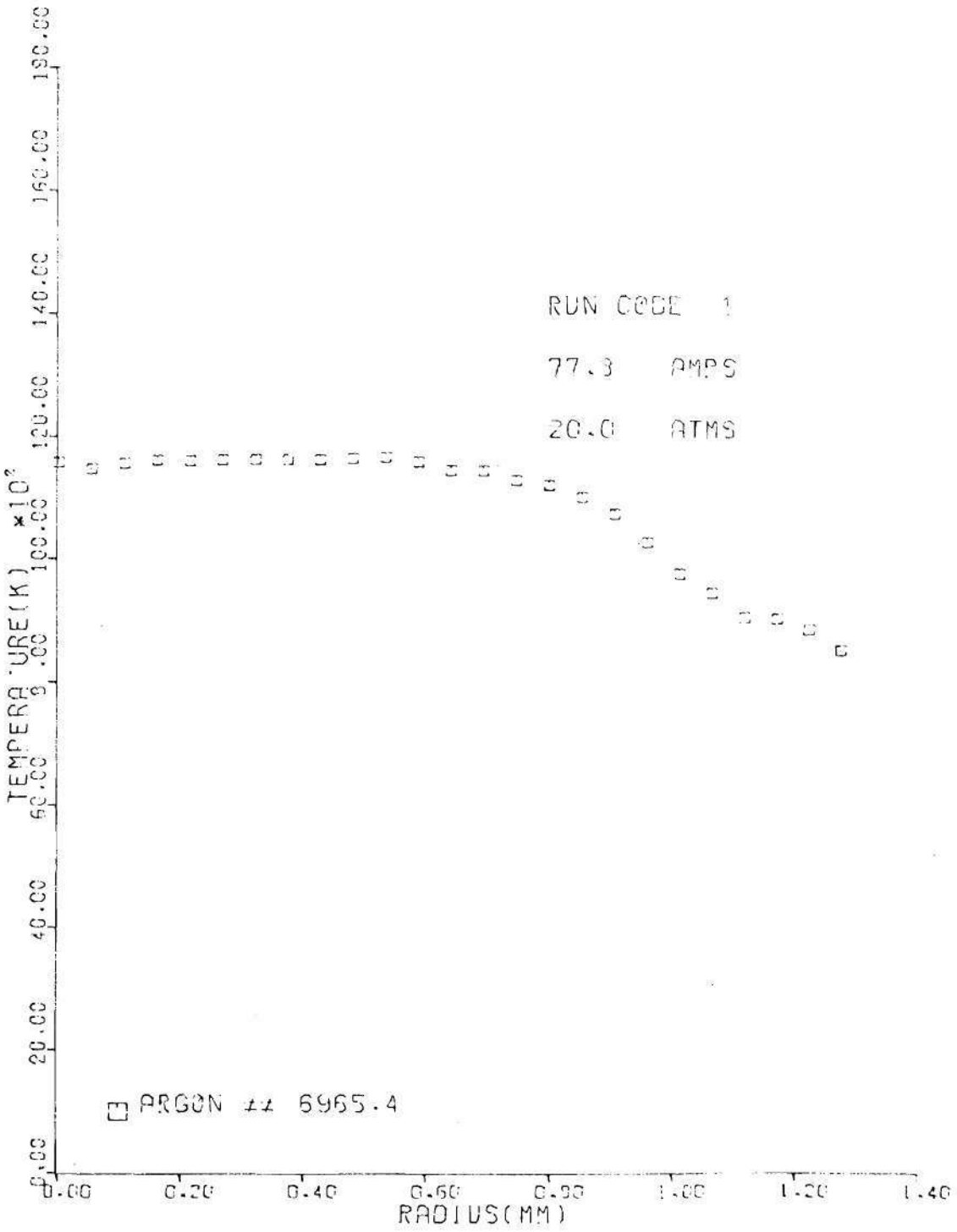
RUN CODE 1
77.3 AMPS
20.0 ATMS
TEMPERATURE(K) ×10²
RADIUS(MM)
ARGON 4A 6965.4
0.00
0.20
0.40
0.60
0.80
1.00
1.20
1.40
20.00
40.00
60.00
80.00
100.00
120.00
140.00
160.00
180.00

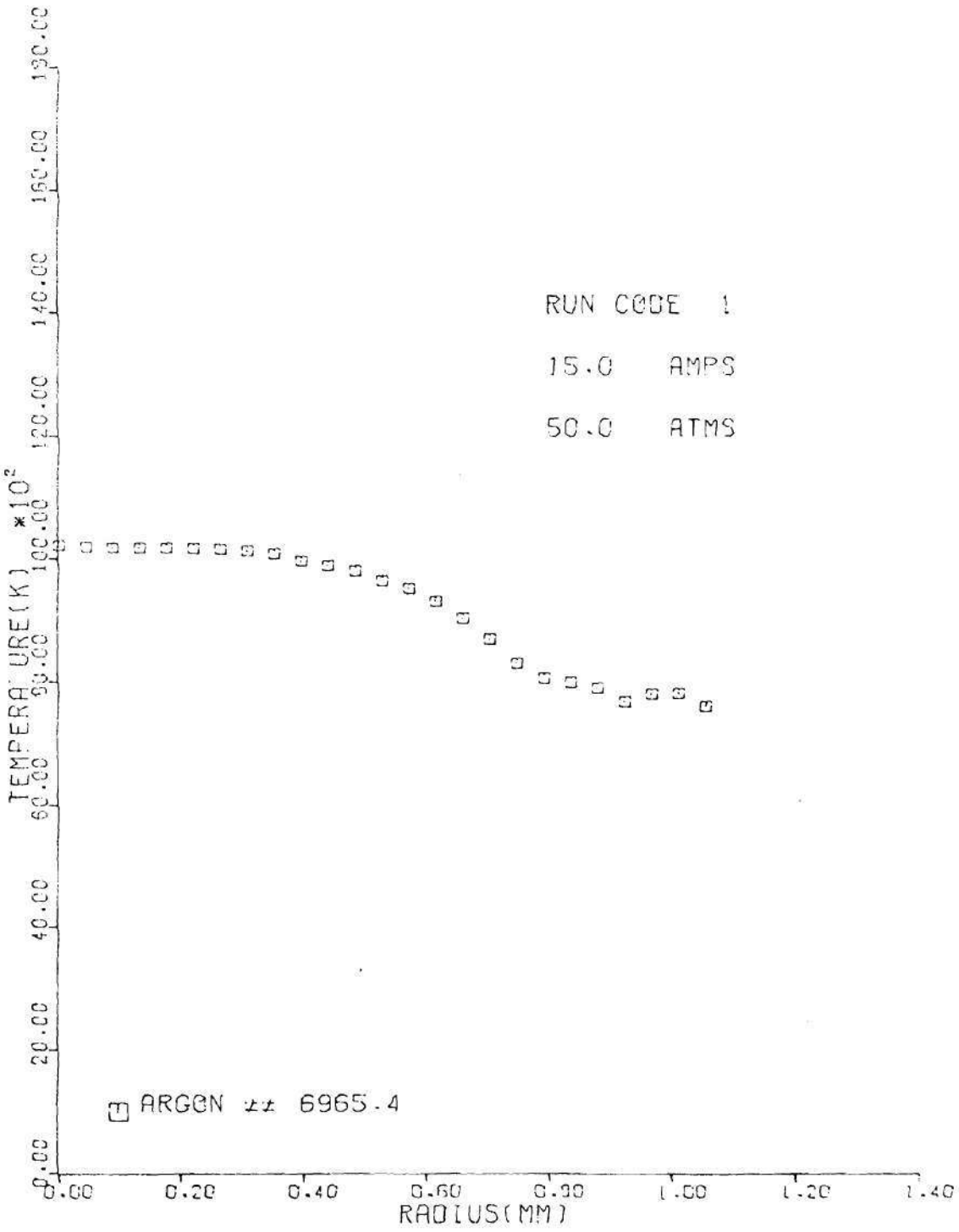
RUN CODE 1
15.0 AMPS
50.0 ATMS
TEMPERATURE(K) *10²
0.00
20.00
40.00
60.00
80.00
100.00
120.00
140.00
160.00
180.00
0.00
0.20
0.40
0.60
0.80
1.00
1.20
1.40
RADIUS(MM)
ARGON ** 6965.4

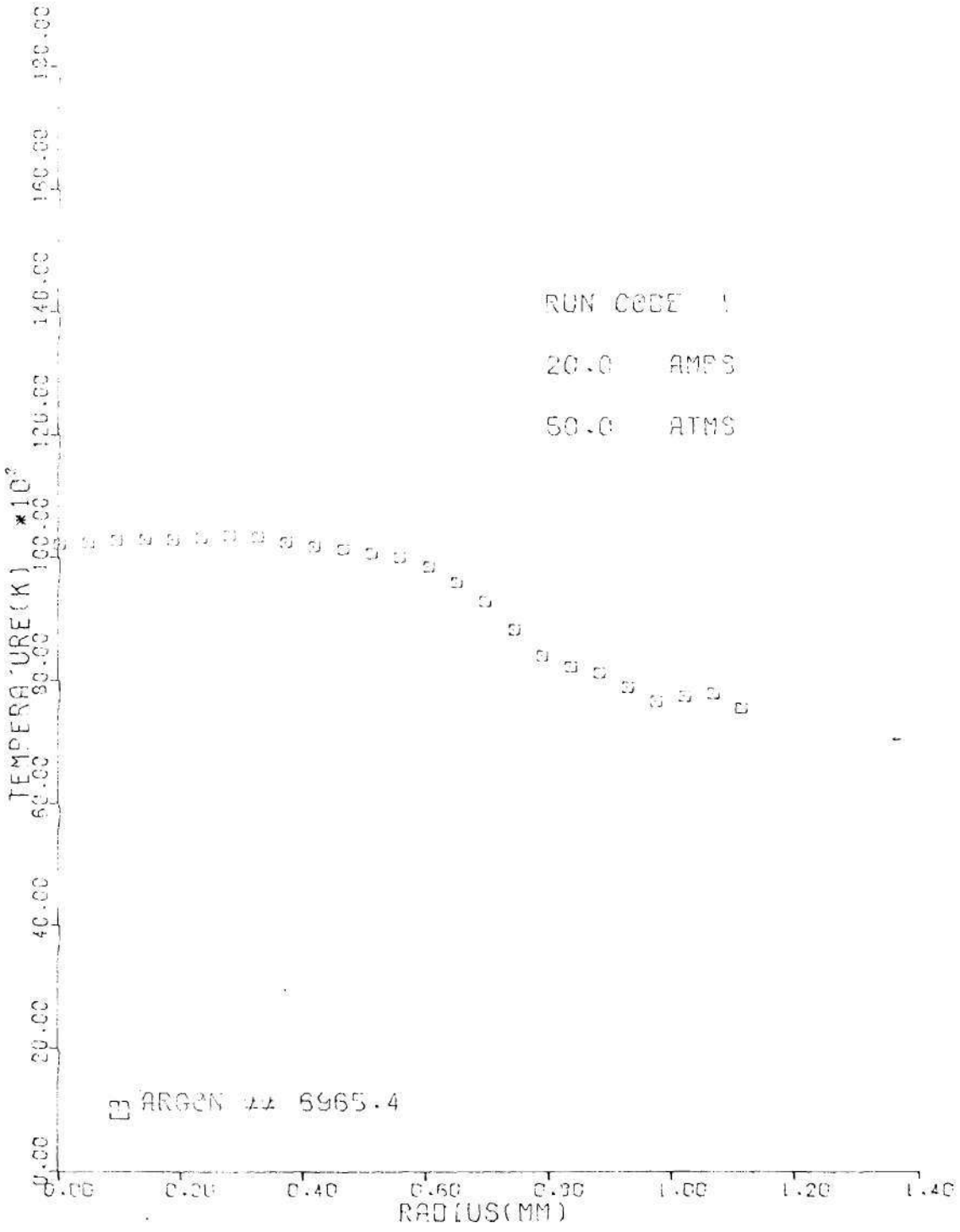
RUN CODE 1
20.0 AMPS
50.0 ATMS
TEMPERATURE(K) *10²
RADIUS(MM)
ARGON AA 6965.4
0.00
20.00
40.00
60.00
80.00
100.00
120.00
140.00
160.00
0.00
0.20
0.40
0.60
0.80
1.00
1.20
1.40

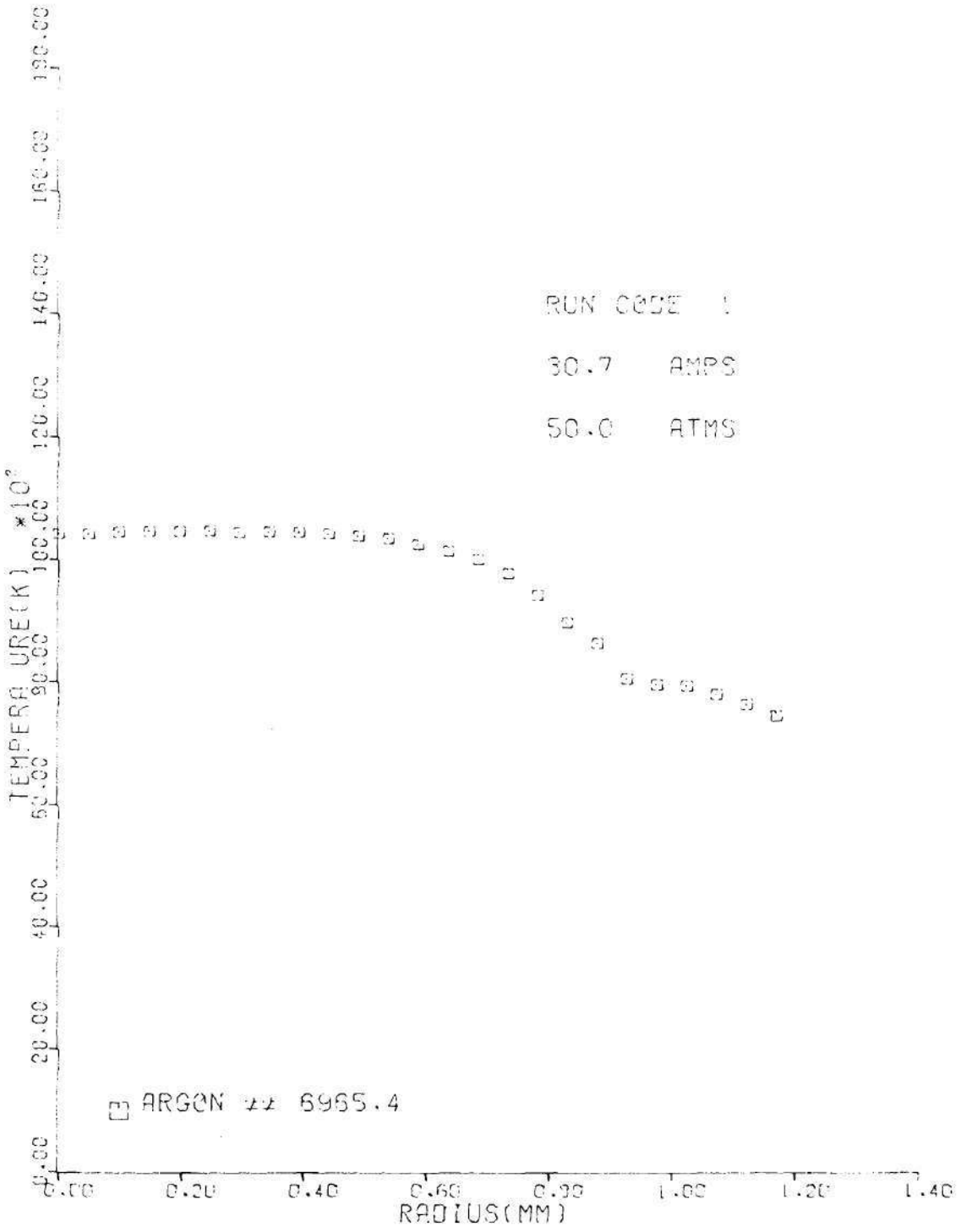
RUN CODE 1
30.7 AMPS
50.0 ATMS
TEMPERATURE(K) *10²
RADIUS(MM)
ARGON ** 6965.4

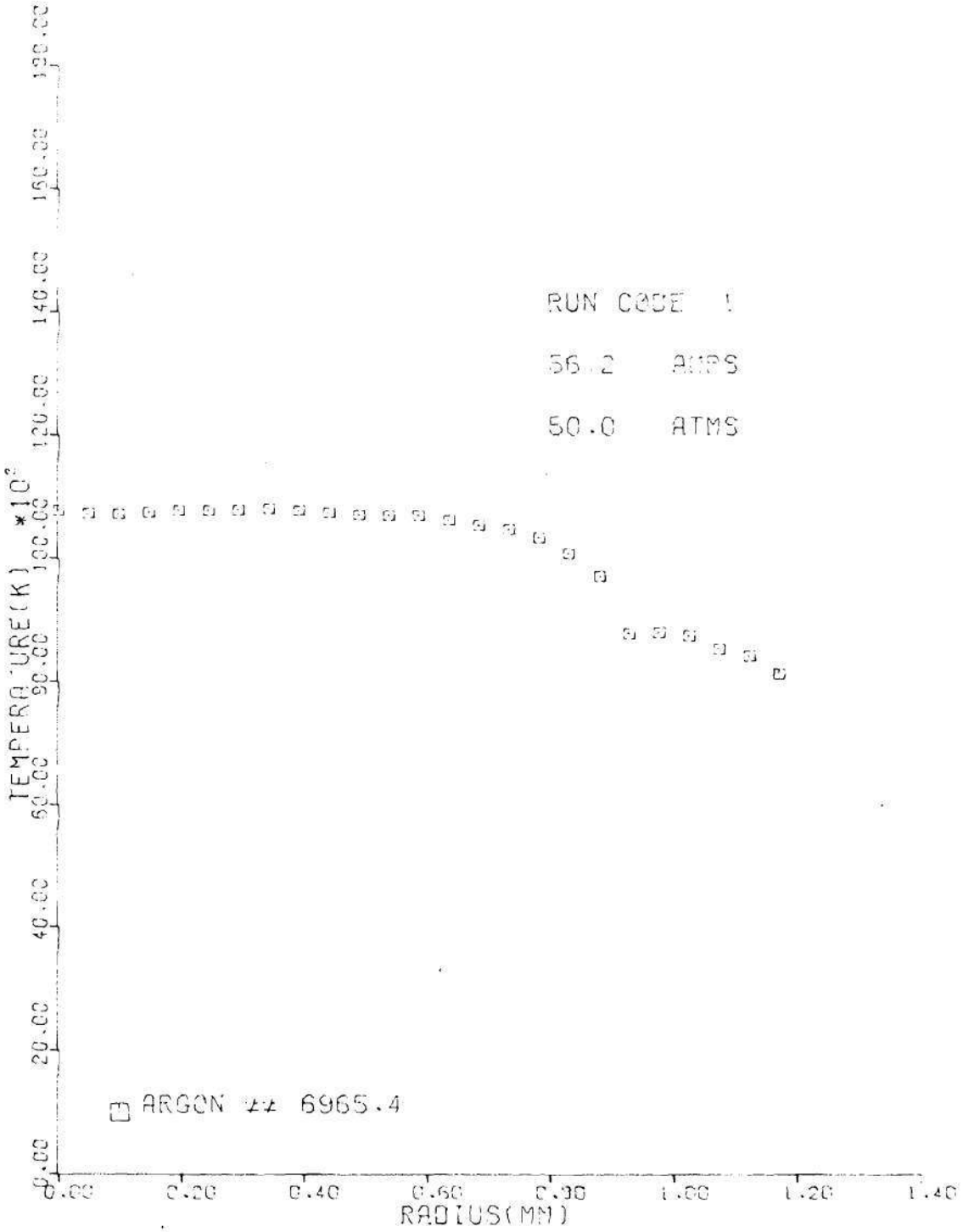
RUN CODE !
56.2 AMPS
50.0 ATMS
TEMPERATURE(K) *10²
0.00
20.00
40.00
60.00
80.00
100.00
120.00
140.00
160.00
180.00
0.00
0.20
0.40
0.60
0.80
1.00
1.20
1.40
RADIUS(MM)
ARGON AT 6965.4

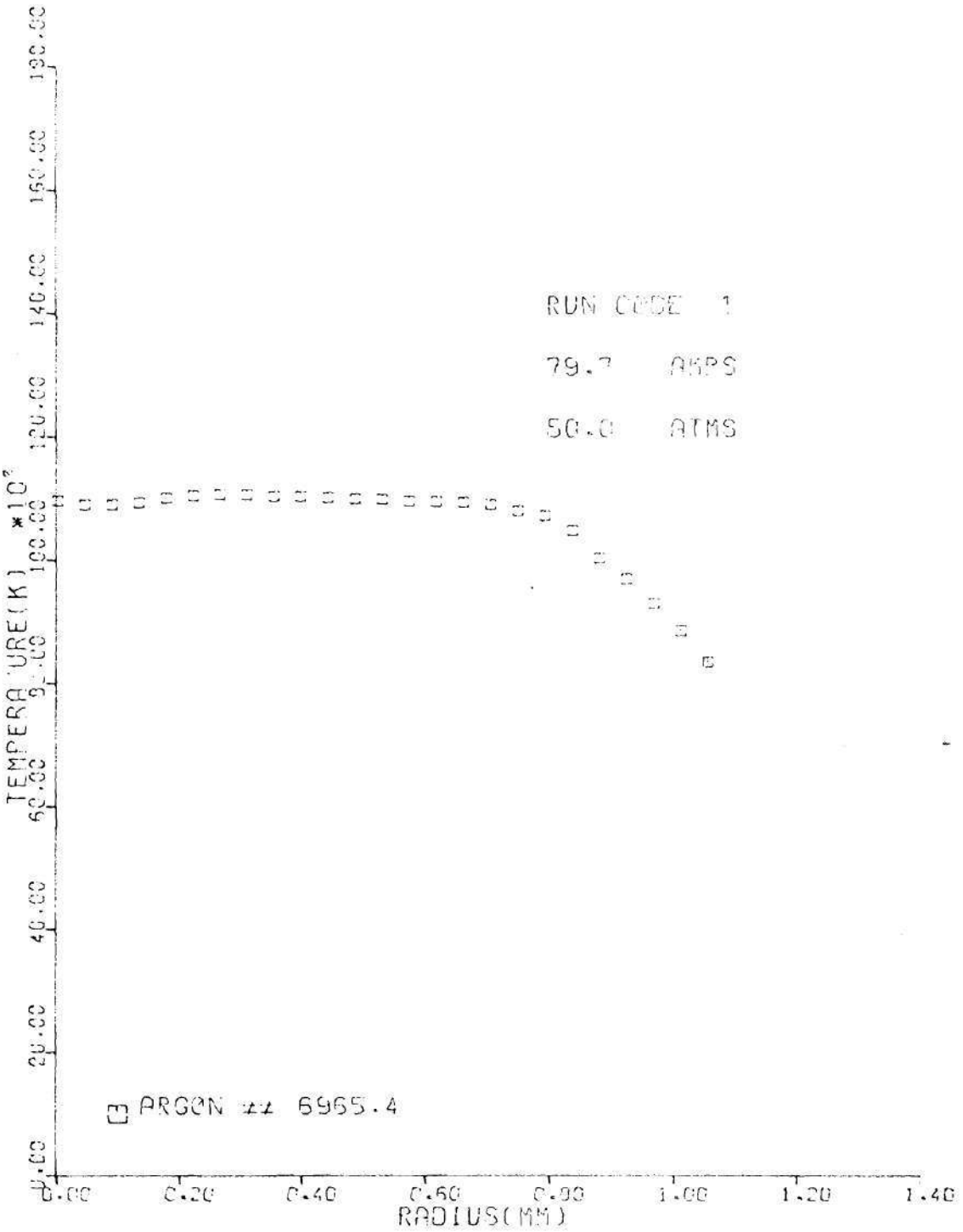
RUN CODE 1
79.7 AMPS
50.0 ATMS
TEMPERATURE(K) *10²
RADIUS(MM)
ARGON #4 6965.4

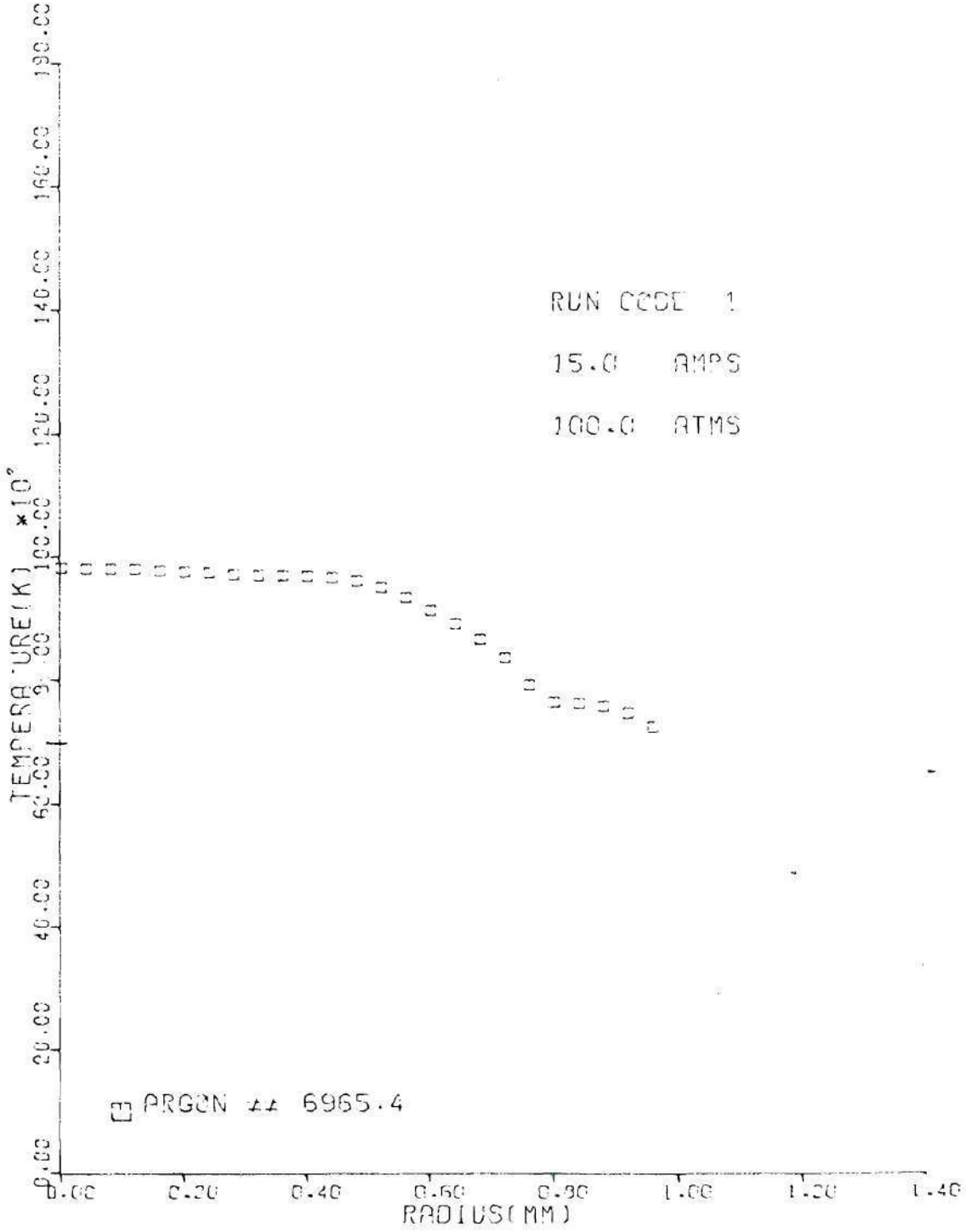
RUN CODE 1
15.0 AMPS
100.0 ATMS
TEMPERATURE(K) *10²
RADIUS(MM)
ARGON AA 6965.4
0.00
0.20
0.40
0.60
0.80
1.00
1.20
1.40
20.00
40.00
60.00
80.00
100.00
120.00
140.00
160.00
180.00

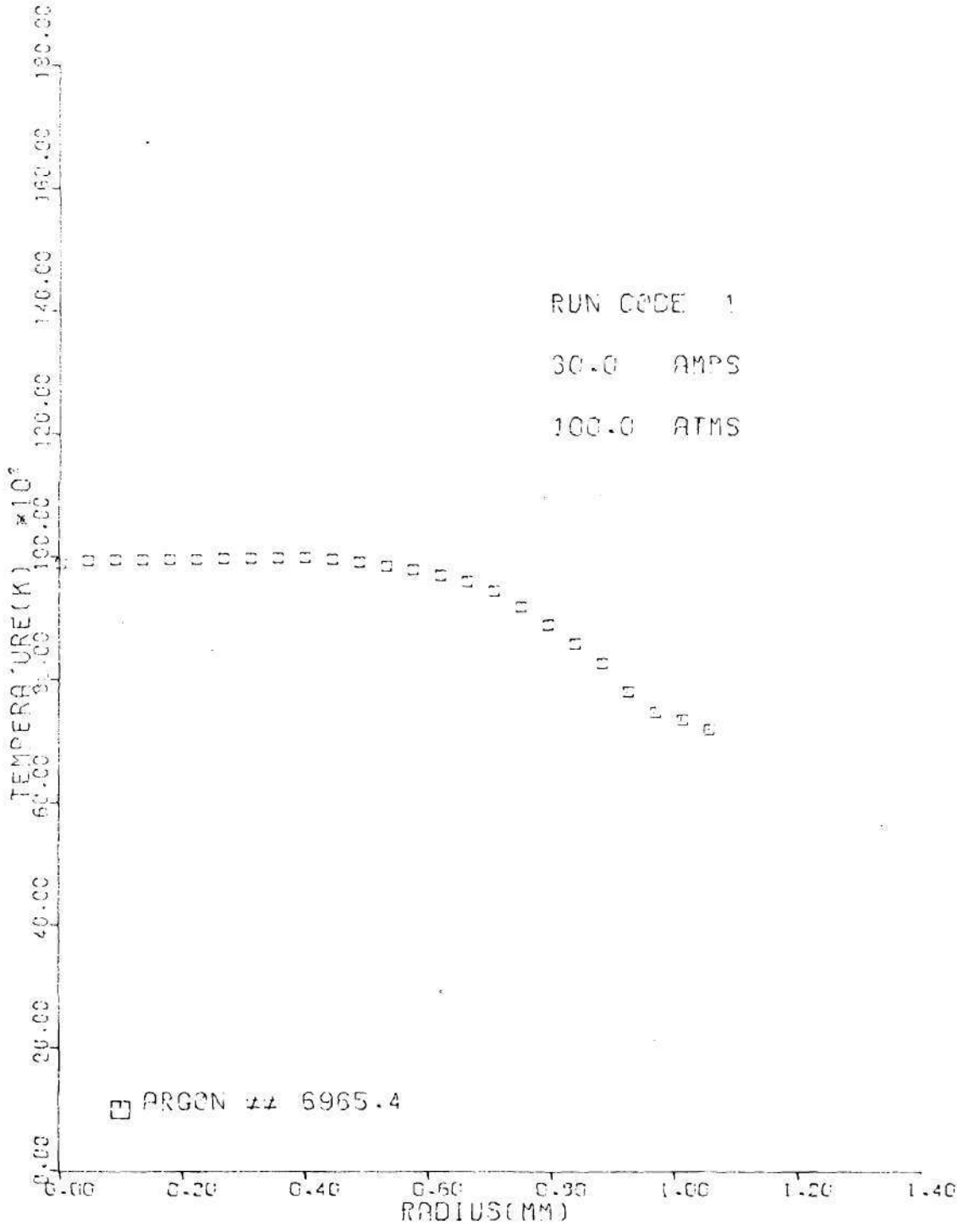
RUN CODE 1
30.0 AMPS
100.0 ATMS
TEMPERATURE(K) *10²
RADIUS(MM)
ARGON AT 6965.4

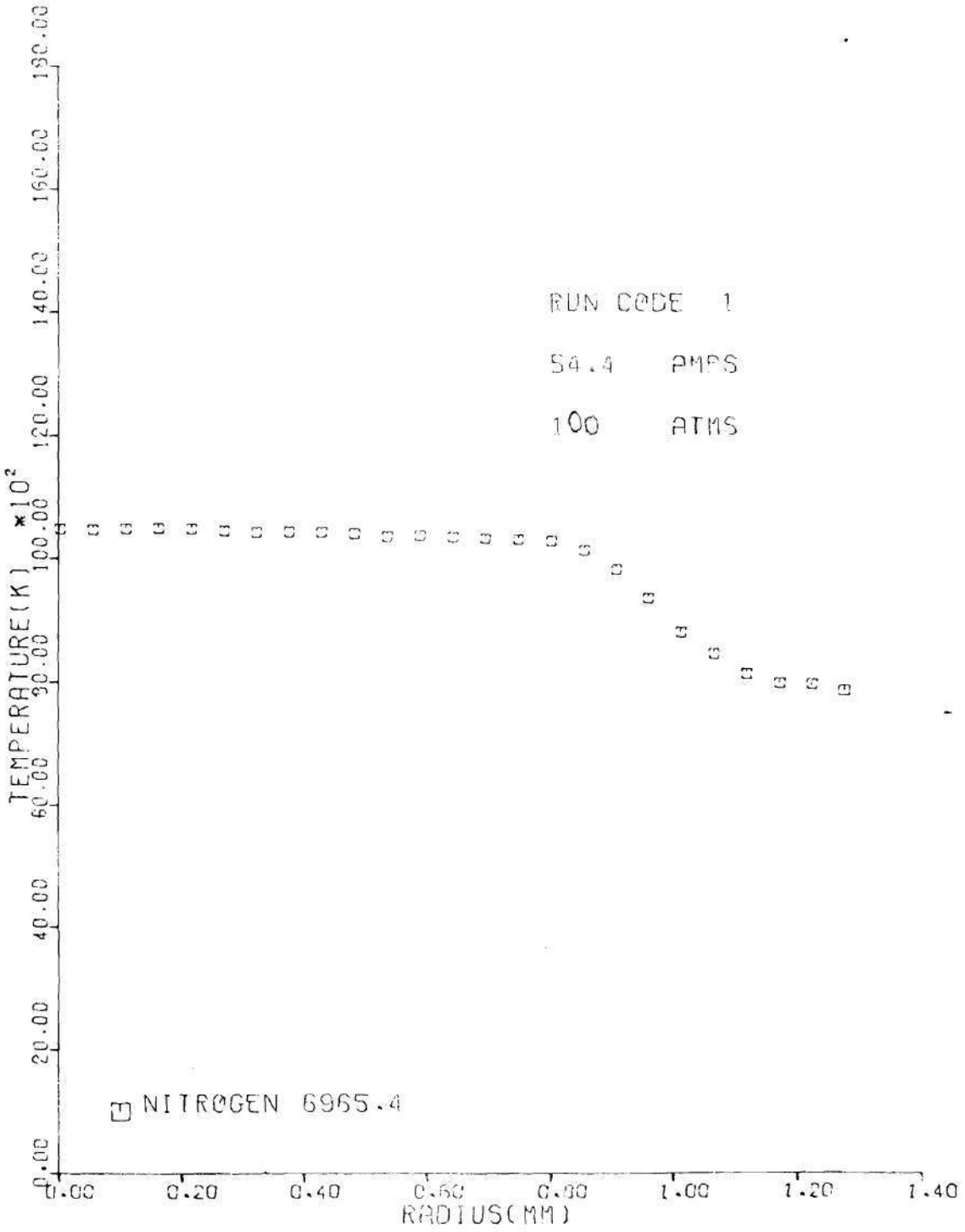
RUN CODE 1
54.4 AMPS
100 ATMS
TEMPERATURE(K) *10²
RADIUS(MM)
NITROGEN 6965.4
0.00
20.00
40.00
60.00
80.00
100.00
120.00
140.00
160.00
180.00
0.00
0.20
0.40
0.60
0.80
1.00
1.20
1.40

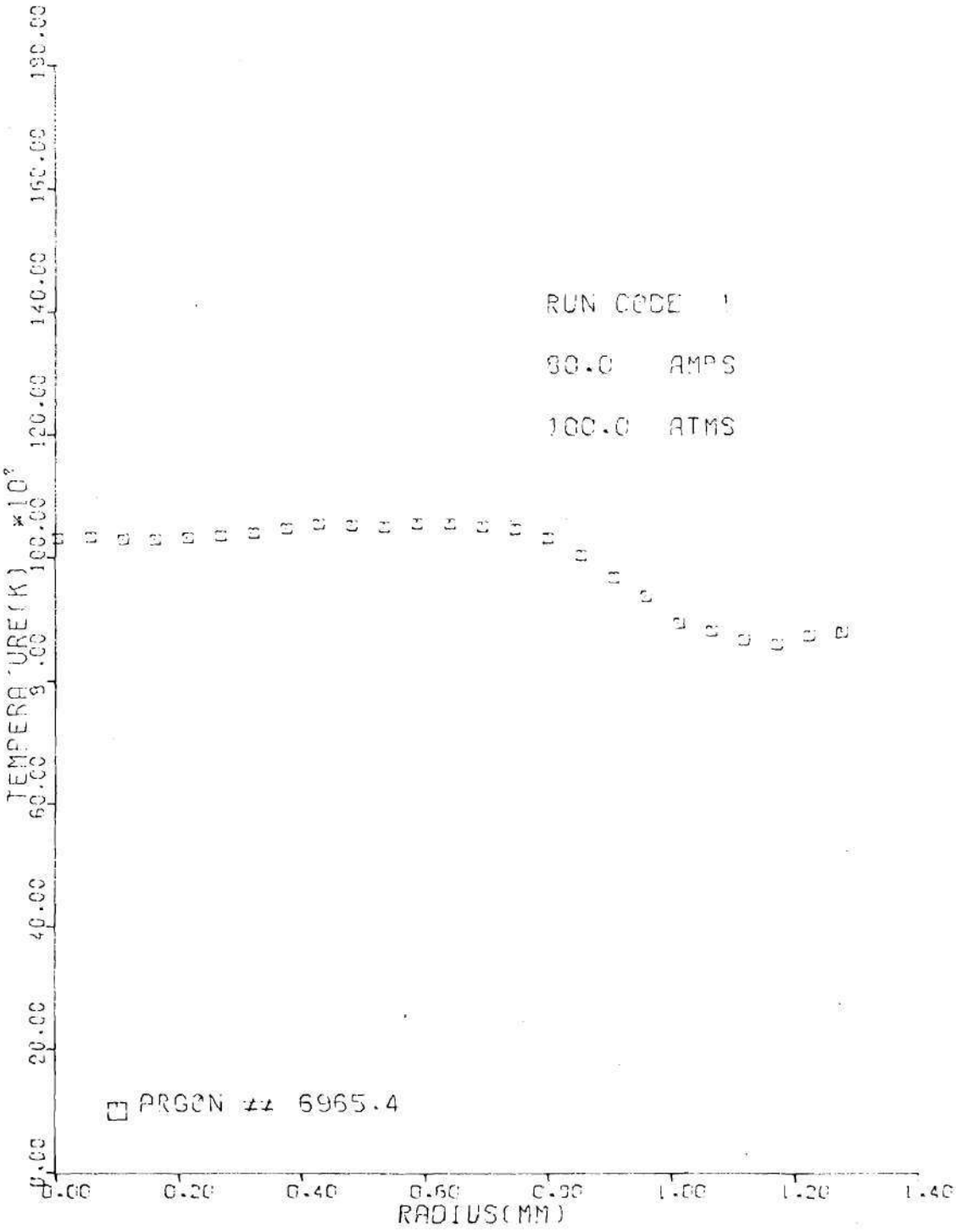
RUN CODE 1
80.0 AMPS
100.0 ATMS
TEMPERATURE(K) *10²
RADIUS(MM)
ARGON ## 6965.4

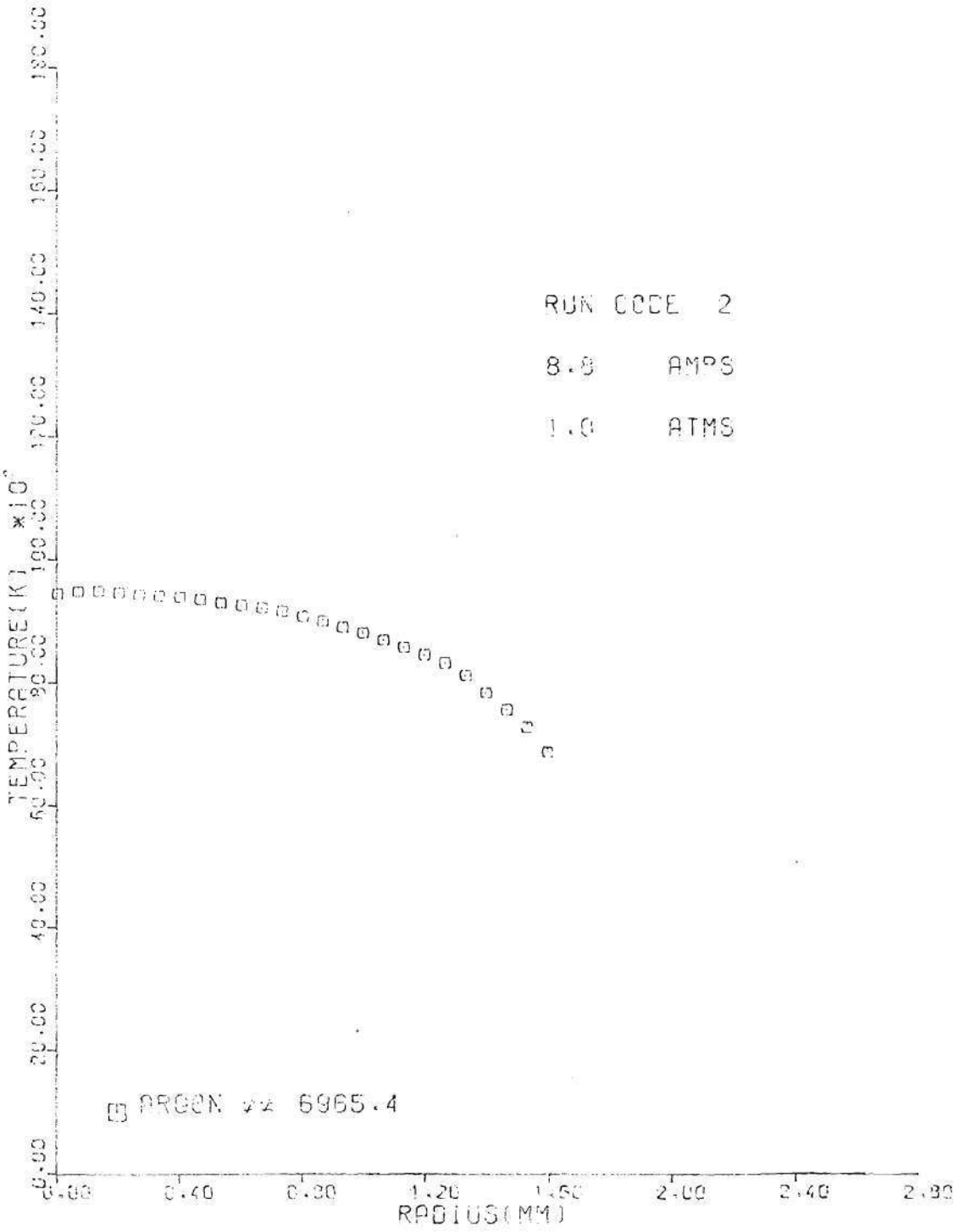
RUN CODE 2
8.0 AMPS
1.0 ATMS
TEMPERATURE(K) *10^
RADIUS(MM)
PROBN ## 6965.4

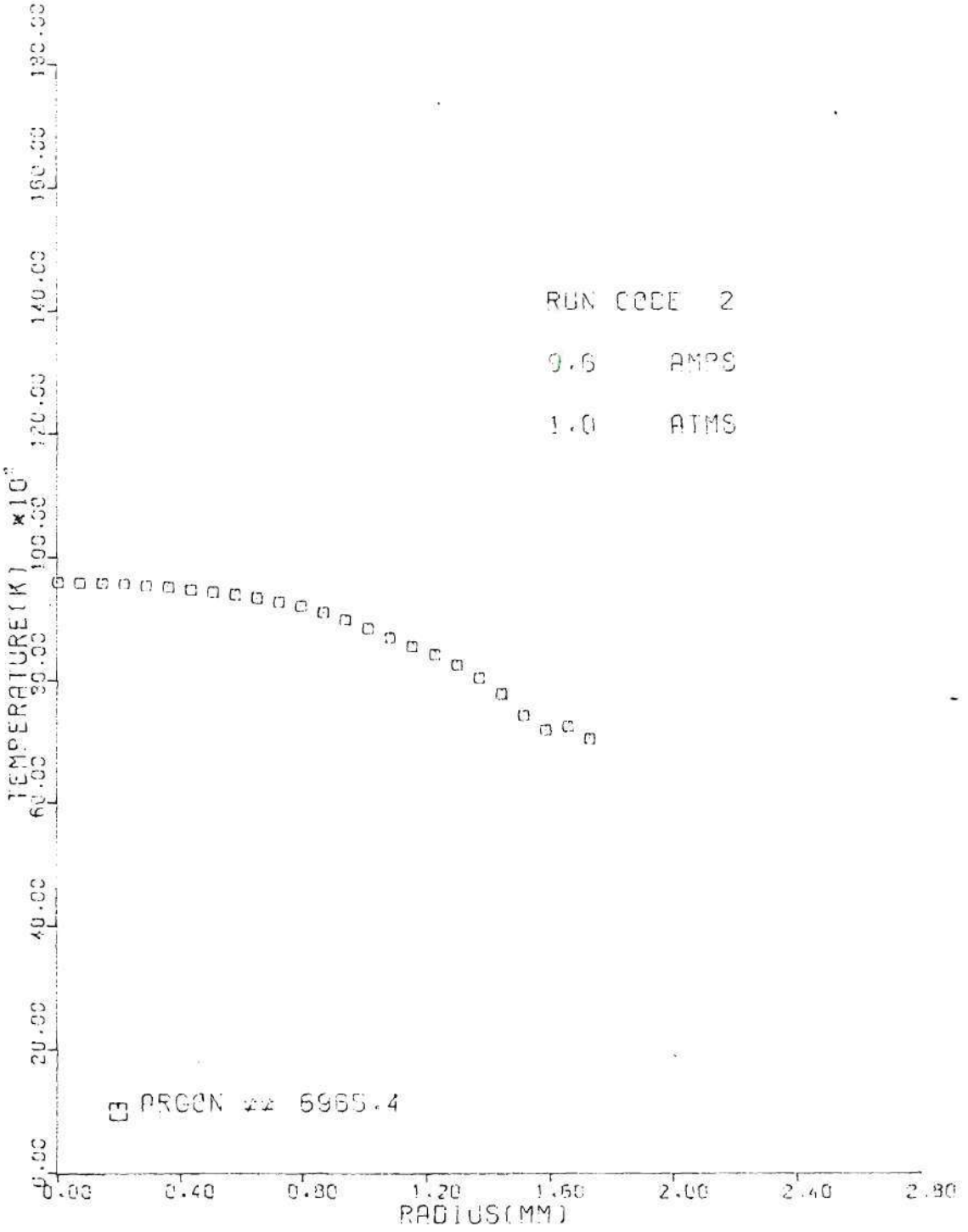
RUN CODE 2
0.6 AMPS
1.0 ATMS
TEMPERATURE(K) *10^
PROGN ** 6965.4
0.00
0.40
0.80
1.20
1.60
2.00
2.40
2.80
RADIUS(MM)

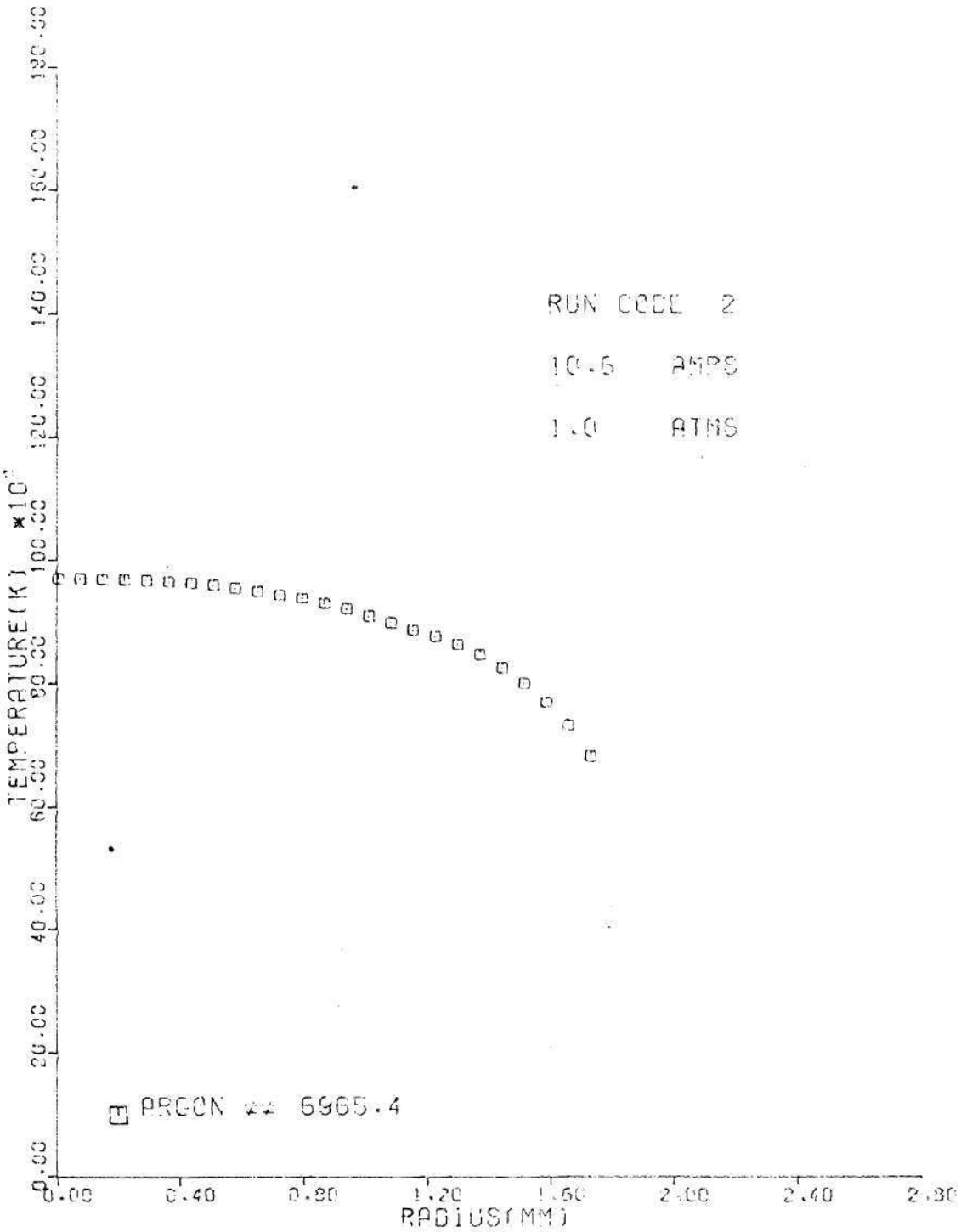
RUN CODE 2
10.6 AMPS
1.0 ATMS
TEMPERATURE(K) *10
0.00
20.00
40.00
60.00
80.00
100.00
120.00
140.00
160.00
180.00
0.00
0.40
0.80
1.20
1.60
2.00
2.40
2.80
RADIUS(MM)
ARGON ** 6965.4

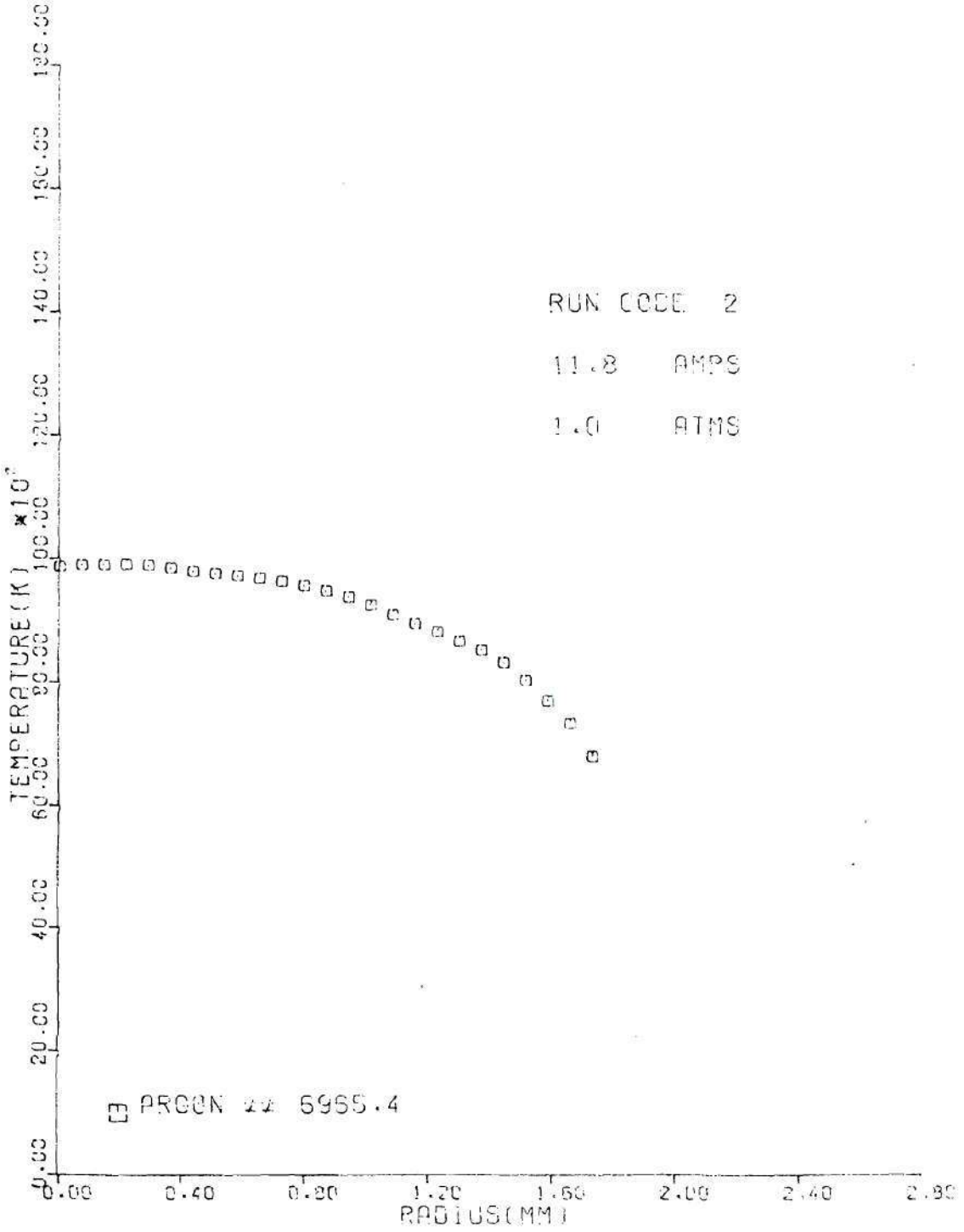
RUN CODE 2
11.8 AMPS
1.0 ATMS
TEMPERATURE(K) *10²
RADIUS(MM)
0.00
0.40
0.80
1.20
1.60
2.00
2.40
2.80
20.00
40.00
60.00
80.00
100.00
120.00
140.00
160.00
180.00
ARGON 2+ 5965.4

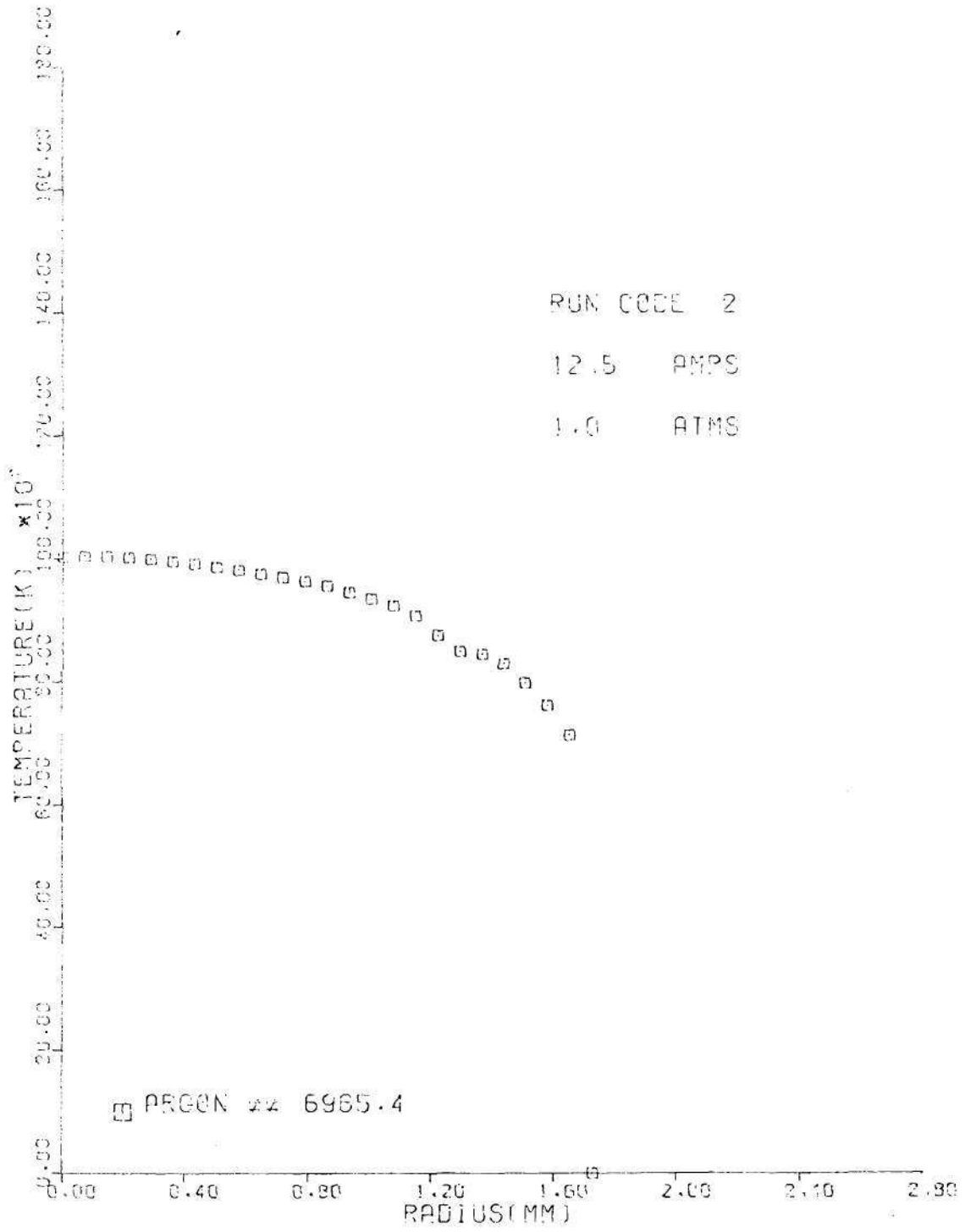
RUN CODE 2
12.5 AMPS
1.0 ATMS
TEMPERATURE(K) x10
RADIUS(MM)
0.00
0.40
0.80
1.20
1.60
2.00
2.40
2.80
PROBN ** 6985.4

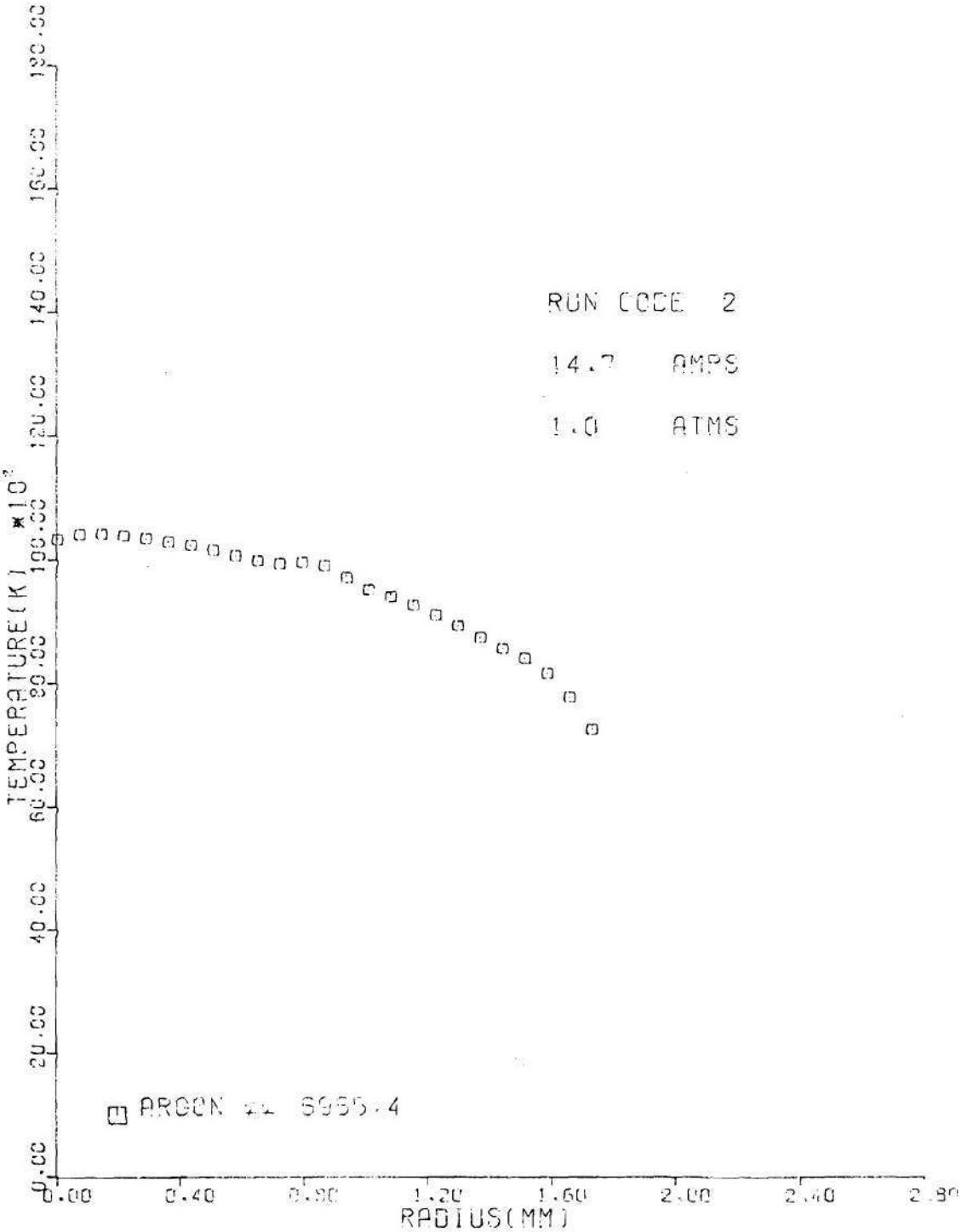
RUN CODE 2
14.7 AMPS
1.0 ATMS
TEMPERATURE(K) *10²
0.00
20.00
40.00
60.00
80.00
100.00
120.00
140.00
160.00
180.00
0.00
0.40
0.80
1.20
1.60
2.00
2.40
2.80
RADIUS(MM)
ARGON

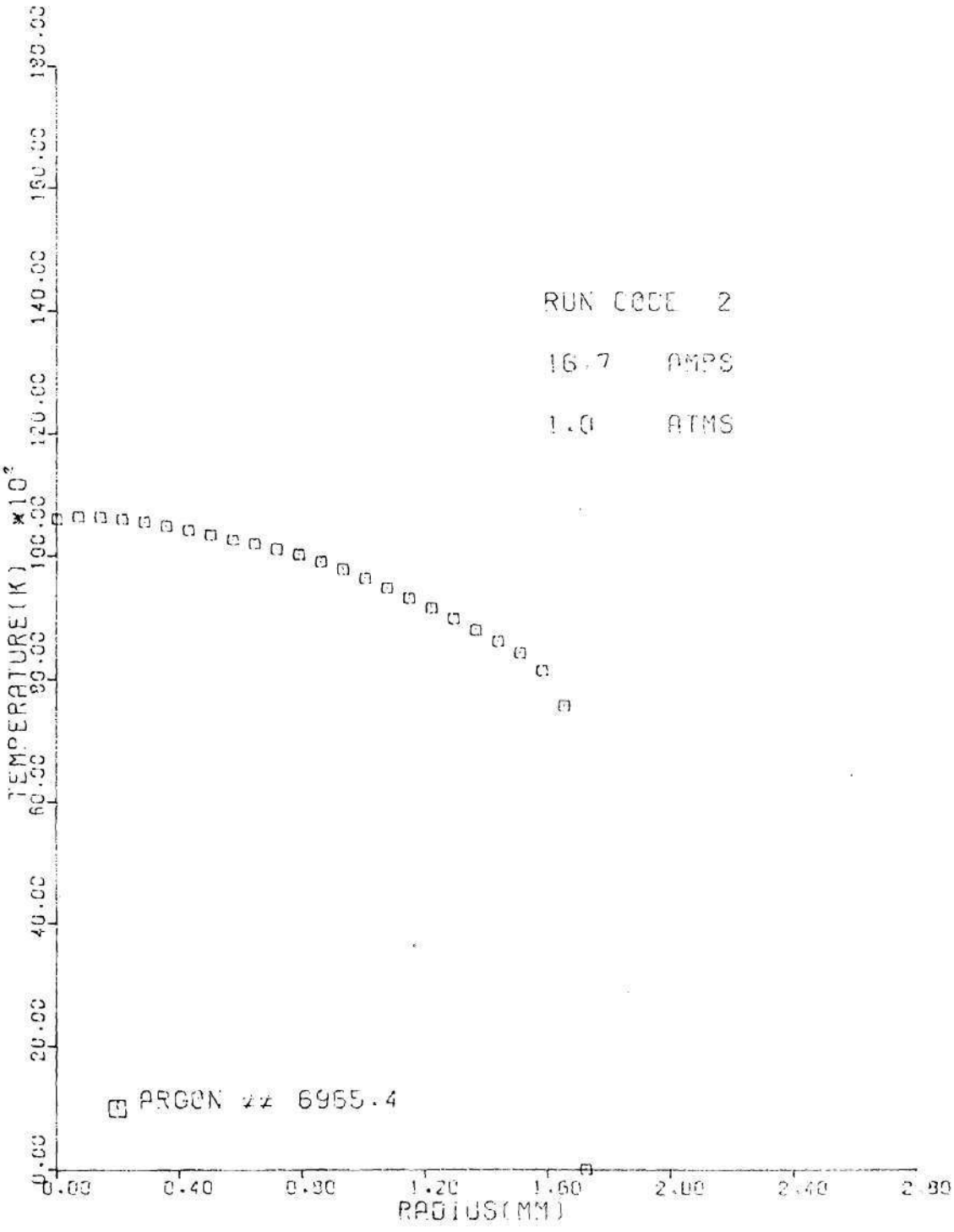
RUN CODE 2
16.7 AMPS
1.0 ATMS
TEMPERATURE(K) *10²
RADIUS(MM)
0.00
0.40
0.80
1.20
1.60
2.00
2.40
2.80
20.00
40.00
60.00
80.00
100.00
120.00
140.00
160.00
180.00
ARGON ** 6965.4

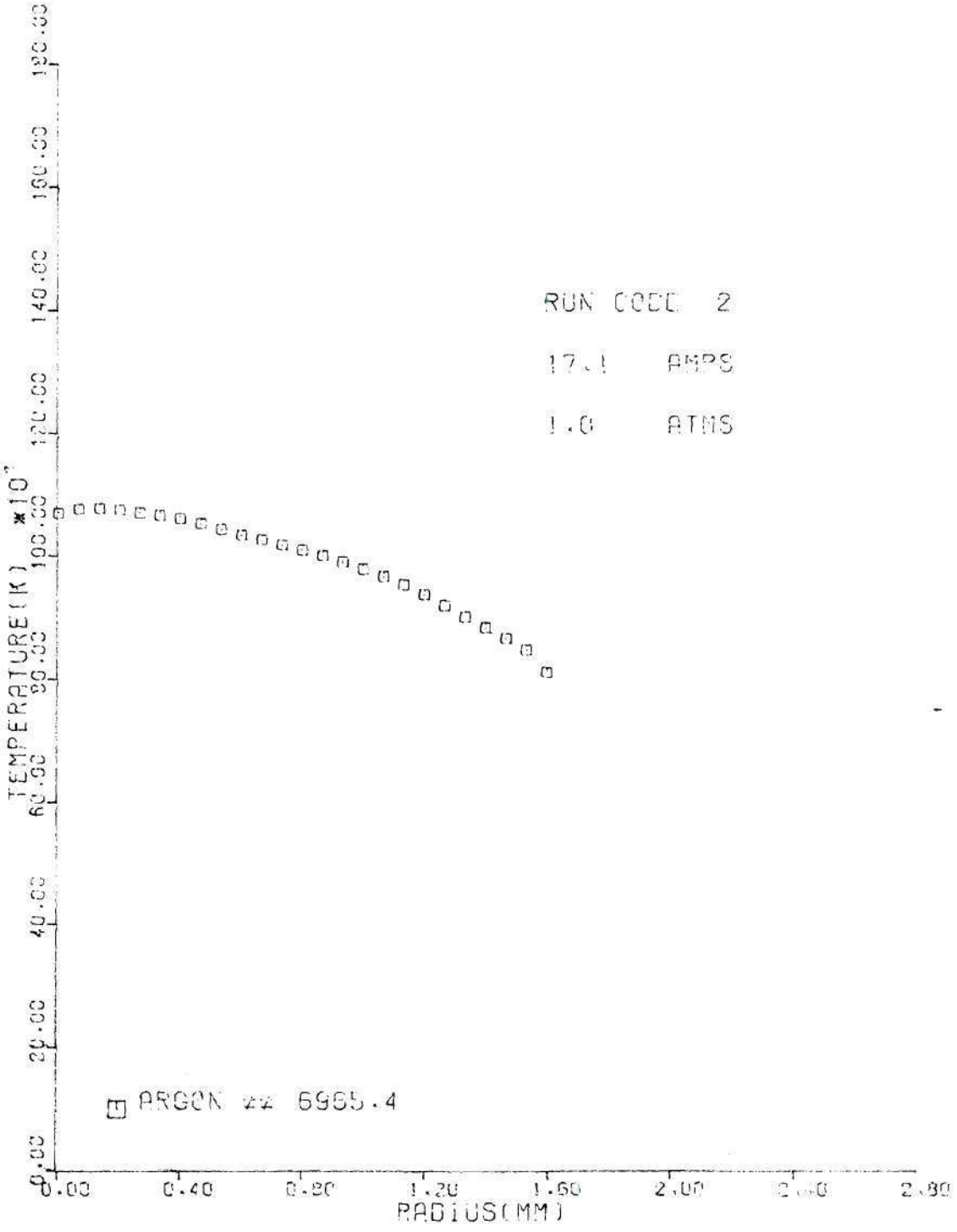
RUN CODE 2
17.1 AMPS
1.0 ATMS
TEMPERATURE(K) *10^
0.00
20.00
40.00
60.00
80.00
100.00
120.00
140.00
160.00
180.00
0.00
0.40
0.80
1.20
1.60
2.00
2.40
2.80
RADIUS(MM)
ARGON ** 6965.4

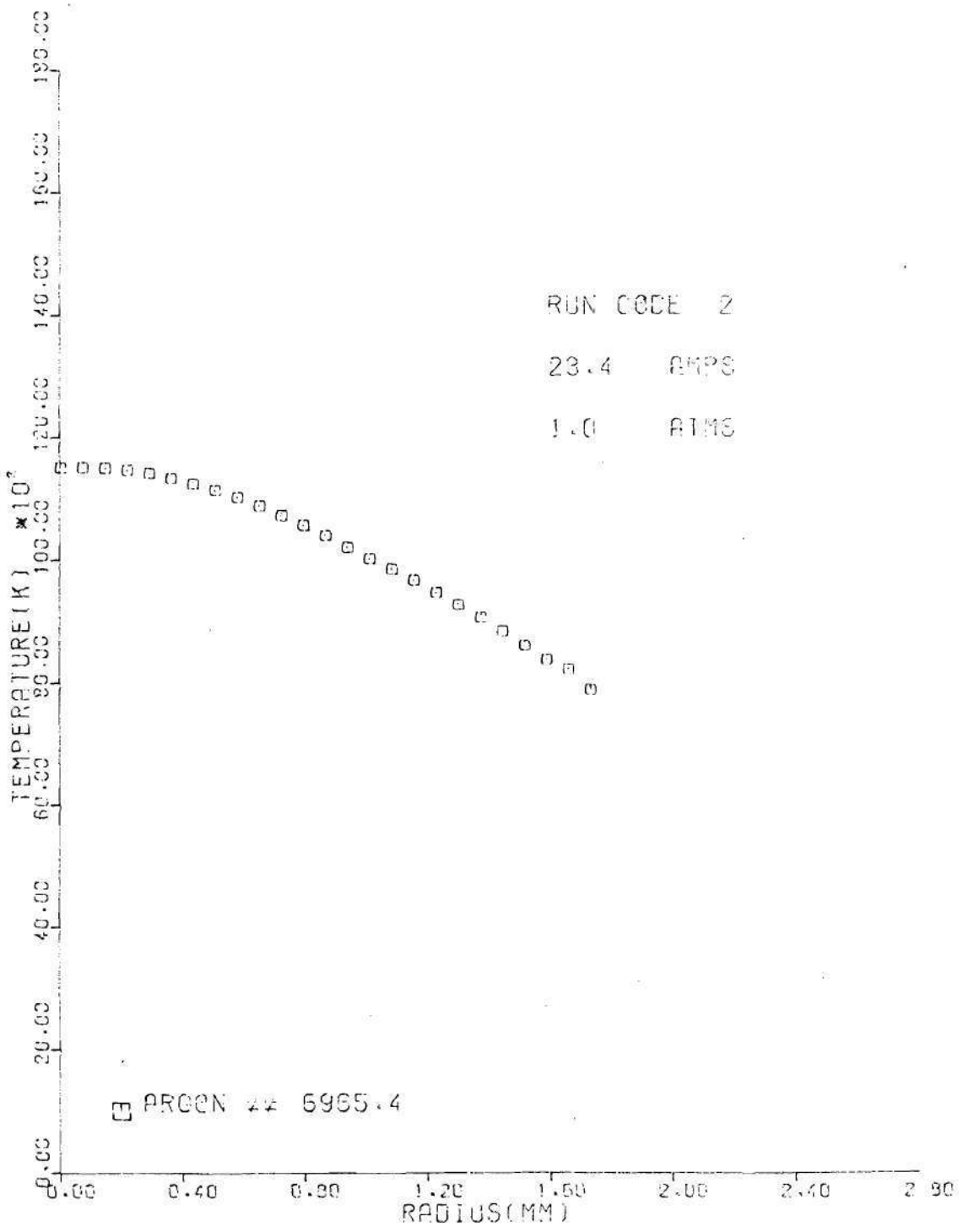
RUN CODE 2
23.4 AMPS
1.0 ATMS
TEMPERATURE(K) *10²
RADIUS(MM)
ARGON ** 6965.4

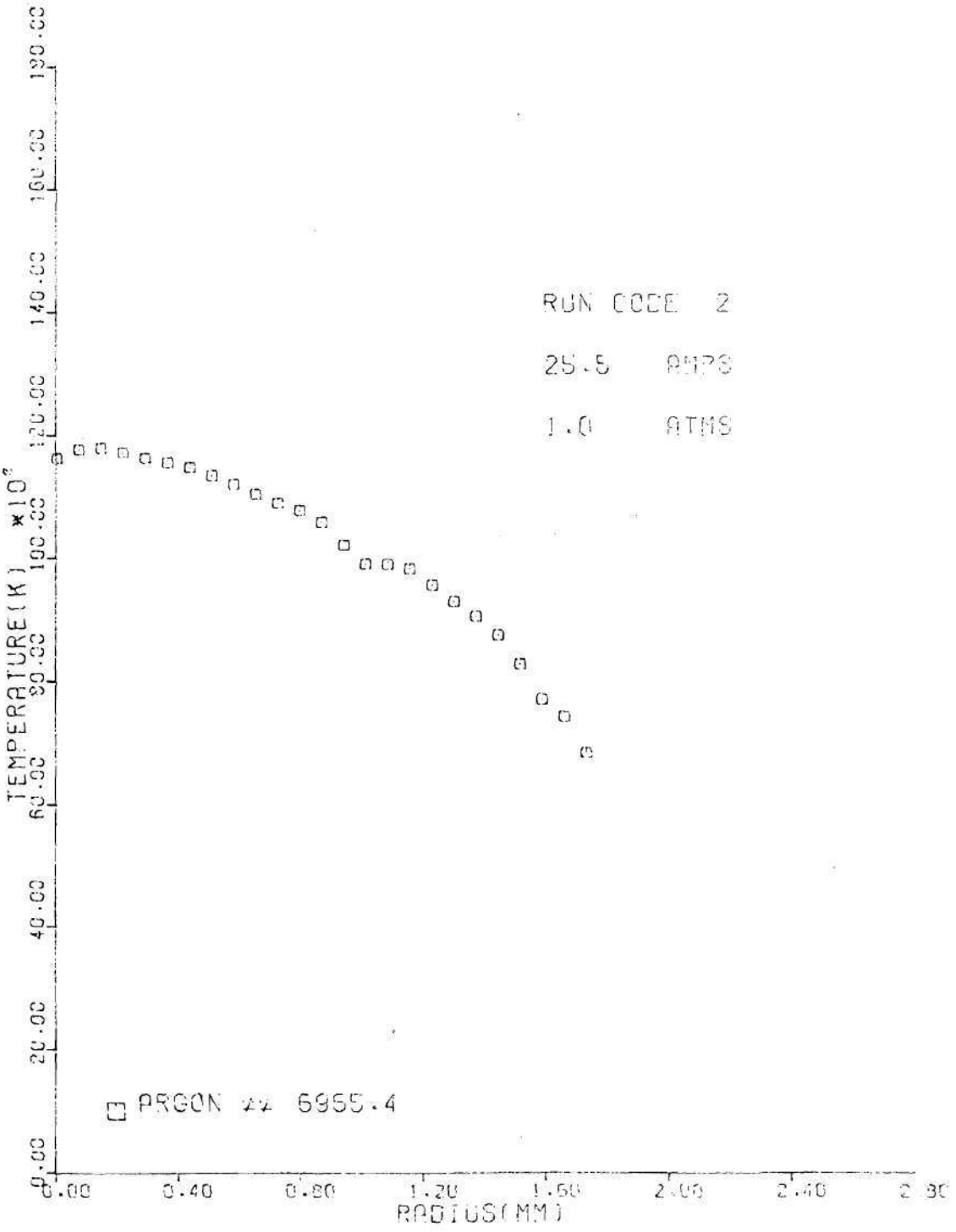
RUN CODE 2
25.5 AMPS
1.0 ATMS
TEMPERATURE(K) *10²
RADIUS(MM)
0.00
0.40
0.80
1.20
1.60
2.00
2.40
2.80
20.00
40.00
120.00
140.00
160.00
180.00
PROBE #2 6955.4

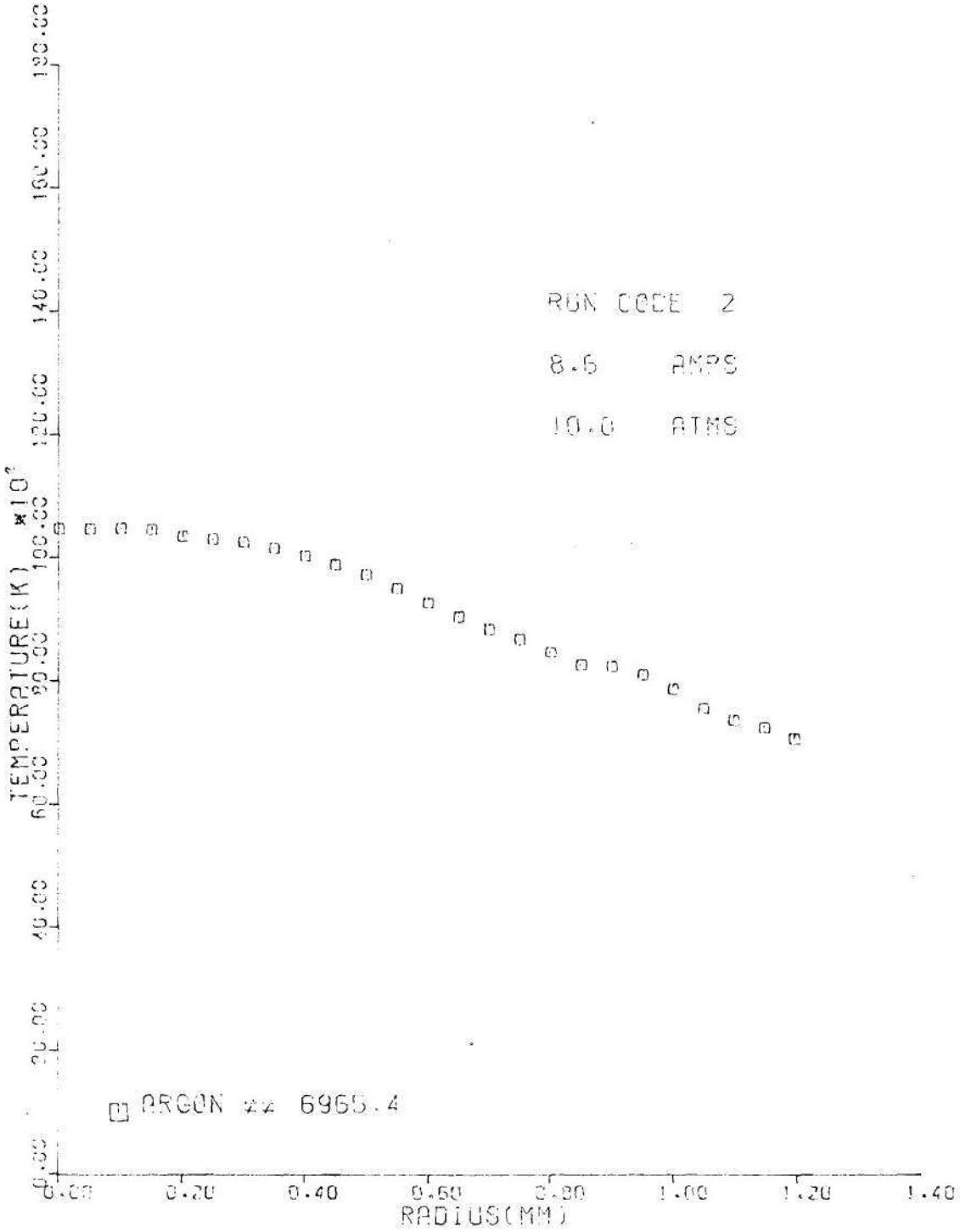
RUN CODE 2
8.6 AMPS
10.0 ATMS
TEMPERATURE(K) *10²
RADIUS(MM)
0.00
0.20
0.40
0.60
0.80
1.00
1.20
1.40
ARGON ** 6965.4

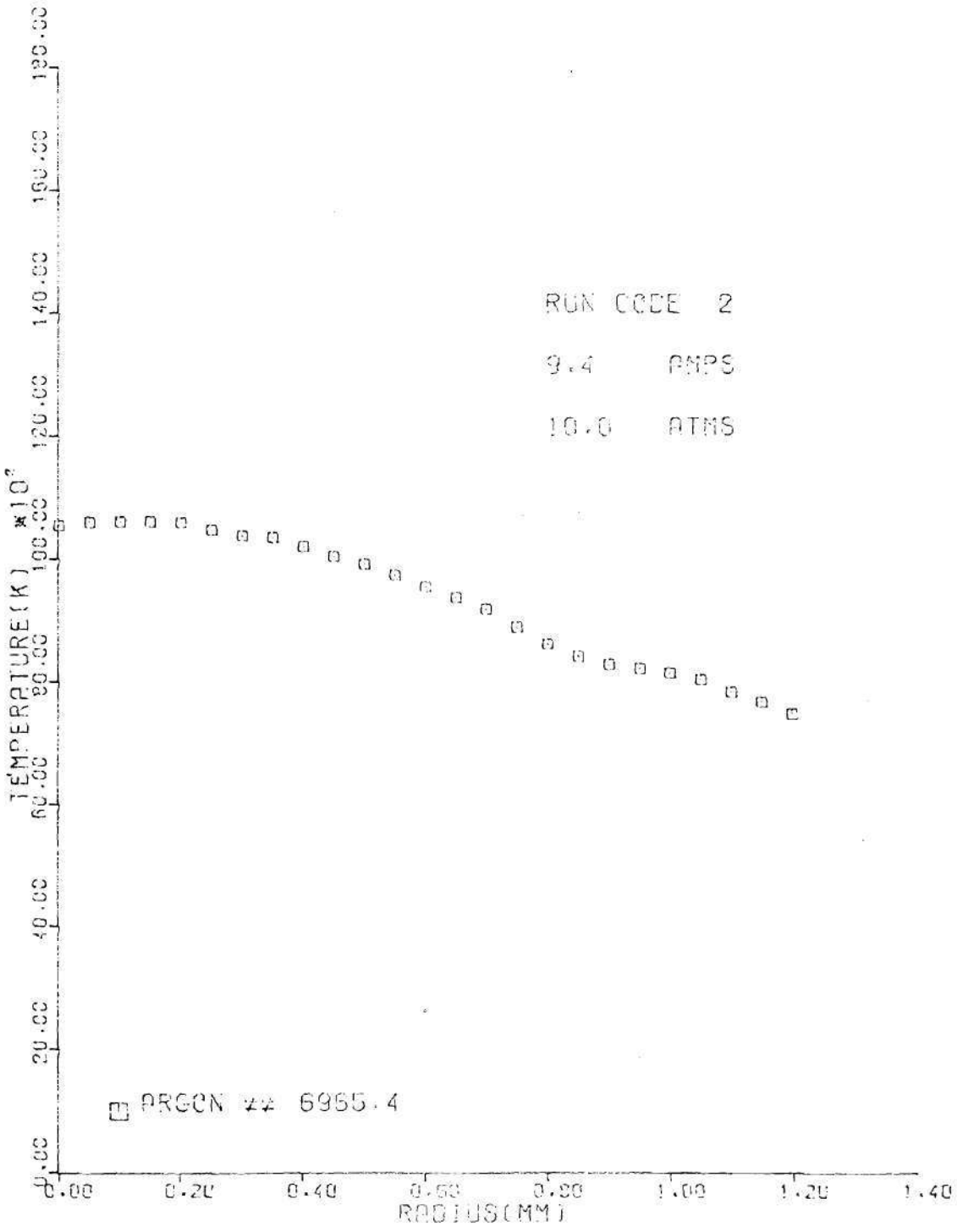
RUN CODE 2
9.4 AMPS
10.0 ATMS
TEMPERATURE(K) *10²
RADIUS(MM)
ARGON AT 6965.4
0.00
20.00
40.00
60.00
80.00
100.00
120.00
140.00
160.00
180.00
0.00
0.20
0.40
0.60
0.80
1.00
1.20
1.40

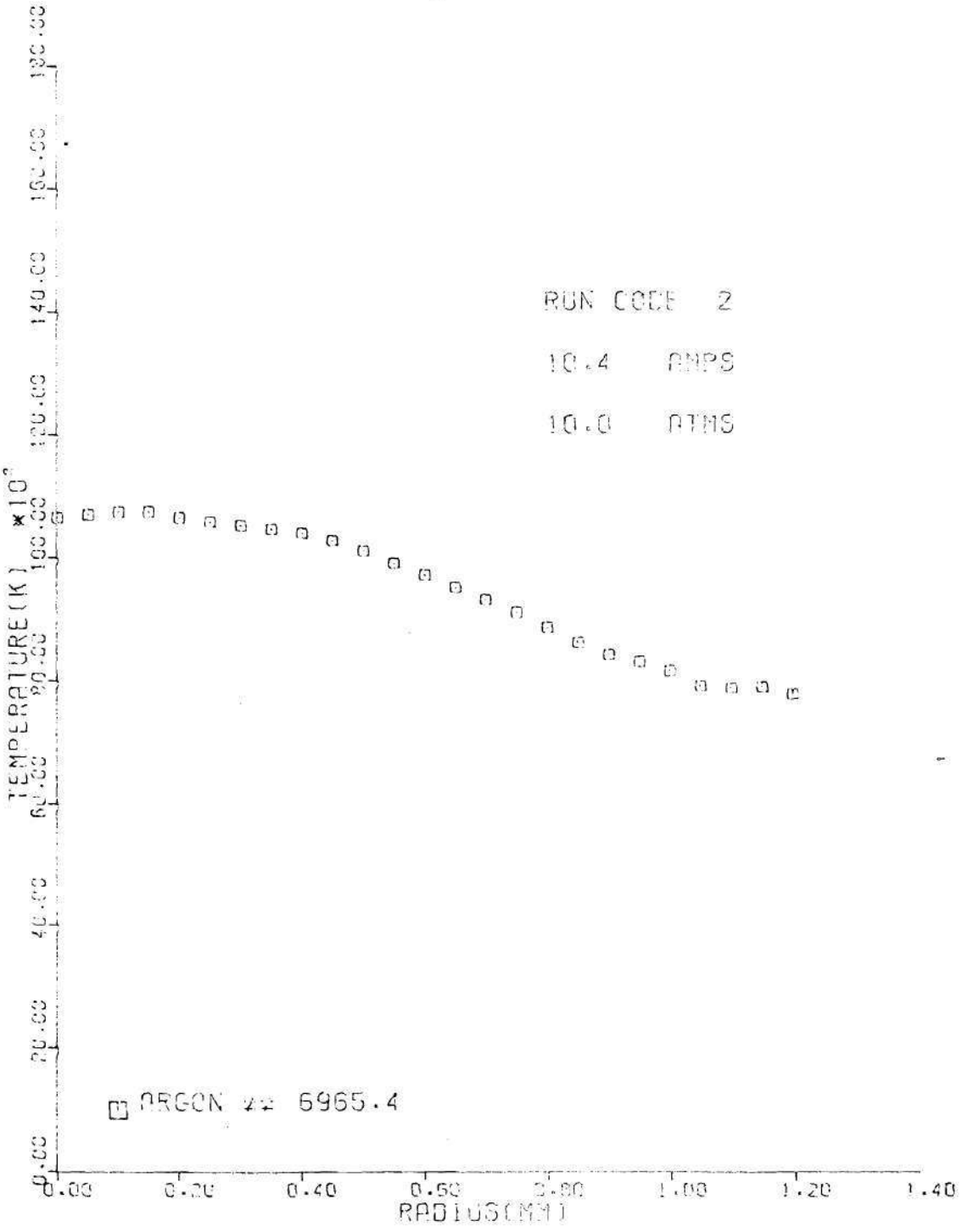
RUN CODE 2
10.4 AMPS
10.0 ATMS
TEMPERATURE(K) *10²
ARGON ## 6965.4
0.00
0.20
0.40
0.60
0.80
1.00
1.20
1.40
RADIUS(MM)

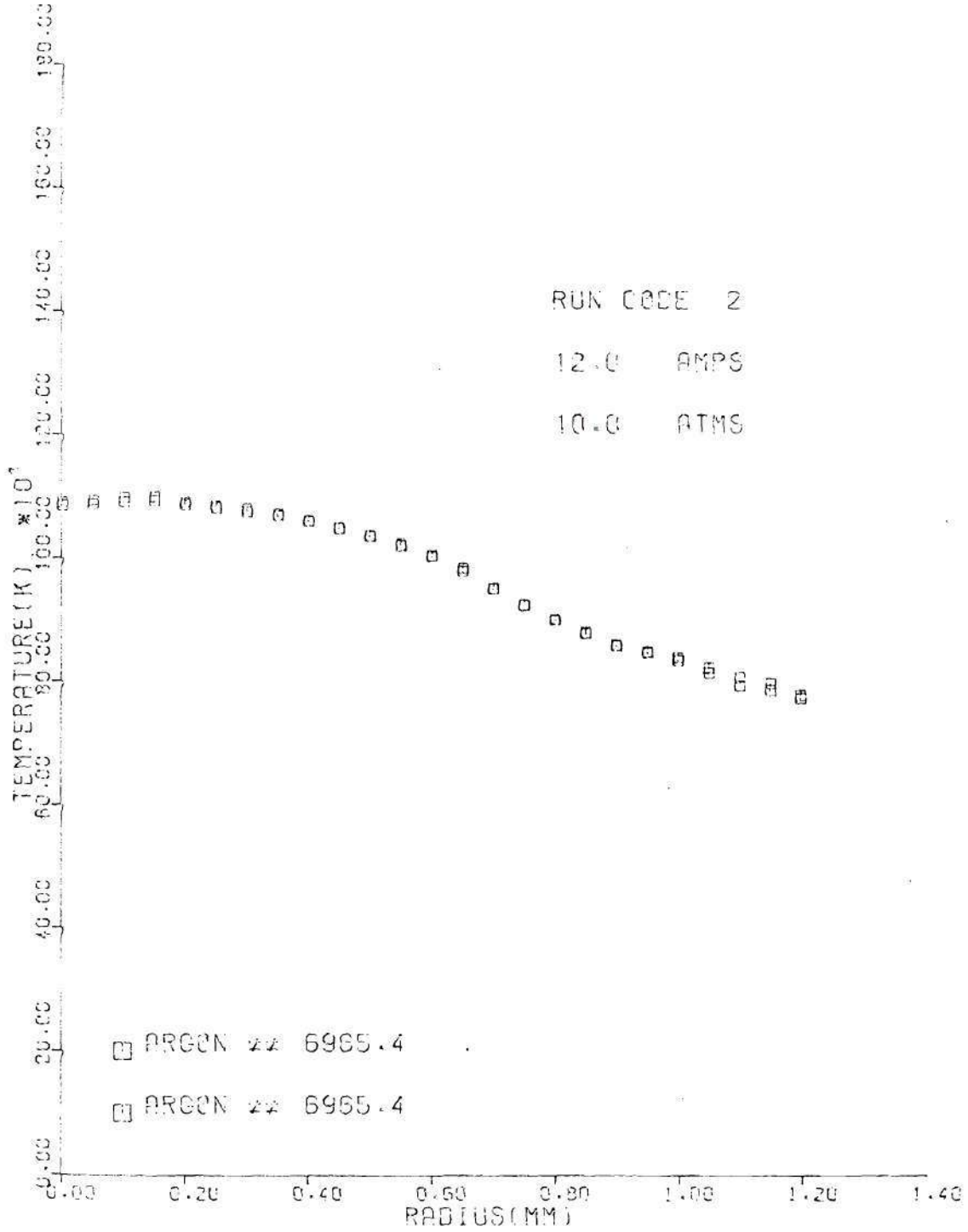
RUN CODE 2
12.0 AMPS
10.0 ATMS
TEMPERATURE(K) *10³
RADIUS(MM)
ARGON ** 6965.4
ARGON ** 6965.4

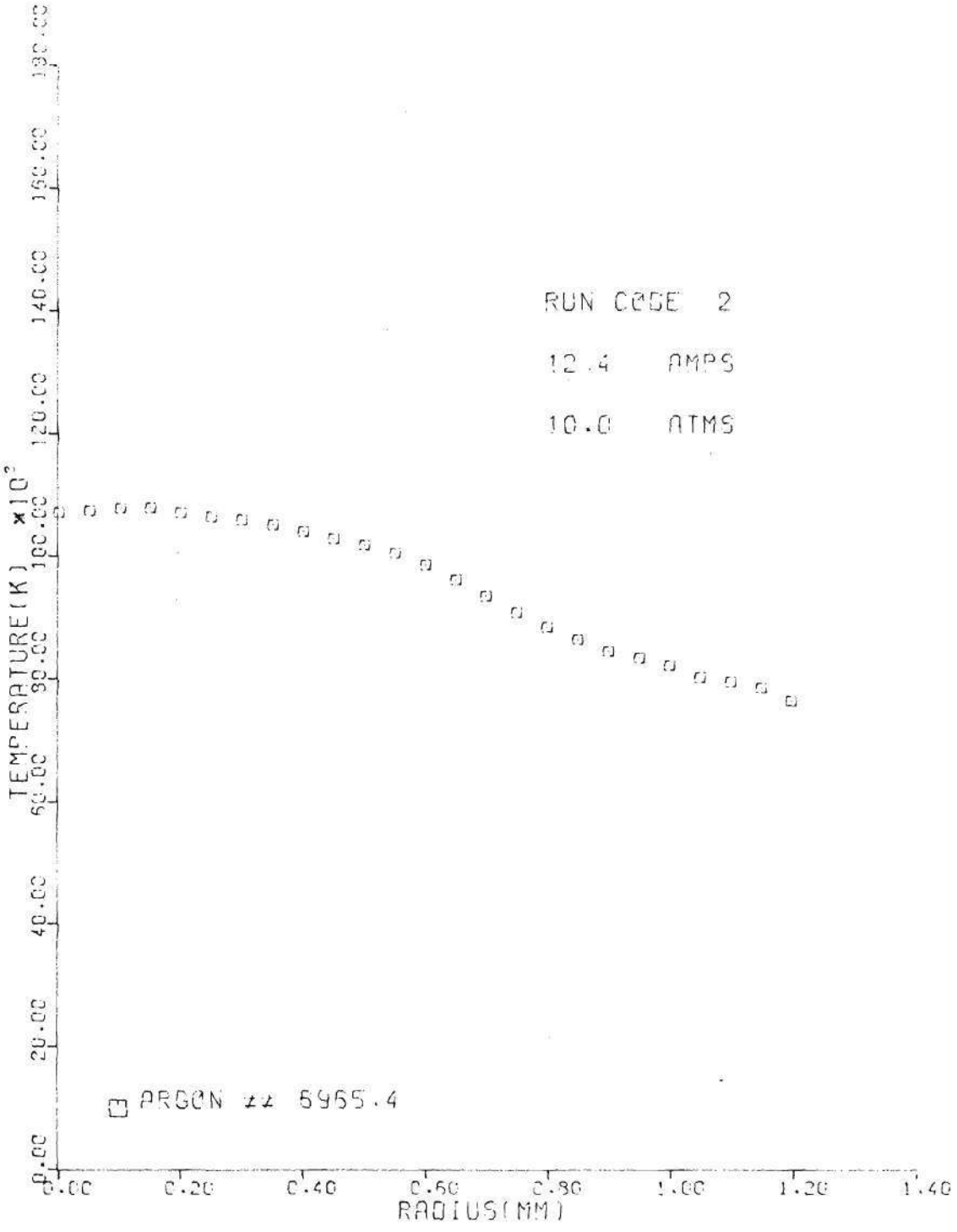
RUN CODE 2
12.4 AMPS
10.0 ATMS
TEMPERATURE(K) x10²
0.00
20.00
40.00
60.00
80.00
100.00
120.00
140.00
160.00
180.00
0.00
0.20
0.40
0.60
0.80
1.00
1.20
1.40
RADIUS(MM)
ARGON II 5965.4

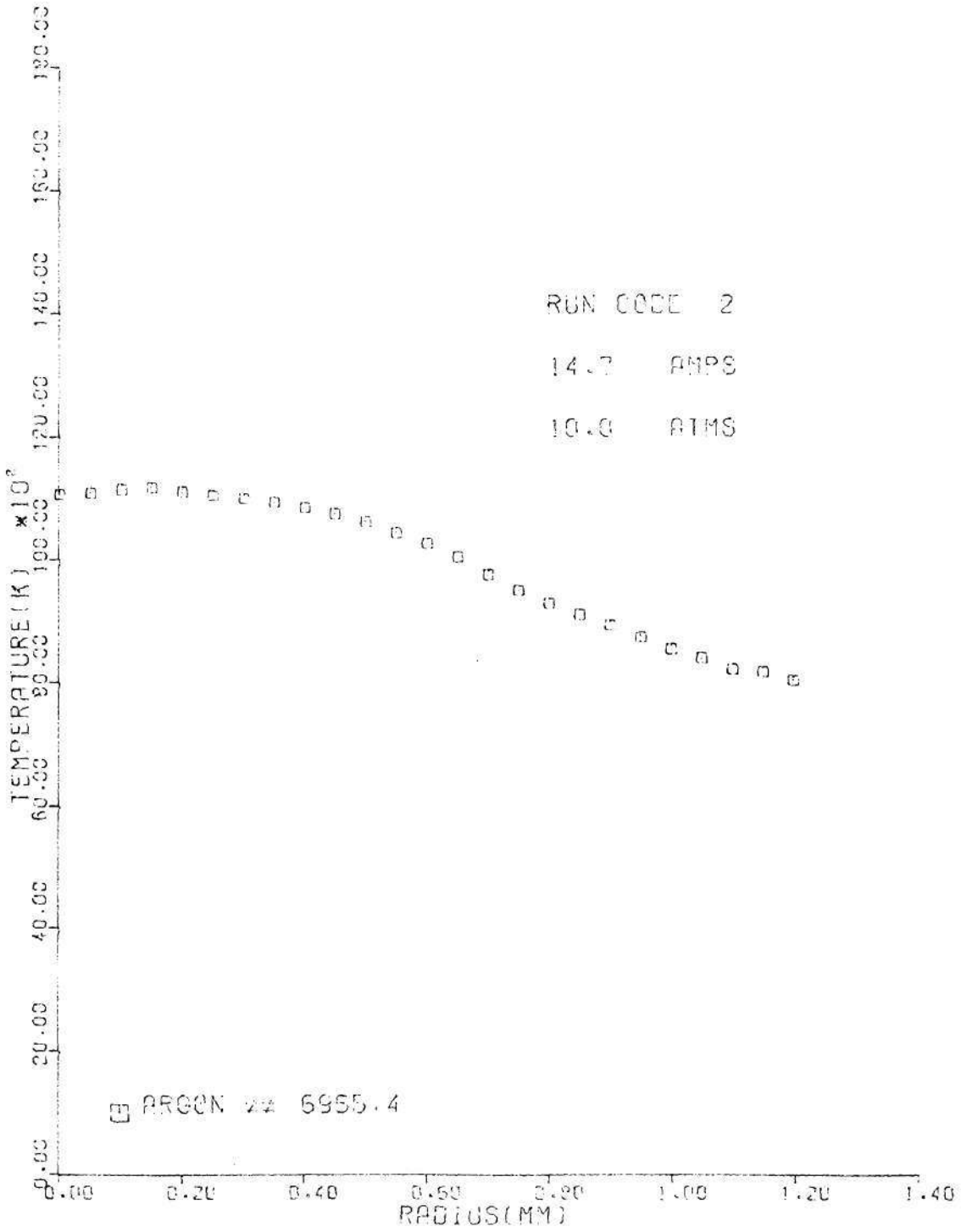
RUN CODE 2
14.7 AMPS
10.0 ATMS
TEMPERATURE(K) *10²
RADIUS(MM)
0.00
0.20
0.40
0.60
0.80
1.00
1.20
1.40
20.00
40.00
60.00
80.00
100.00
120.00
140.00
160.00
180.00
ARGON 2+ 6965.4

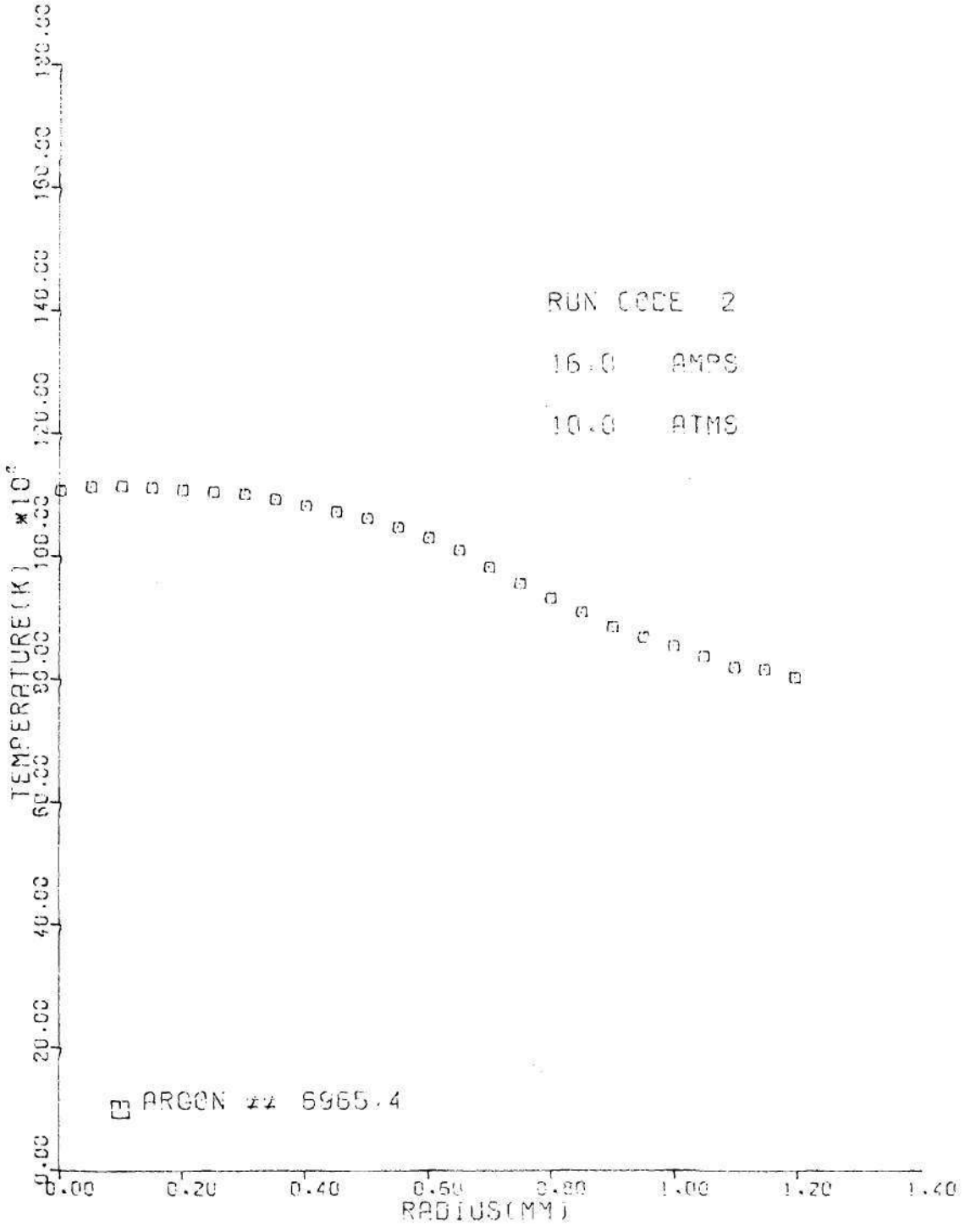
RUN CODE 2
16.0 AMPS
10.0 ATMS
TEMPERATURE(K) *10^2
0.00
20.00
40.00
60.00
80.00
100.00
120.00
140.00
160.00
180.00
0.00
0.20
0.40
0.60
0.80
1.00
1.20
1.40
RADIUS(MM)
ARGON ** 6965.4

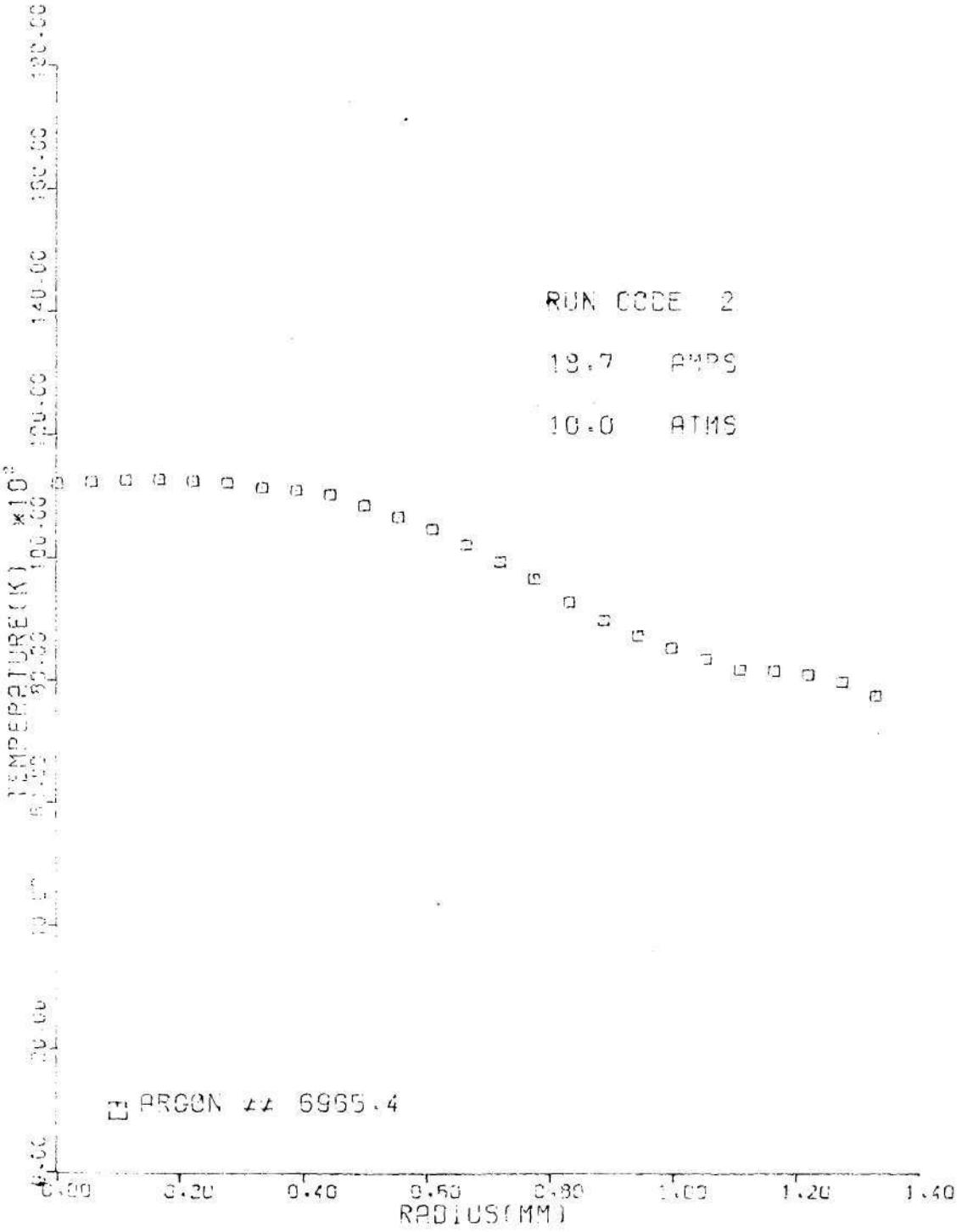
RUN CODE 2
19.7 AMPS
10.0 ATMS
TEMPERATURE(K) *10³
RADIUS(MM)
0.00
0.20
0.40
0.60
0.80
1.00
1.20
1.40
ARGON AA 6965.4

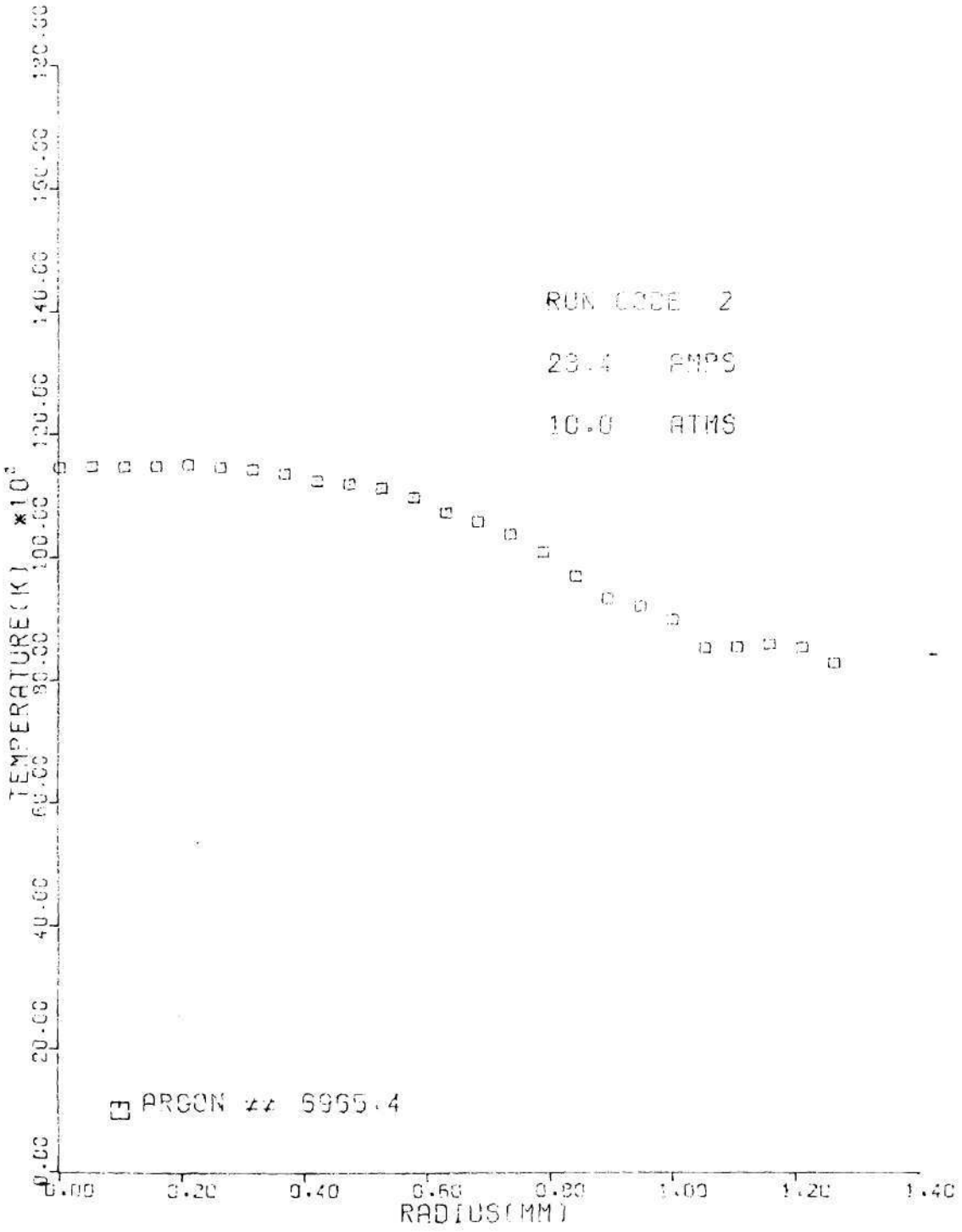
RUN CODE 2
23.4 AMPS
10.0 ATMS
TEMPERATURE(K) *10³
RADIUS(MM)
ARGON ** 6965.4

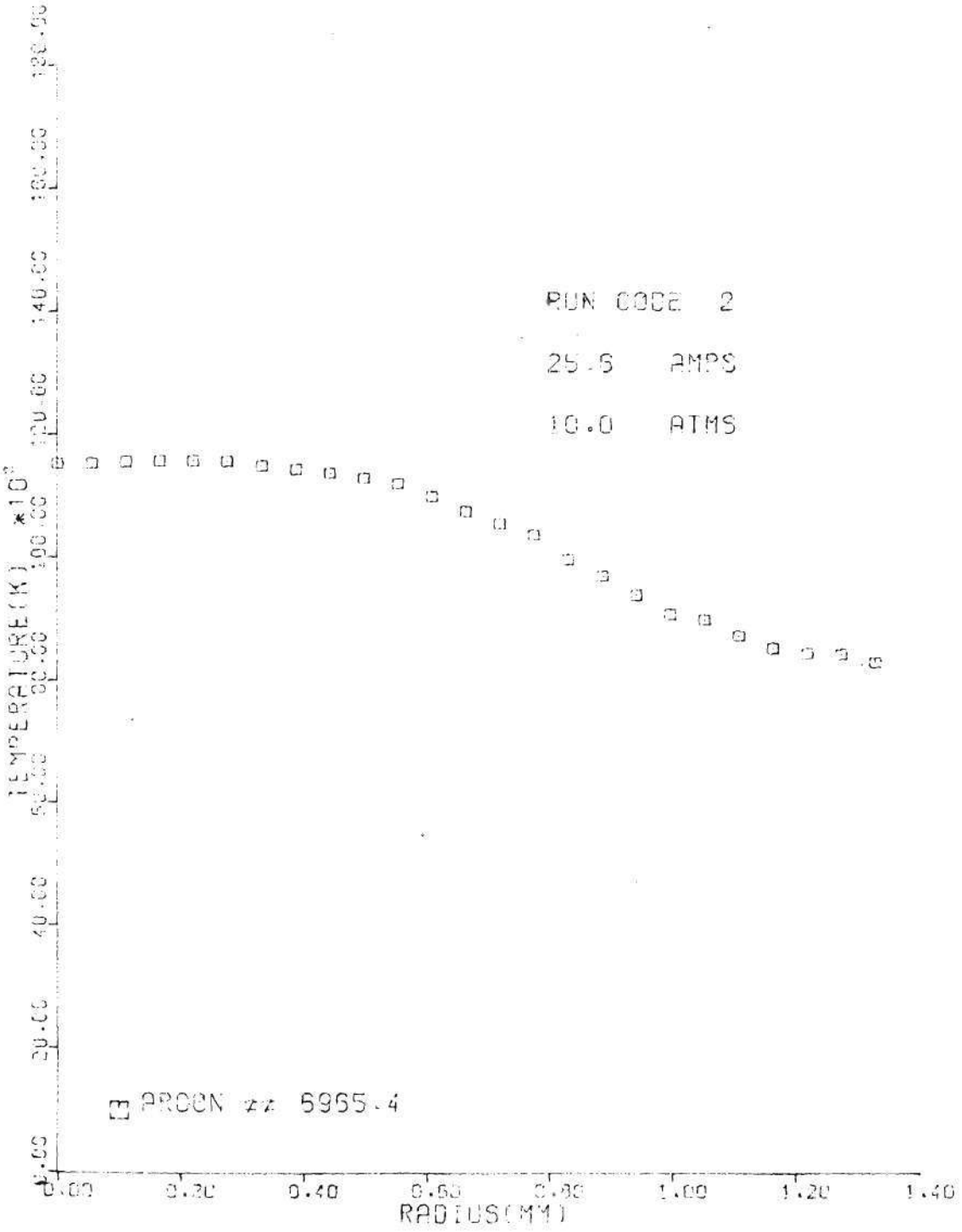
RUN CODE 2
25.6 AMPS
10.0 ATMS
TEMPERATURE(K) *10³
RADIUS(MM)
PROBN ** 5965.4

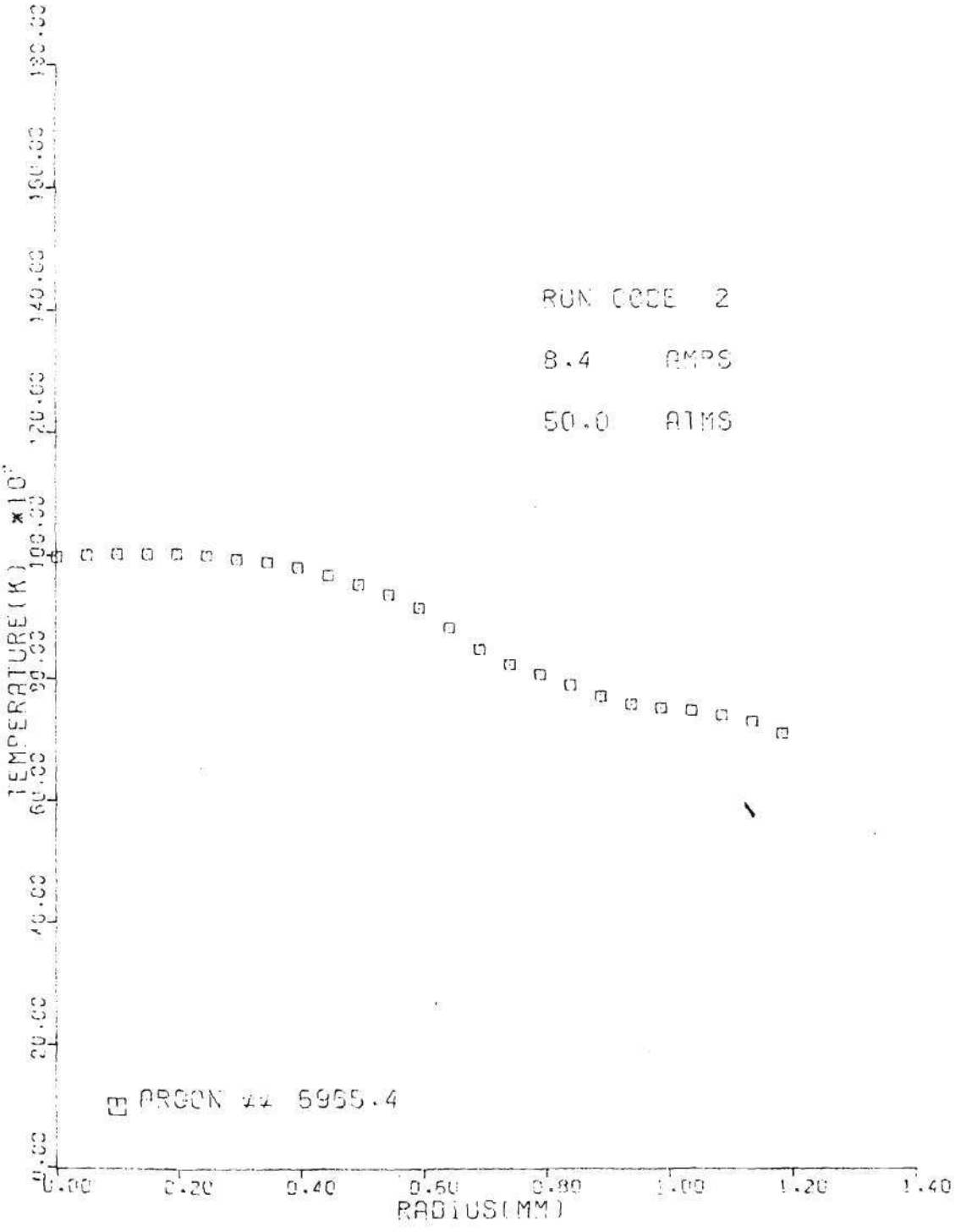
RUN CODE 2
8.4 AMPS
50.0 ATMS
TEMPERATURE(K) *10^
ARGON AT 5965.4
0.00
0.20
0.40
0.60
0.80
1.00
1.20
1.40
RADIUS(MM)

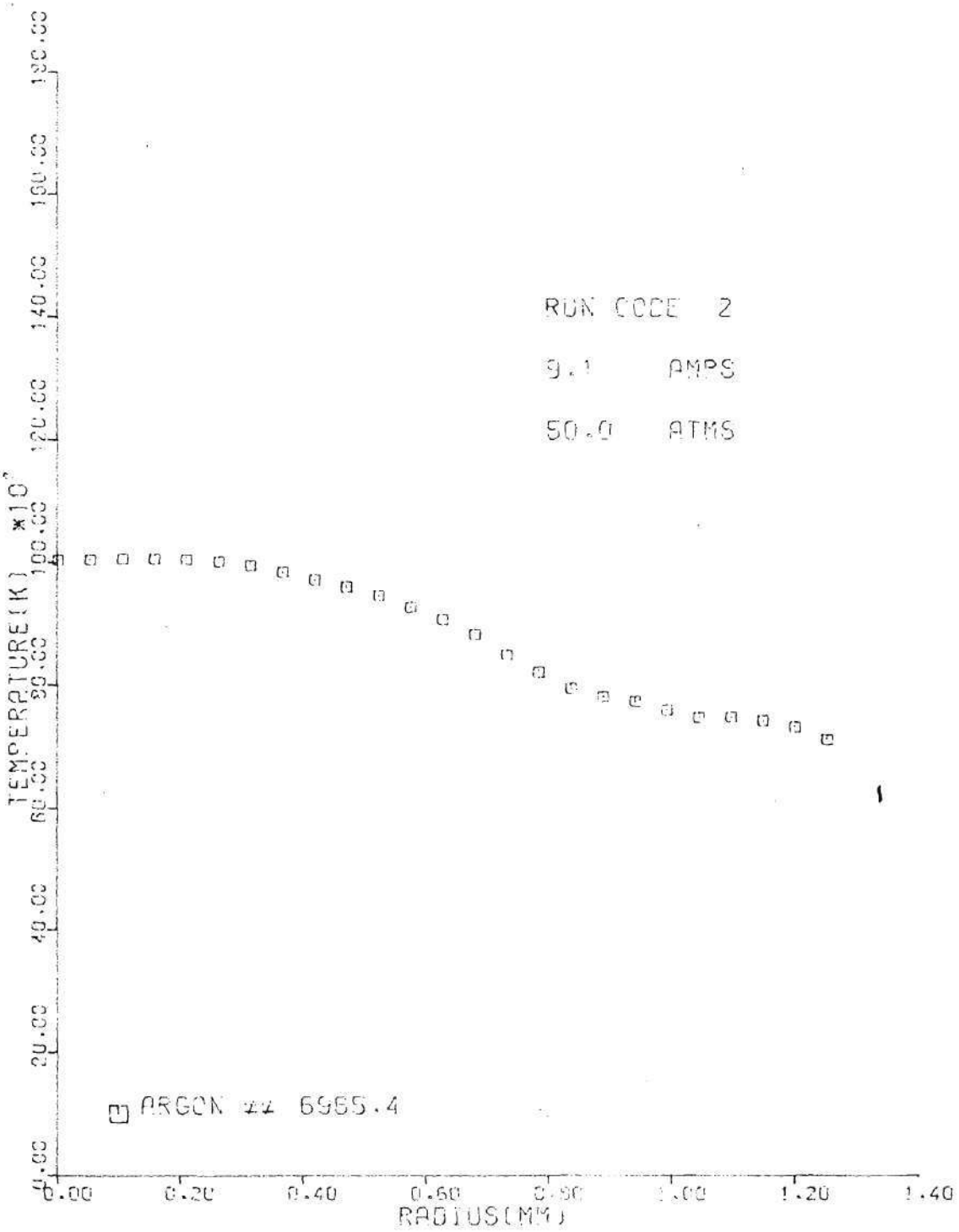
RUN CODE 2
9.1 AMPS
50.0 ATMS
TEMPERATURE(K) *10³
ARGON ## 6965.4
RADIUS(MM)
0.00
0.20
0.40
0.60
1.00
1.20
1.40
20.00
40.00
60.00
80.00
100.00
120.00
140.00
160.00

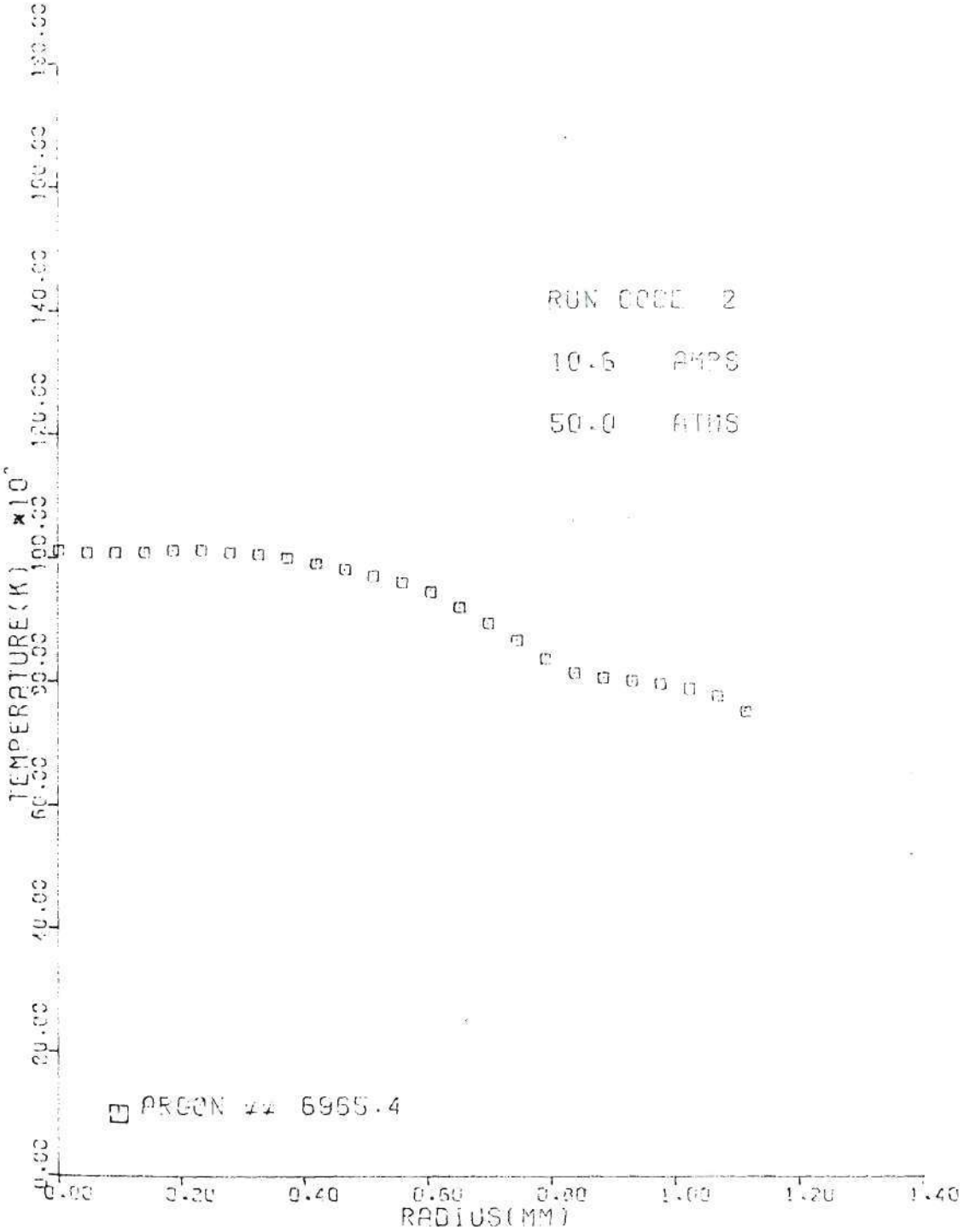
RUN CODE 2
10.6 AMPS
50.0 ATMS
TEMPERATURE(K) ×10²
ARGON ** 6955.4
0.00
0.20
0.40
0.60
0.80
1.00
1.20
1.40
RADIUS(MM)

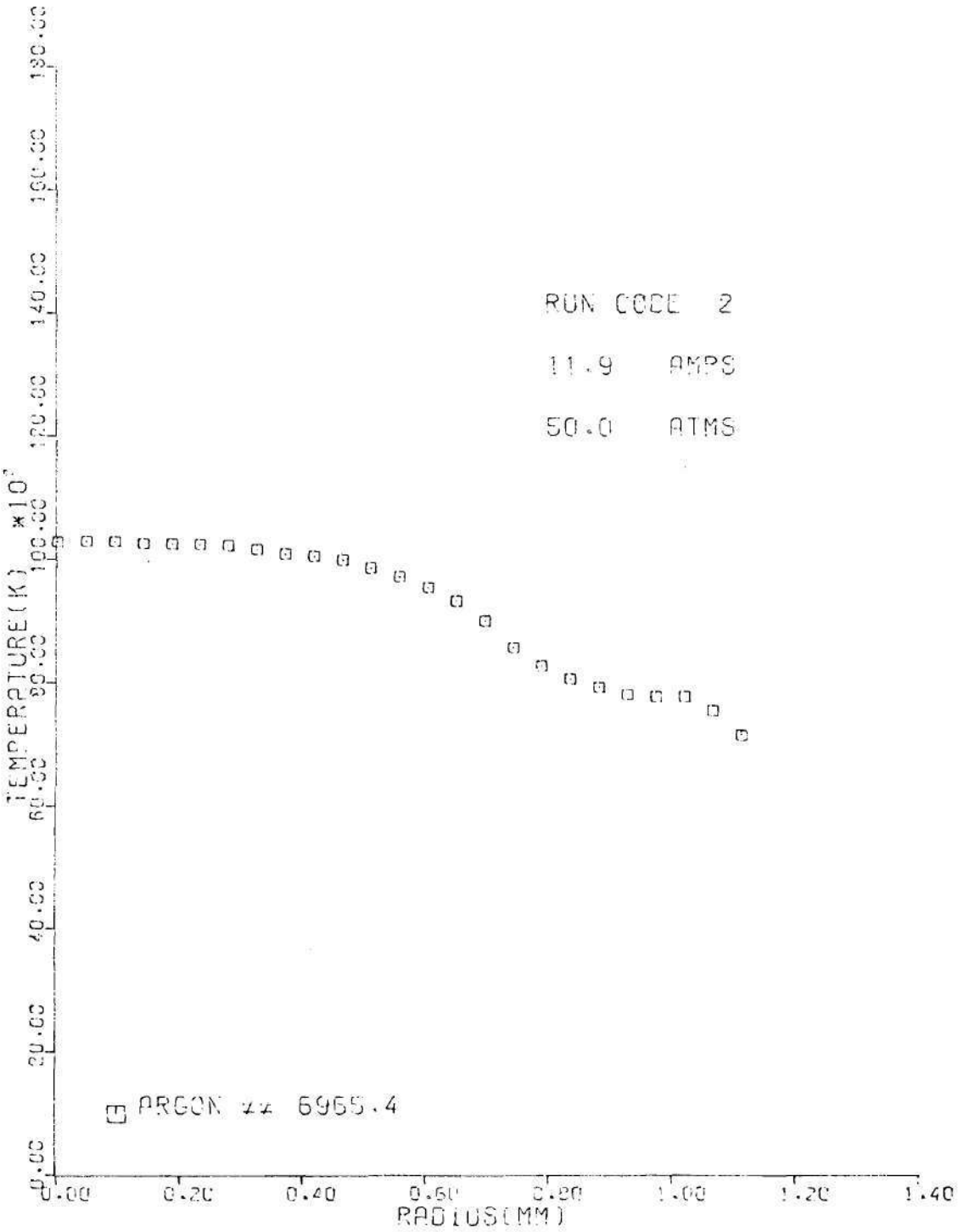
RUN CODE 2
11.9 AMPS
50.0 ATMS
TEMPERATURE(K) *10
ARGON ** 6965.4
RADIUS(MM)
0.00
0.20
0.40
0.60
0.80
1.00
1.20
1.40

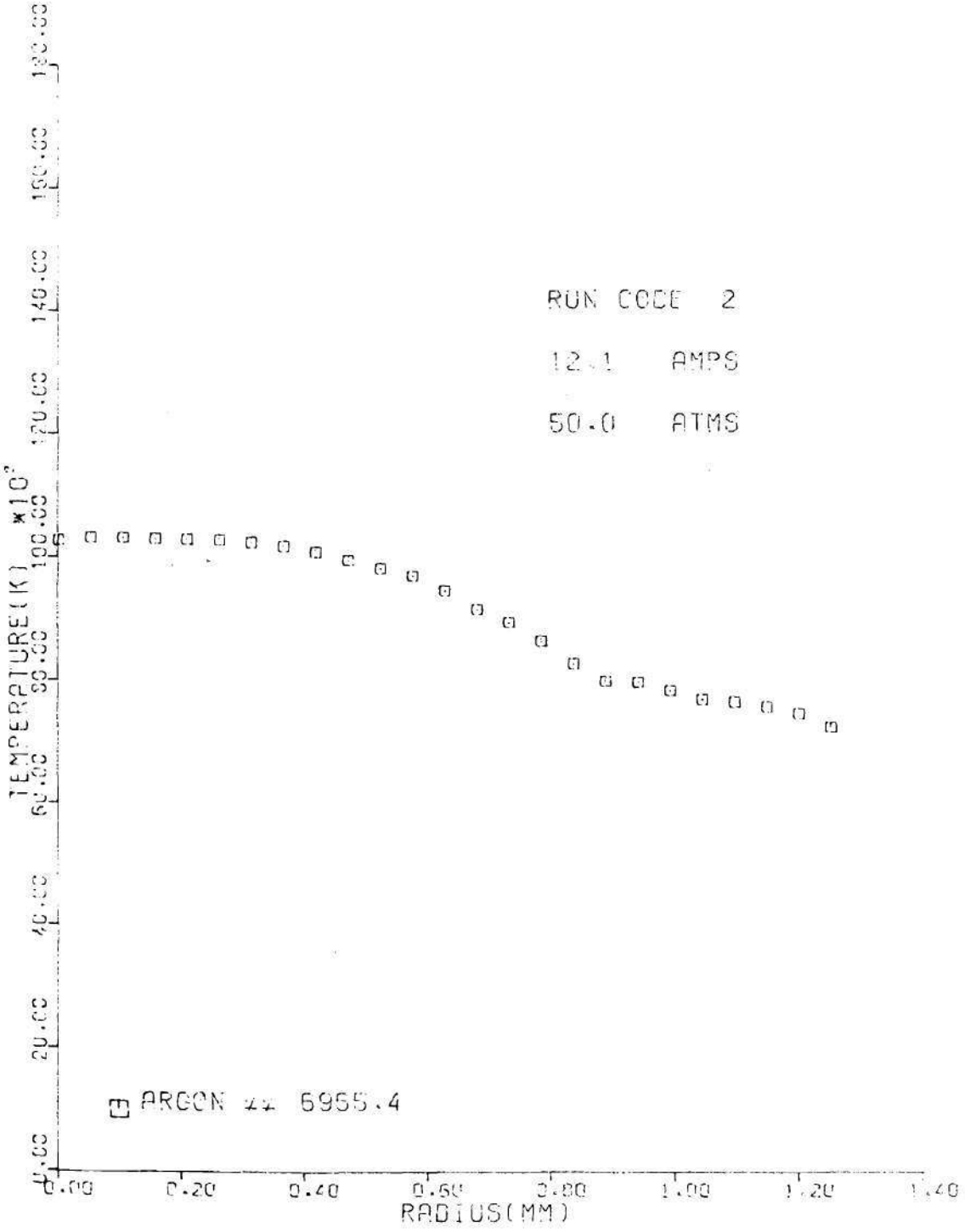
RUN CODE 2
12.1 AMPS
50.0 ATMS
TEMPERATURE(K) *10²
ARGON ++ 6965.4
RADIUS(MM)

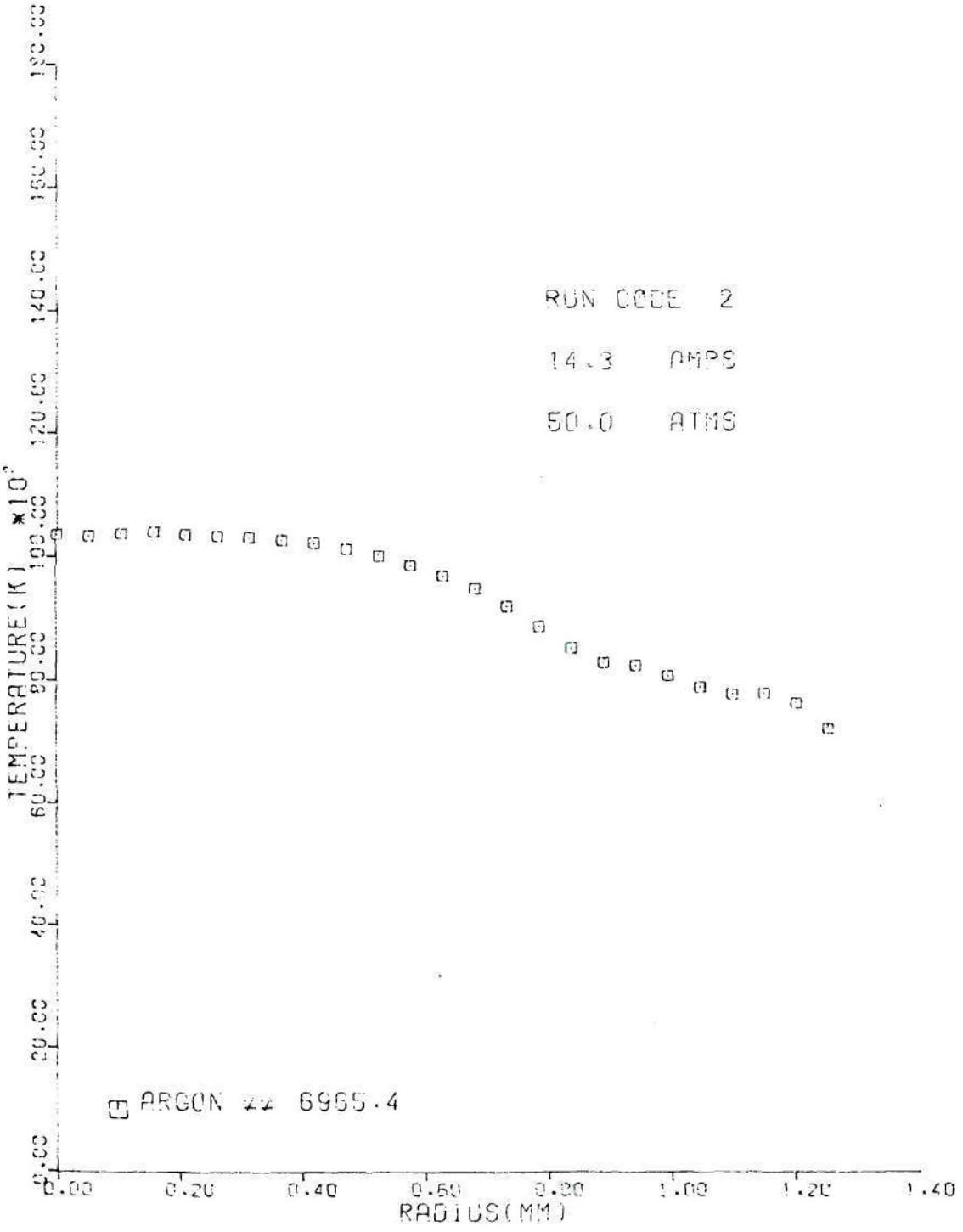
RUN CODE 2
14.3 AMPS
50.0 ATMS
TEMPERATURE(K) *10²
RADIUS(MM)
ARGON ** 6965.4

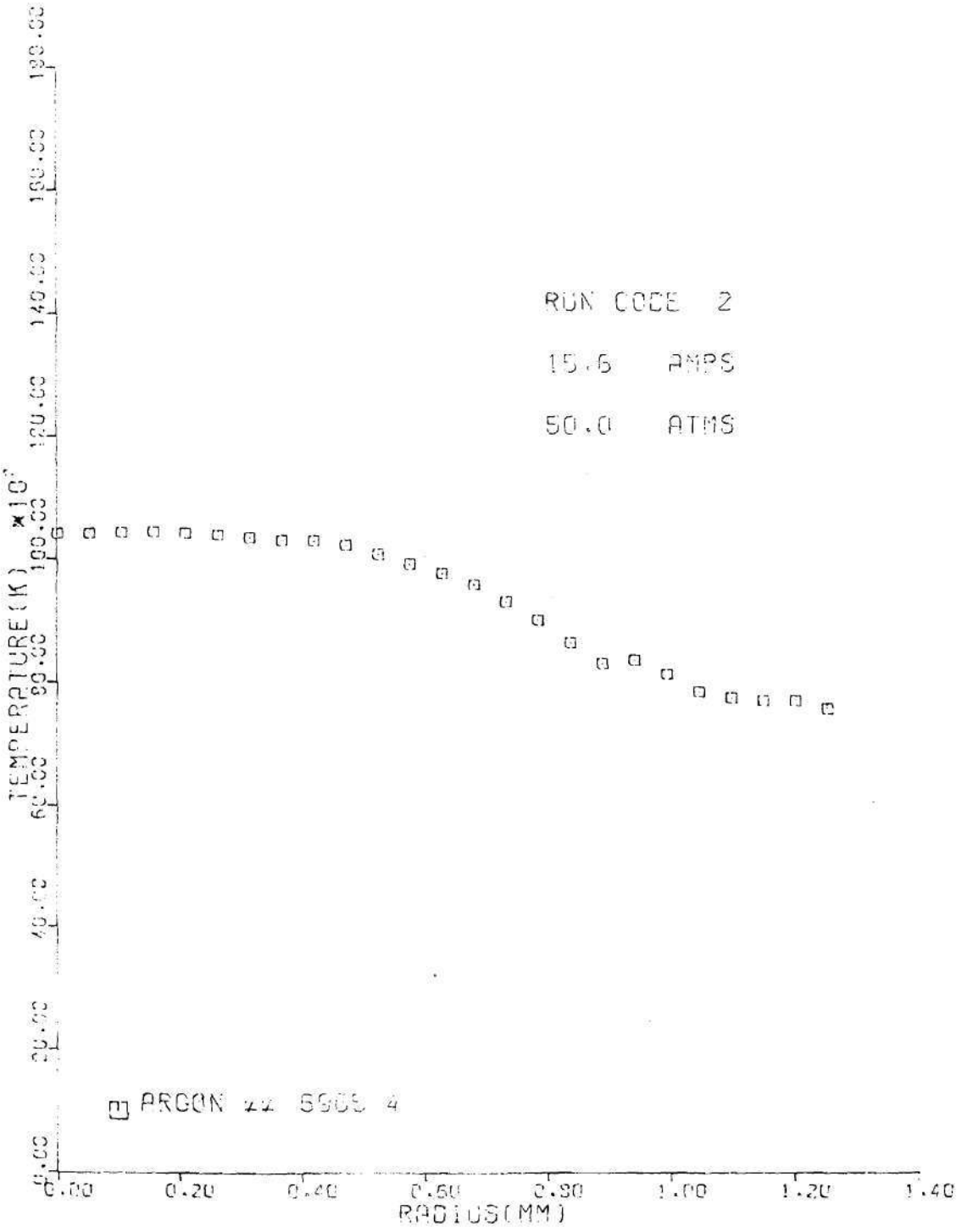
RUN CODE 2
15.6 AMPS
50.0 ATMS
TEMPERATURE(K) *10^
RADIUS(MM)
0.00
0.20
0.40
0.60
0.80
1.00
1.20
1.40
ARGON

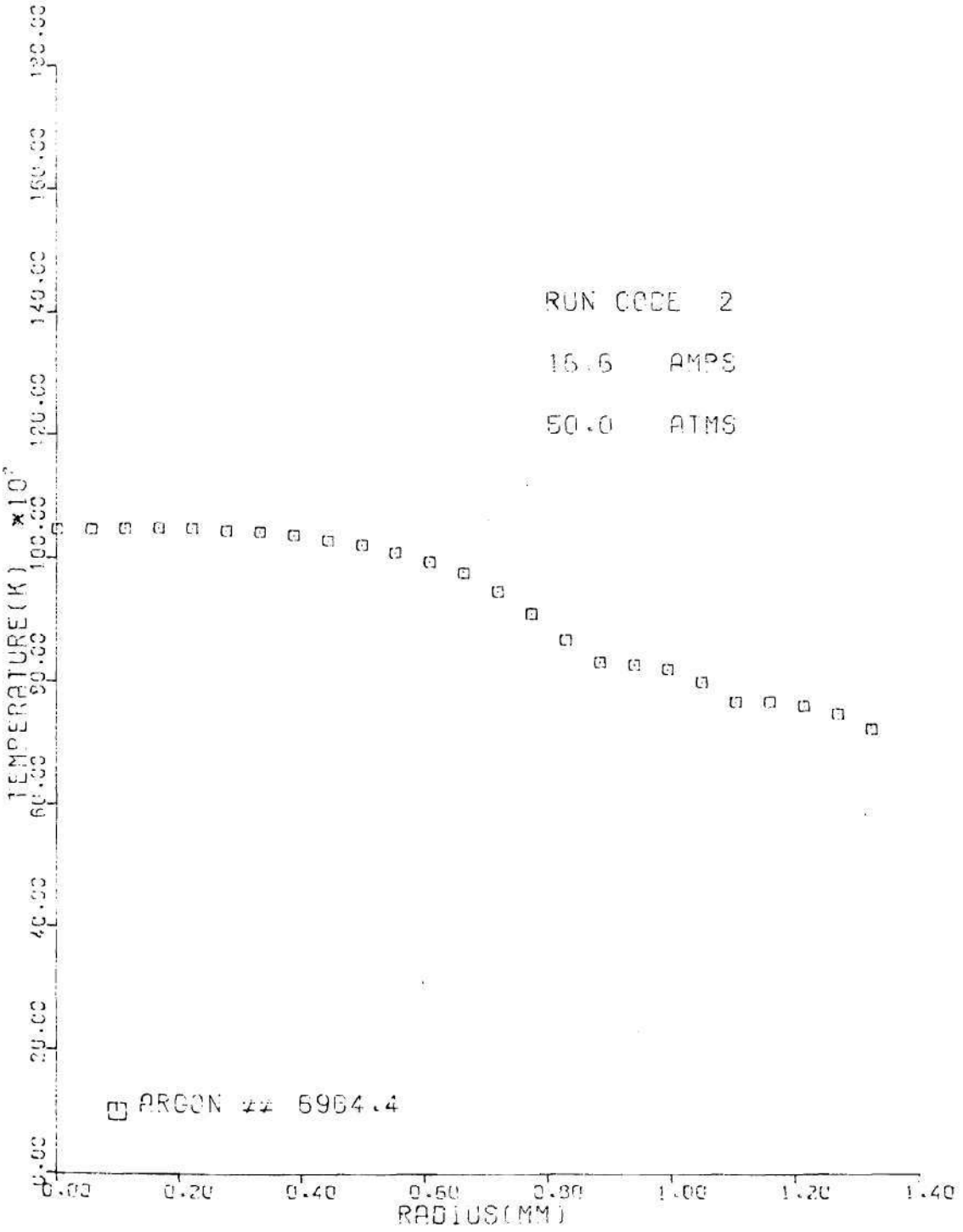
RUN CODE 2
16.6 AMPS
50.0 ATMS
TEMPERATURE(K) *10²
RADIUS(MM)
0.00
0.20
0.40
0.60
0.80
1.00
1.20
1.40
ARGON ## 6964.4

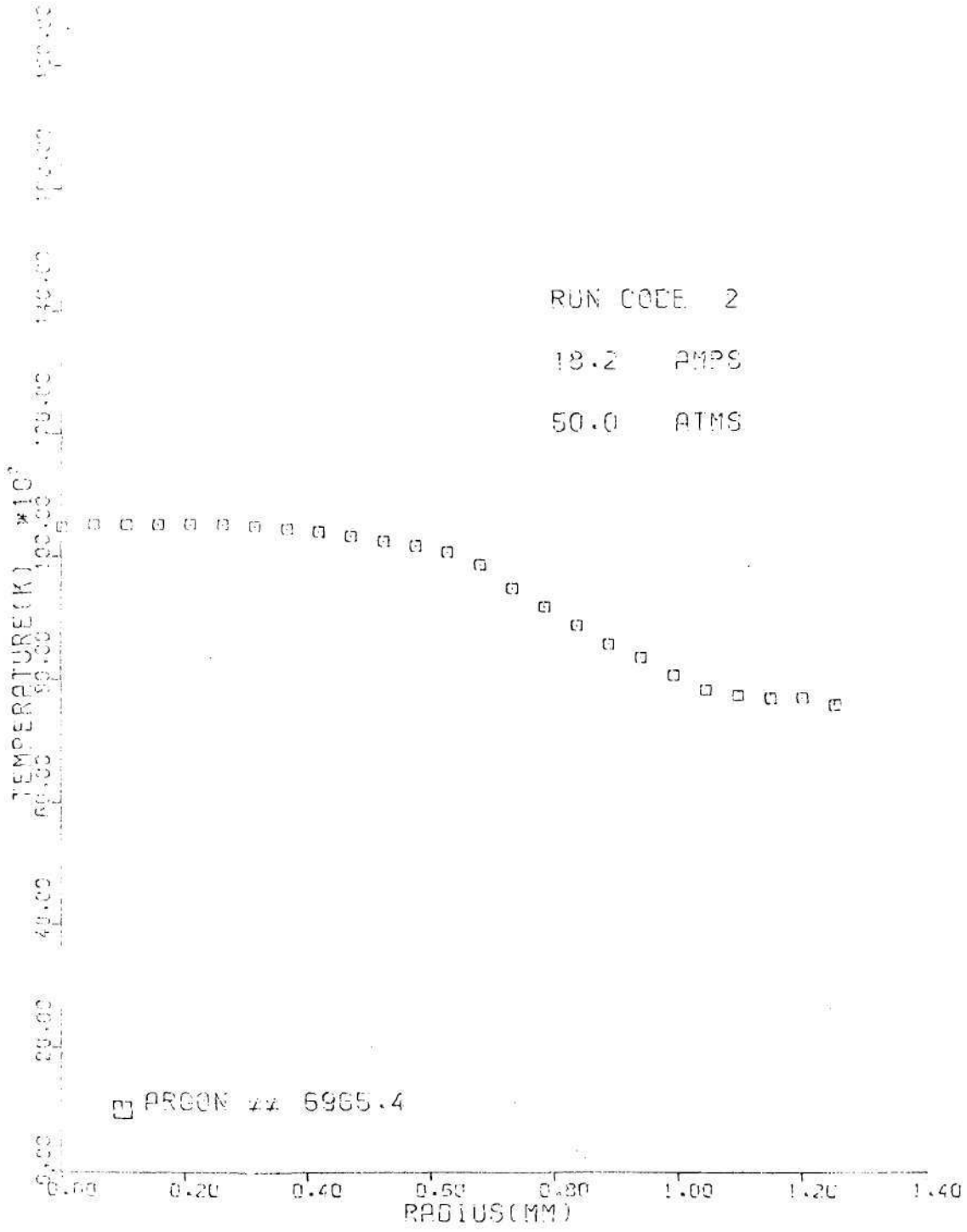
RUN CODE 2
18.2 AMPS
50.0 ATMS
TEMPERATURE(K) *10³
PROON ** 6985.4
0.00
0.20
0.40
0.60
0.80
1.00
1.20
1.40
RADIUS(MM)

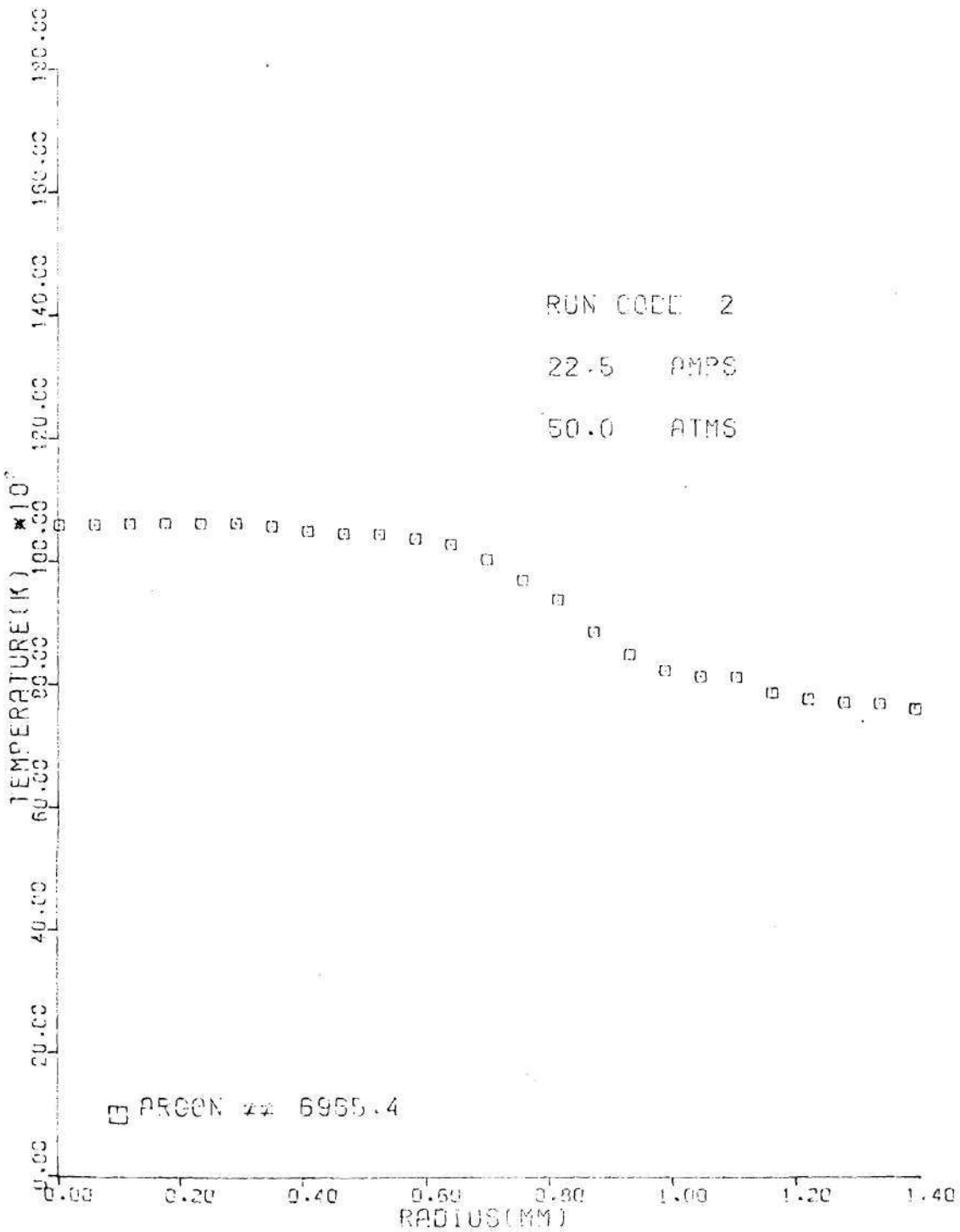
RUN CODE 2
22.5 AMPS
50.0 ATMS
TEMPERATURE(K) *10
RADIUS(MM)
0.00
0.20
0.40
0.60
0.80
1.00
1.20
1.40
ARGON ** 6965.4

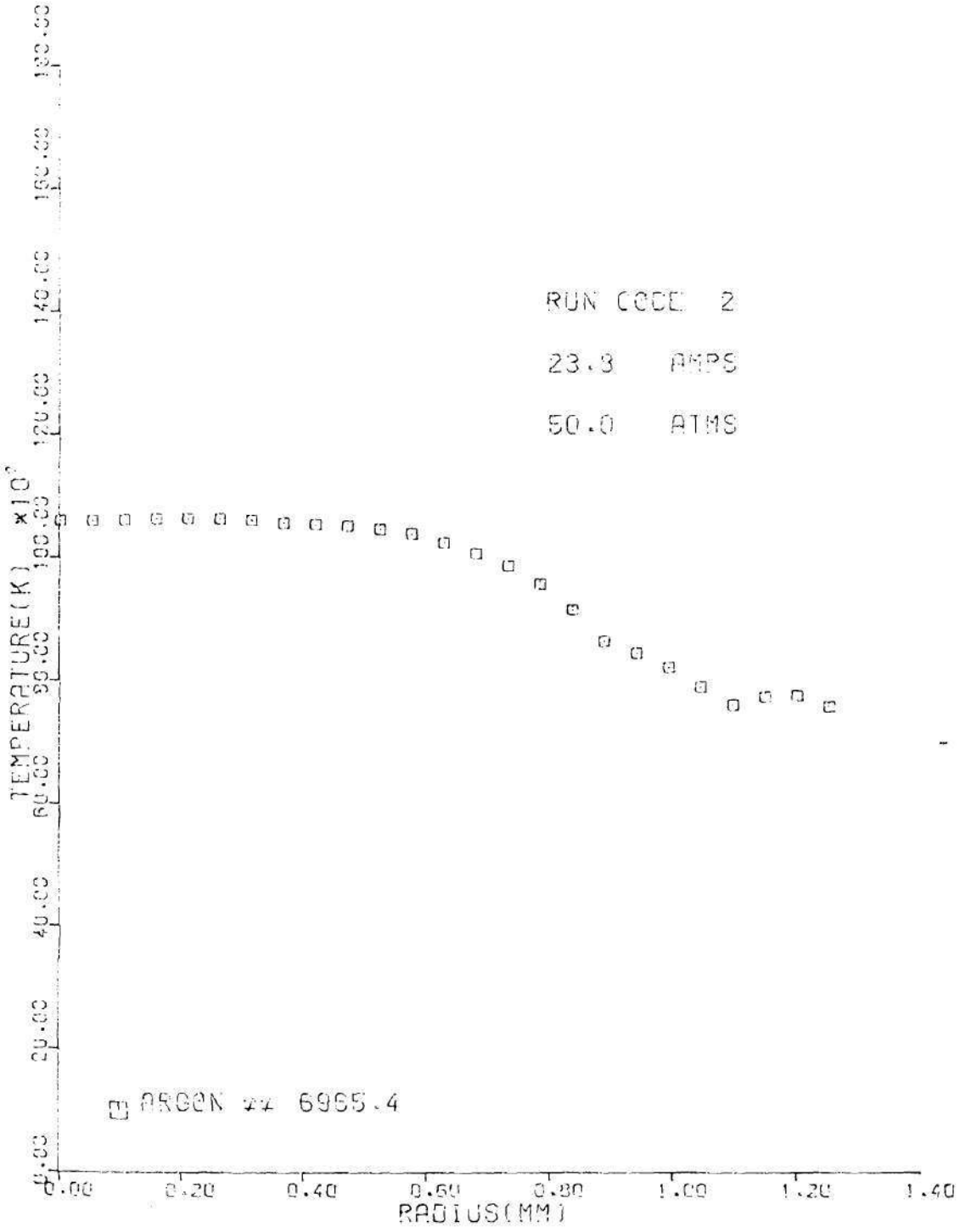
RUN CODE 2
23.3 AMPS
50.0 ATMS
TEMPERATURE(K) x10³
RADIUS(MM)
0.00
0.20
0.40
0.60
0.80
1.00
1.20
1.40
ARGON ** 6995.4

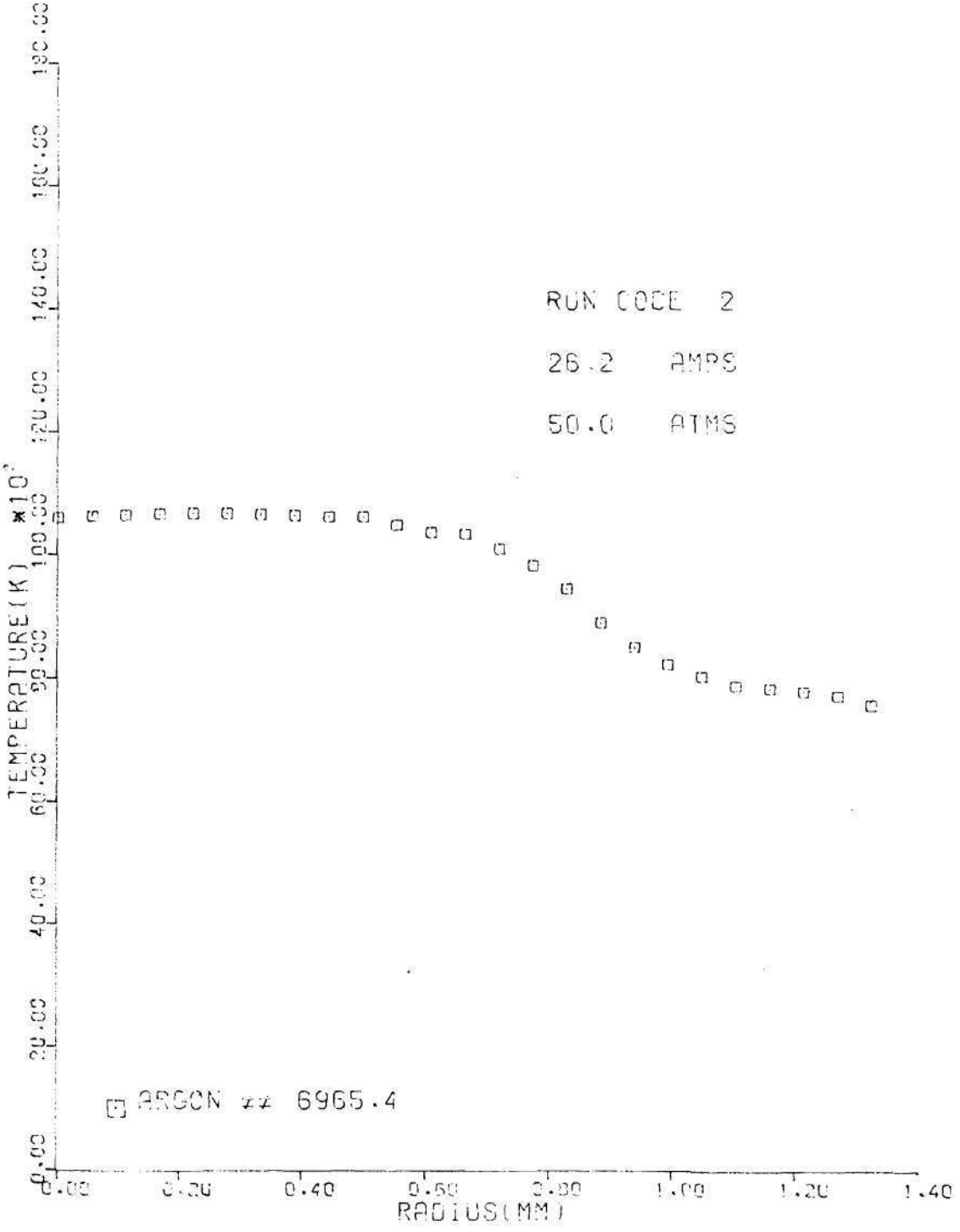
RUN CODE 2
26.2 AMPS
50.0 ATMS
TEMPERATURE(K) *10²
RADIUS(MM)
ARGON ** 6965.4
0.00
20.00
40.00
60.00
80.00
100.00
120.00
140.00
160.00
180.00
0.00
0.20
0.40
0.60
0.80
1.00
1.20
1.40

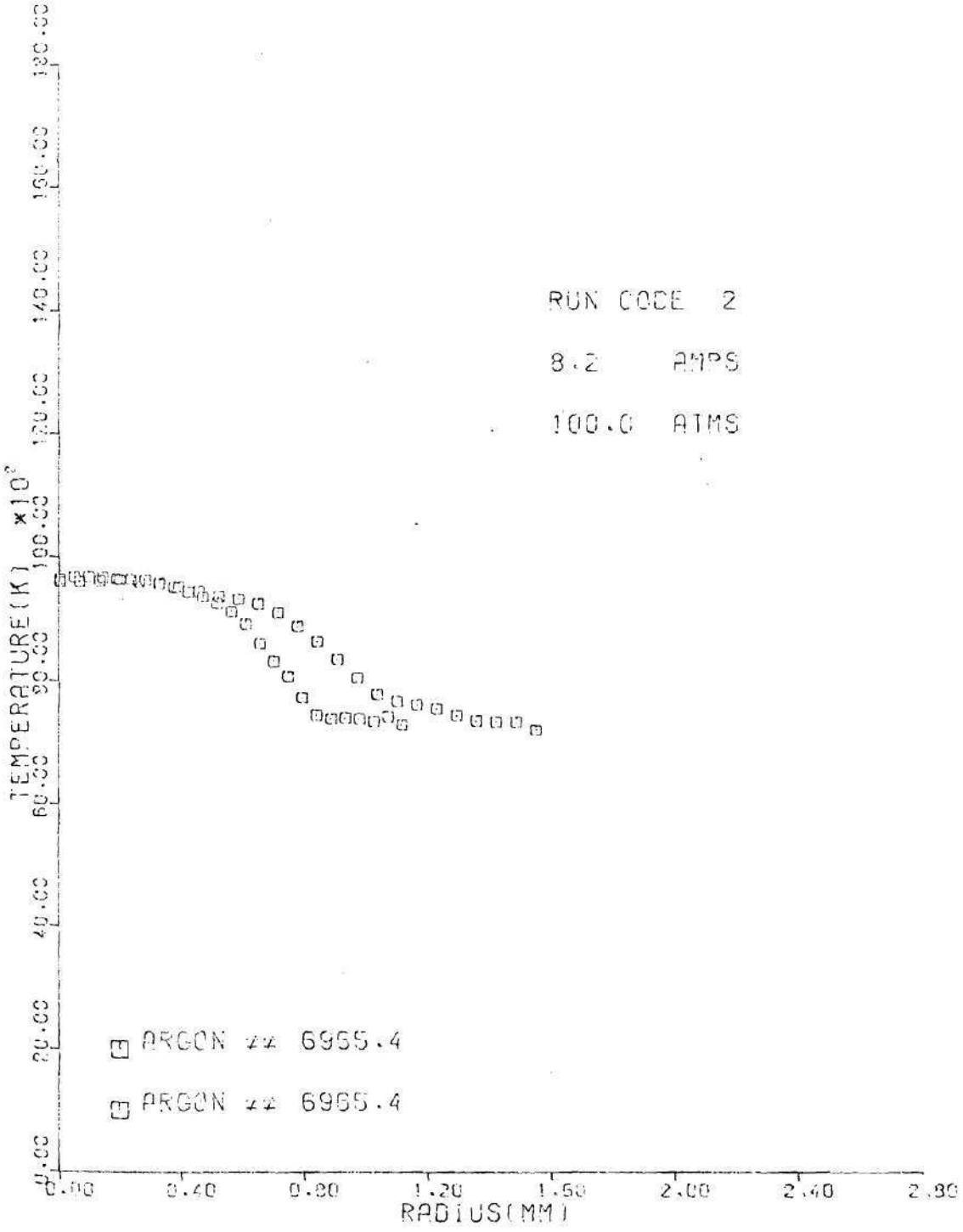
RUN CODE 2
8.2 AMPS
100.0 ATMS
TEMPERATURE(K) *10²
RADIUS(MM)
ARGON ** 6965.4
ARGON ** 6965.4

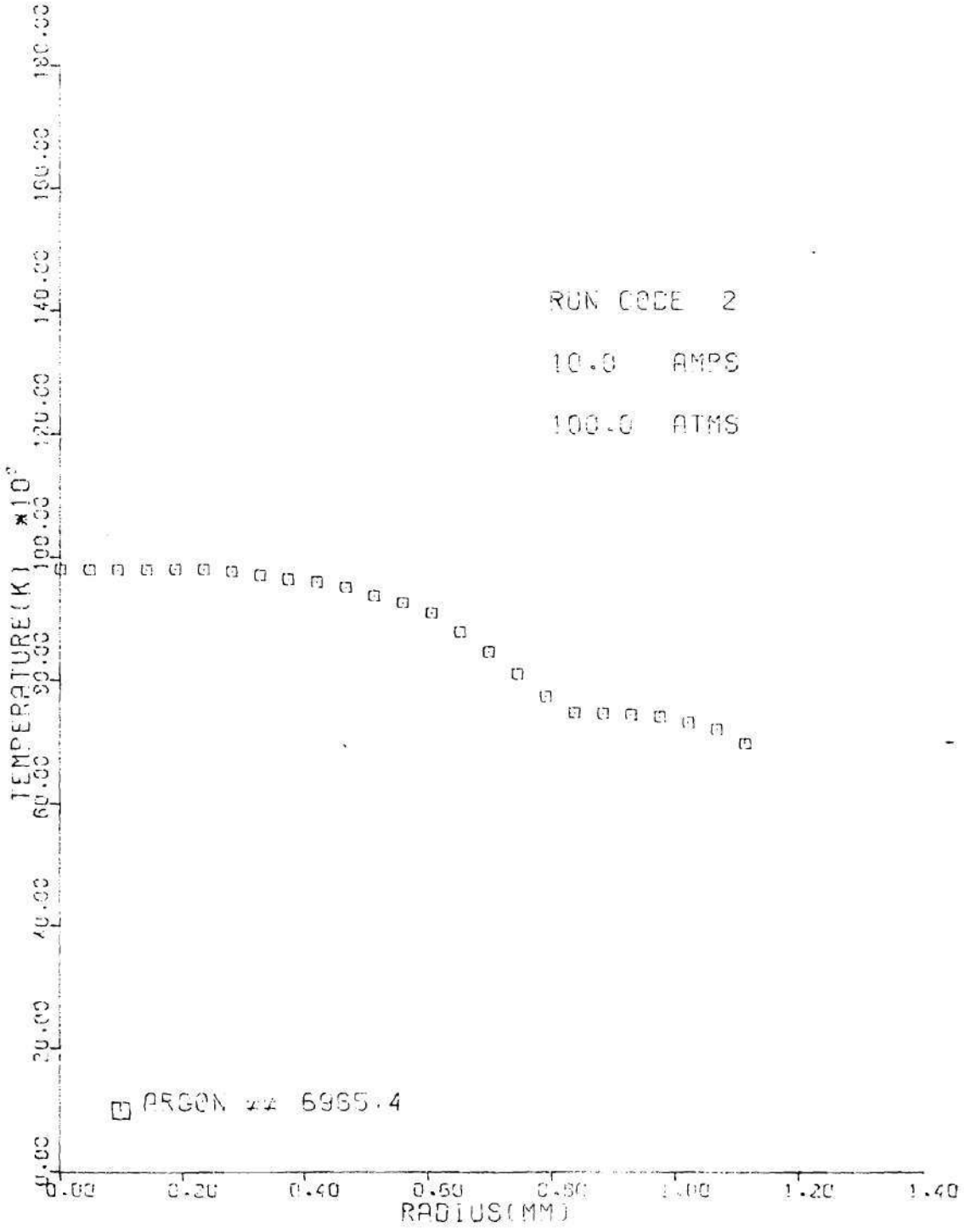
RUN CODE 2
10.0 AMPS
100.0 ATMS
TEMPERATURE(K) *10^3
RADIUS(MM)
ARGON ** 6965.4

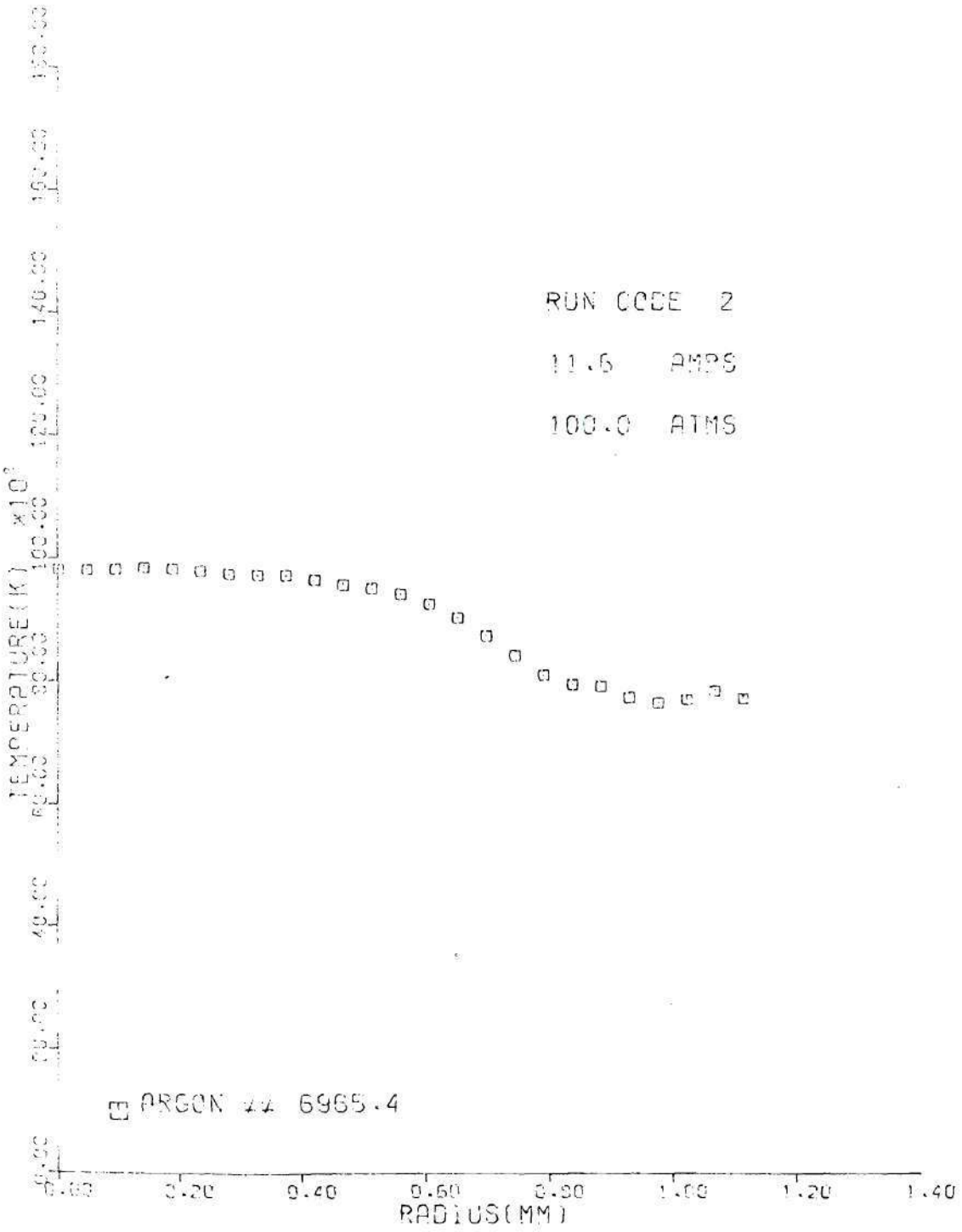
RUN CODE 2
11.6 AMPS
100.0 ATMS
TEMPERATURE(K) x10³
80.00
100.00
120.00
140.00
160.00
180.00
40.00
20.00
0.00
ARGON AA 6965.4
0.00
0.20
0.40
0.60
0.80
1.00
1.20
1.40
RADIUS(MM)

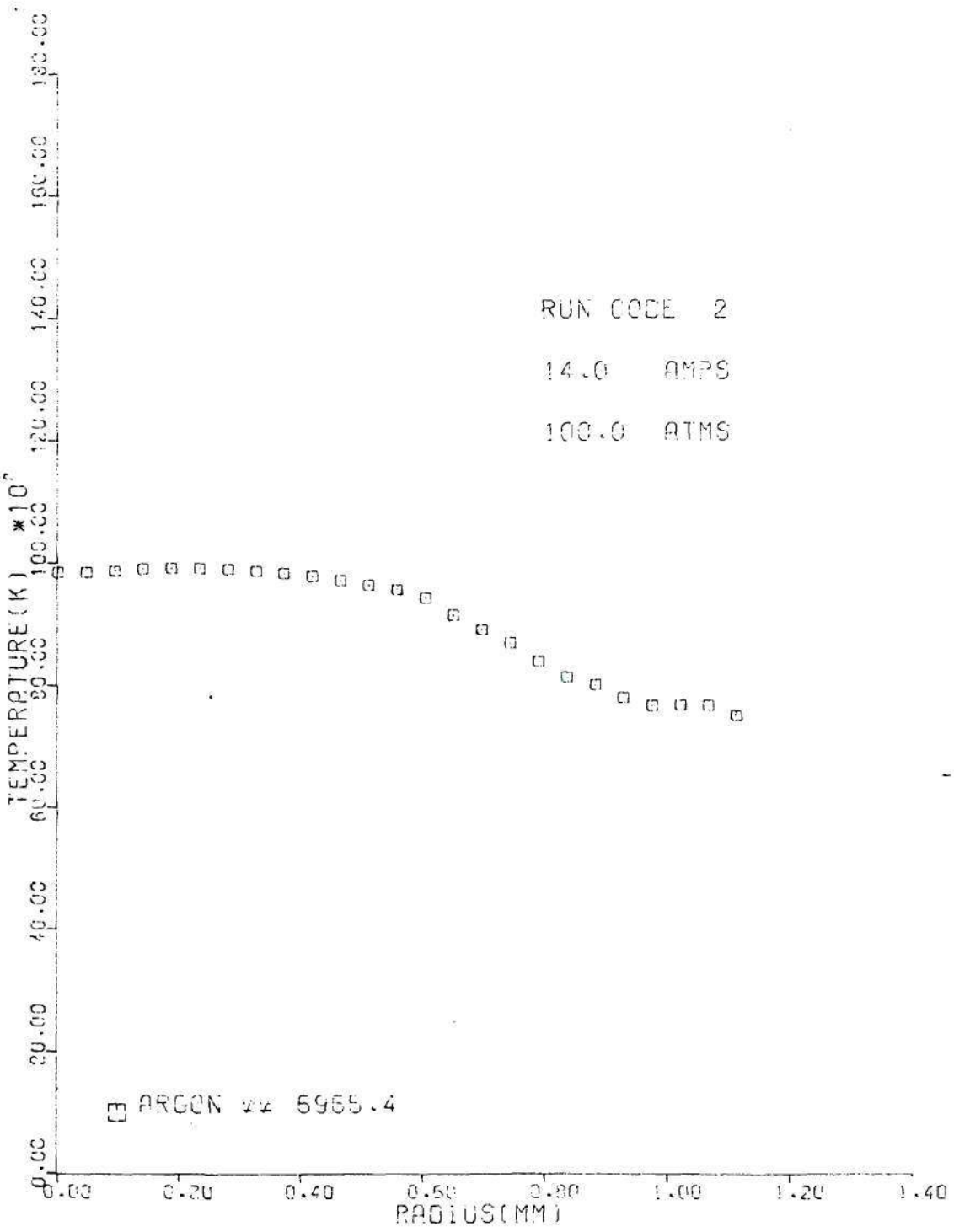
RUN CODE 2
14.0 AMPS
100.0 ATMS
TEMPERATURE(K) *10^
ARGON ** 5965.4
RADIUS(MM)
0.00
0.20
0.40
0.60
0.80
1.00
1.20
1.40

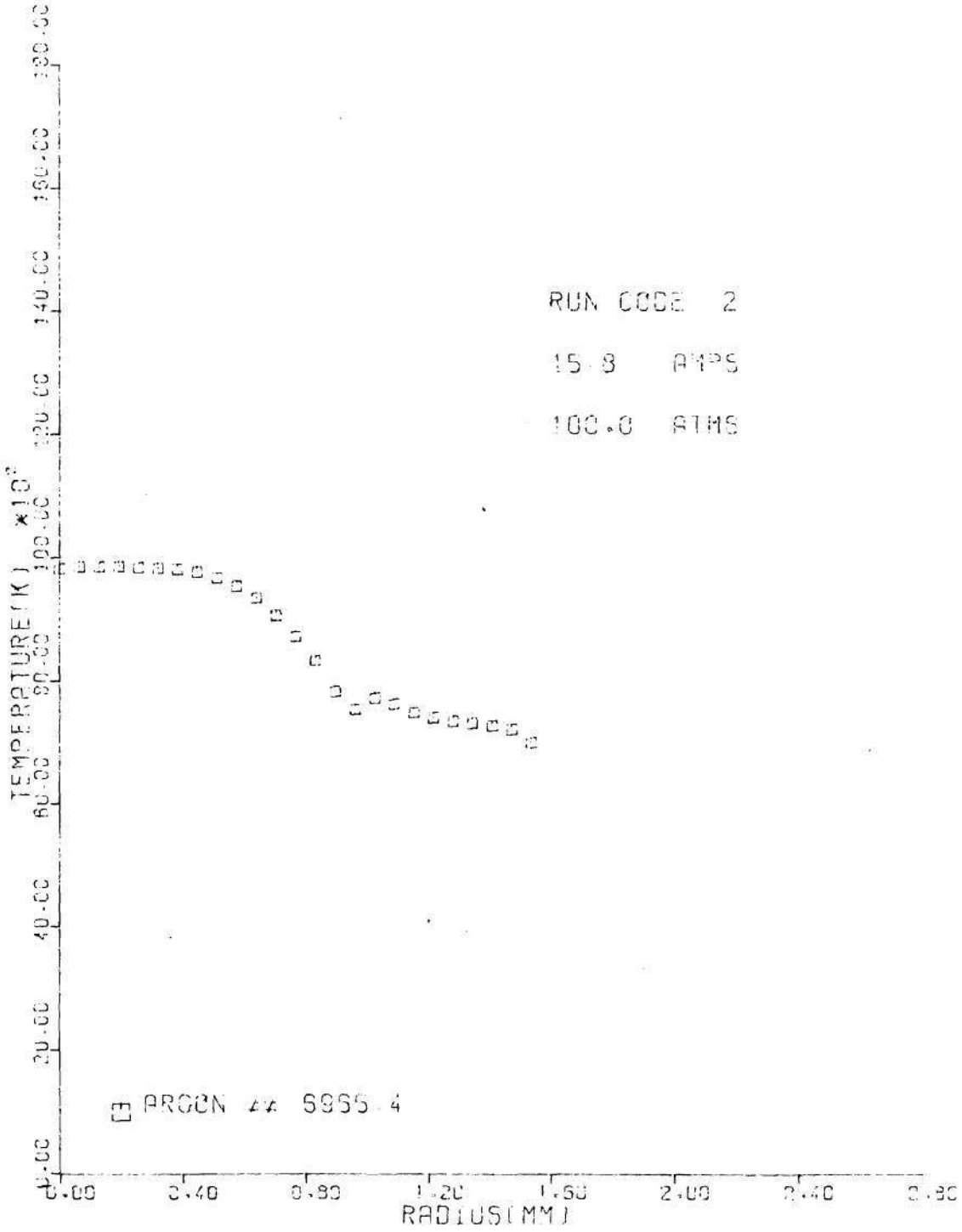
RUN CODE 2
15.8 AMPS
100.0 ATMS
TEMPERATURE(K) *10^3
RADIUS(MM)
ARGON AT 5955.4

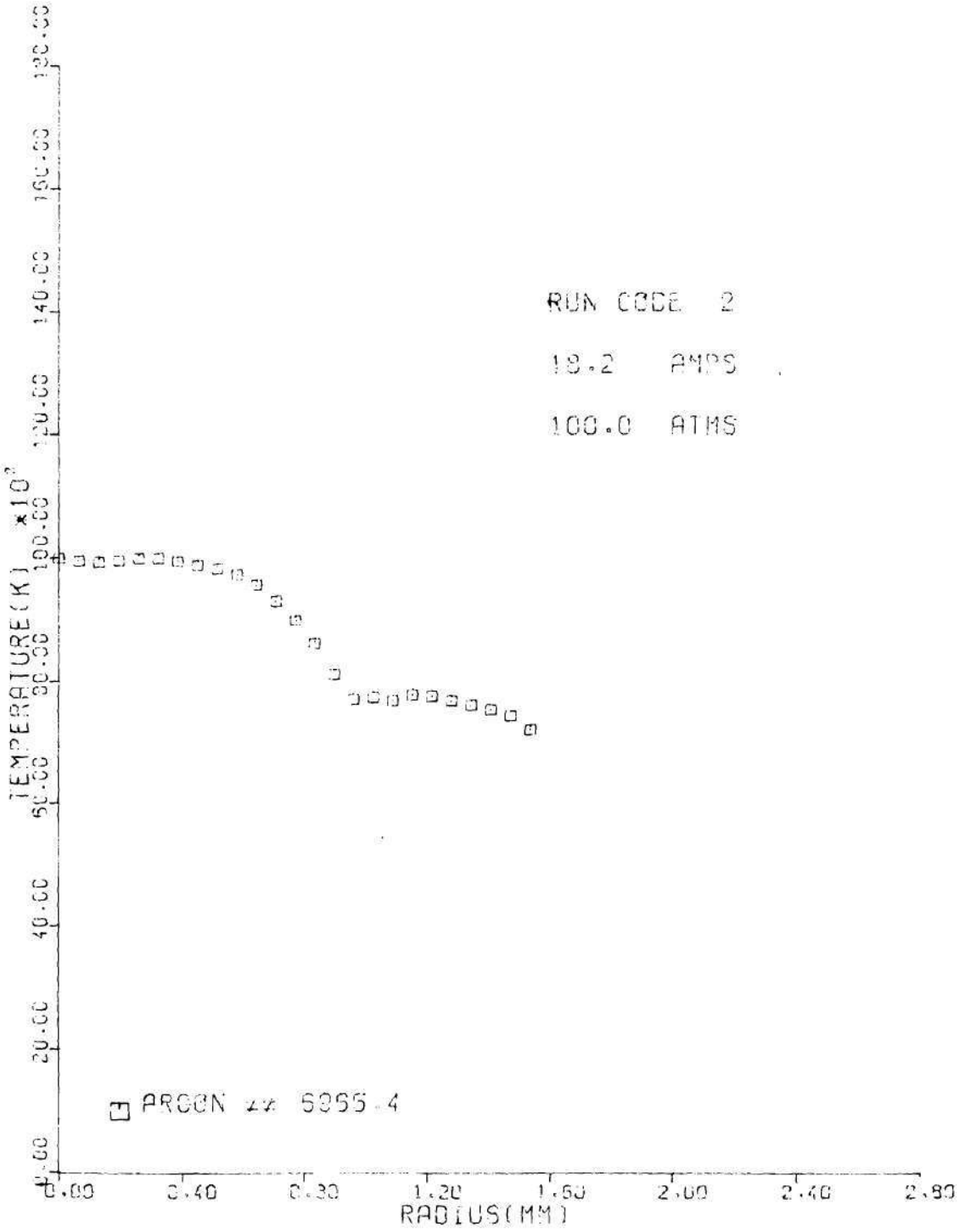
RUN CODE 2
10.2 AMPS
100.0 ATMS
TEMPERATURE(K) *10²
RADIUS(MM)
ARGON ** 5955.4

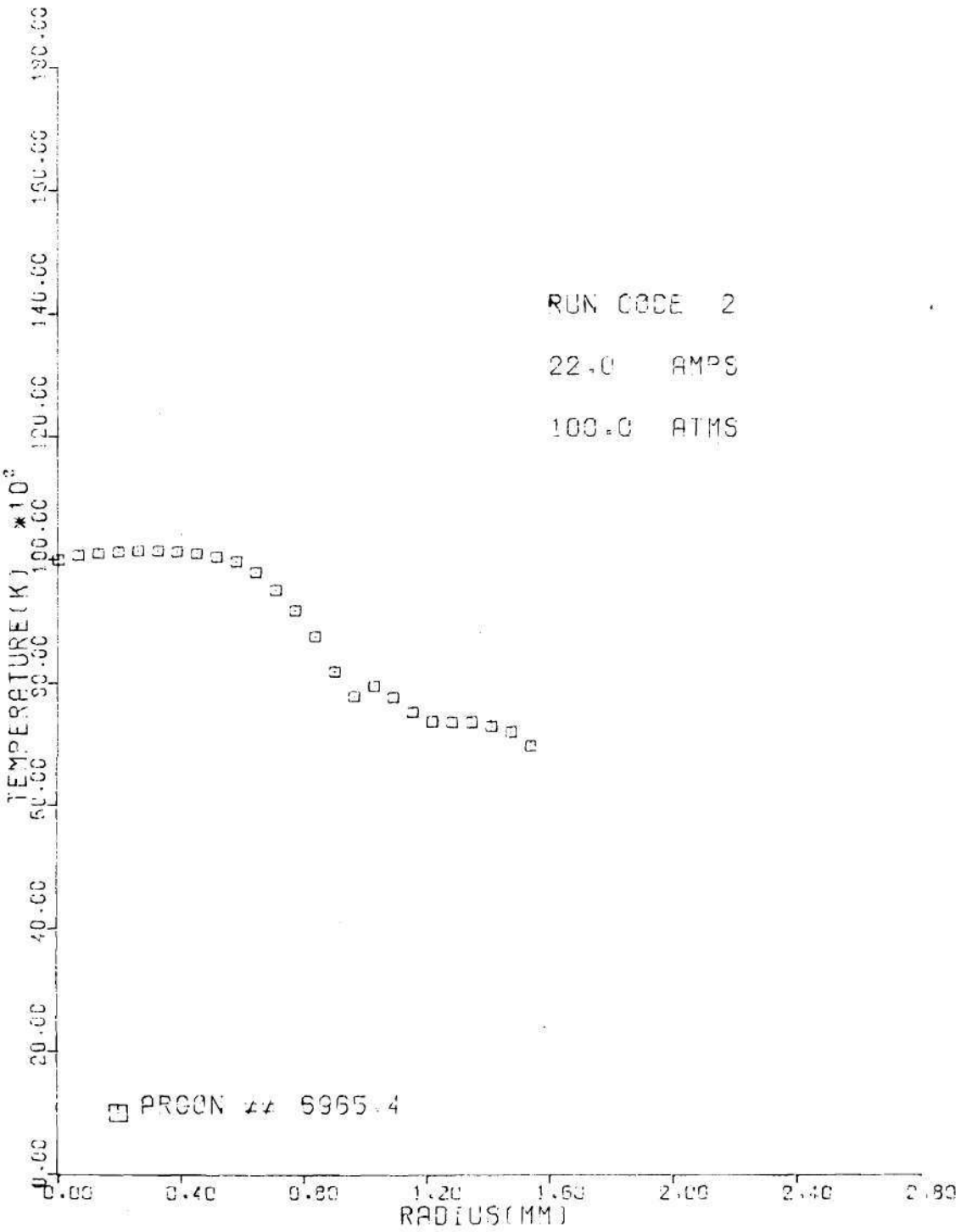
RUN CODE 2
22.0 AMPS
100.0 ATMS
TEMPERATURE(K) *10²
0.00
20.00
40.00
60.00
80.00
100.00
120.00
140.00
160.00
180.00
PROBN ## 5965.4
0.00
0.40
0.80
1.20
1.60
2.00
2.40
2.80
RADIUS(MM)

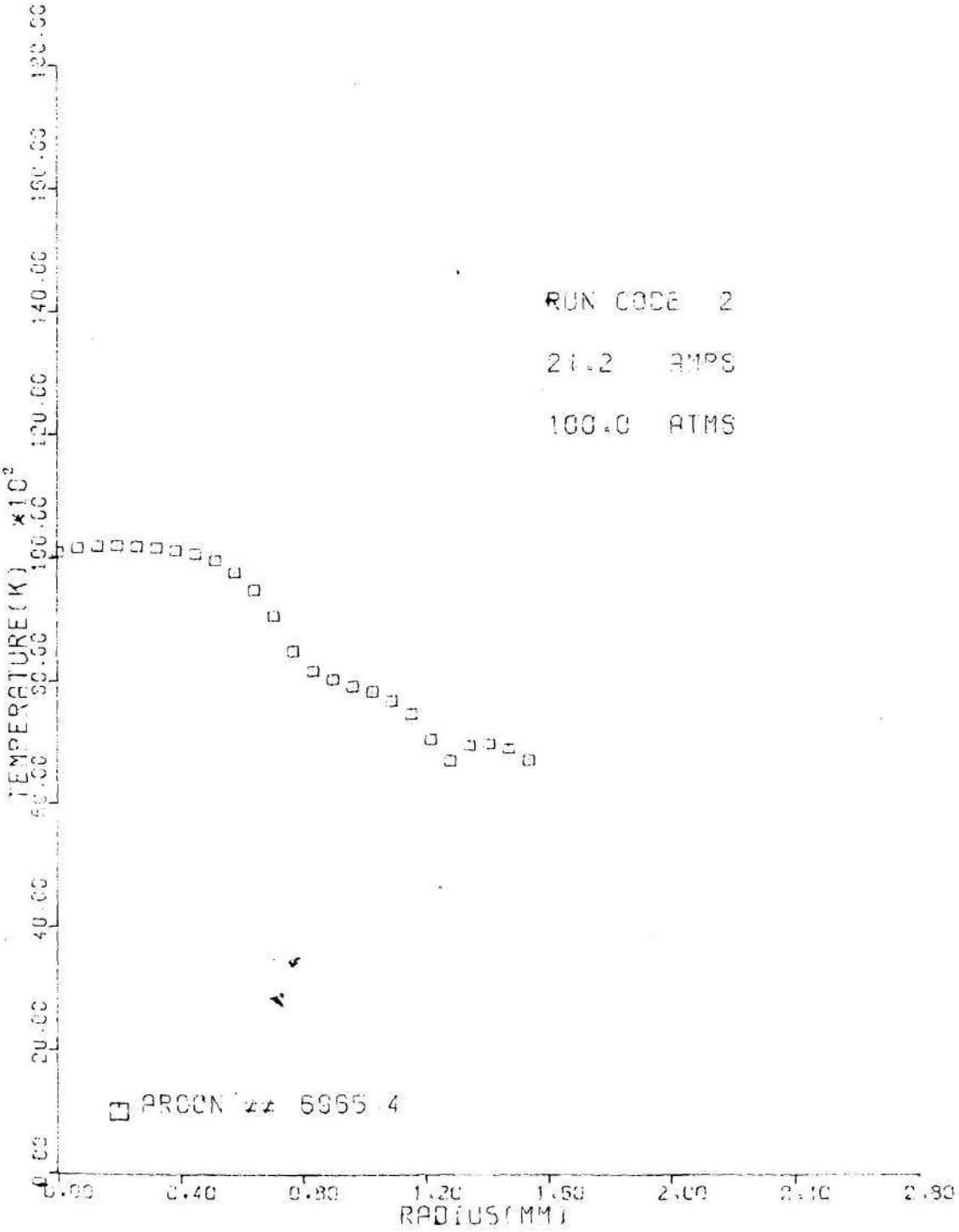
RUN CODE 2
21.2 AMPS
100.0 ATMS
TEMPERATURE(K) *10²
RADIUS(MM)
ARGON ** 6965 4

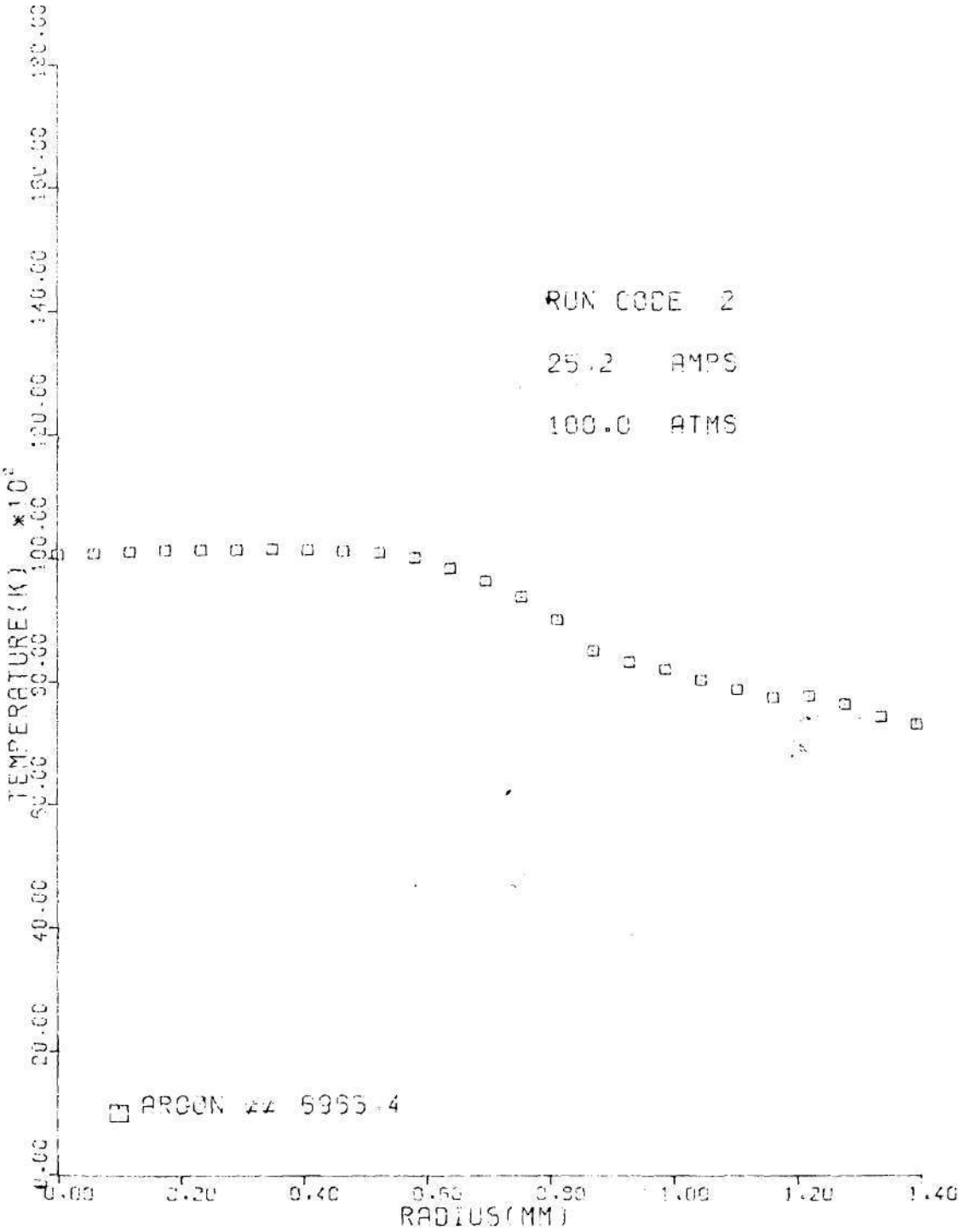
RUN CODE 2
25.2 AMPS
100.0 ATMS
TEMPERATURE(K) *10²
RADIUS(MM)
ARGON ## 5965.4

APPENDIX C

CAM OPERATOR

It was desired to speed up the data acquisition process to prolong the cascade life and data accuracy, especially at higher current and pressure regimes where pulsed currents were used to prevent damage to the cascade. The data acquisition process consisted of six steps once the pressure had been set to the desired value and the arc was operating at a low current:

(1) starting strip chart recorder;

(2) pulse desired current in by activating one or both power supplies;

(3) activate mirror scan motor;

(4) after time for a scan in one direction, a motor changes spectrometer setting to nearby continuum from line;

(5) reversible mirror motor returns mirror back to initial position, sweeping arc image back across entrance slit; and

(6) pulse power supply out and return arc to a safer "cooking" current.

It was also desired, if possible,to sample pressure, current, voltage, field strength, and to activate the stepper motor to complete the entire data cycle. If the automation could have been made complete, the arc would "see" only about two seconds of strenuous operation instead of the several minutes necessary to complete the cycle by hand, thereby extending cascade life considerably.

A motor-driven cam-type automatic operator was chosen for the task. There were twenty cams on the shaft. One was to be used as a time zero, leaving nineteen cams to operate the data cycle.

Each cam operated a micro-switch by depressing a lever on the switch with a raised portion of the cam disc. This raised portion could be adjusted to depress the lever for 100% of the revolution or any lesser fraction down to 50% of an entire revolution.

The first nine cam discs were set to depress the contacts on the first nine micro-switches in succession. The first switch was set to be off for the first 5% of the revolution, on for the next 5% and finally off for the remainder of the revolution. The second cam was set to activate its switch after 9% of the revolution, remain activated for the next 5% of a revolution and then stay on for the following 30% simply by jumpering switches 1 through 6 together.

The micro-switches had three connections; a common, a normally closed, and a normally open. By connecting a device to the common and normally open terminals, the depression of the switch lever would activate it. By changing the normally open lead to the normally closed one, depression of the switch lever would break the circuit, de-activating it. In this way, the choice of cams arranged as above would allow a device to be activated at a certain point in the data cycle or de-activated at that point. The duration of the switch signal depended on the way the cam switches were jumpered together.

The tenth cam was set to be time zero; that is, the first perceptible motion of the shaft activated the switch behind the cam. It was thought to use this switch to trigger an oscilloscope trace of current or

voltage to allow a photographic record.

Cams eleven through twenty were set to have the switches off for a set time, t_s, and then activated for one-half revolution minus t_s. It was decided to lag cam eleven behind time zero for 10% of a revolution, so the first of this series of cams had a raised portion for 50% of a revolution and a lowered portion of the disc for the remaining 50%.

In this way, cam eleven was off for 10%, on for 50% and back off for 40%. Similarly, cam twelve had its closed portion covering 10% more of the disc, so it was off for 20% and on for 40%, then off for the remaining 40%. As in the case of the first nine cams, the choice of having the switch open or closed when the lever is depressed depended on the choice of switch terminals.

A time chart depicting the combination of cam pulses is shown in Figure 22. By varying the openings on the cam discs and the selections of switch leads, many permutations were possible.

The cam operator came equipped with two dc driving motors of different speeds and several combinations of gears, allowing a complete revolution in as much as 5 minutes and in as little as 1 second.

The switch terminals from the cam operator were connected to a patchboard which was mounted on the front console. Remote leads to the automated equipment also were connected to different jacks on the patchboard. Connection of a device to a cam switch or set of switches automatically operated the device at the present point in the data cycle.

Next, automation of several portions of the measuring equipment was begun. A precision time was put in a circuit with a dc motor attached to the spectrometer wavelength counter. A 24 volt power supply triggered

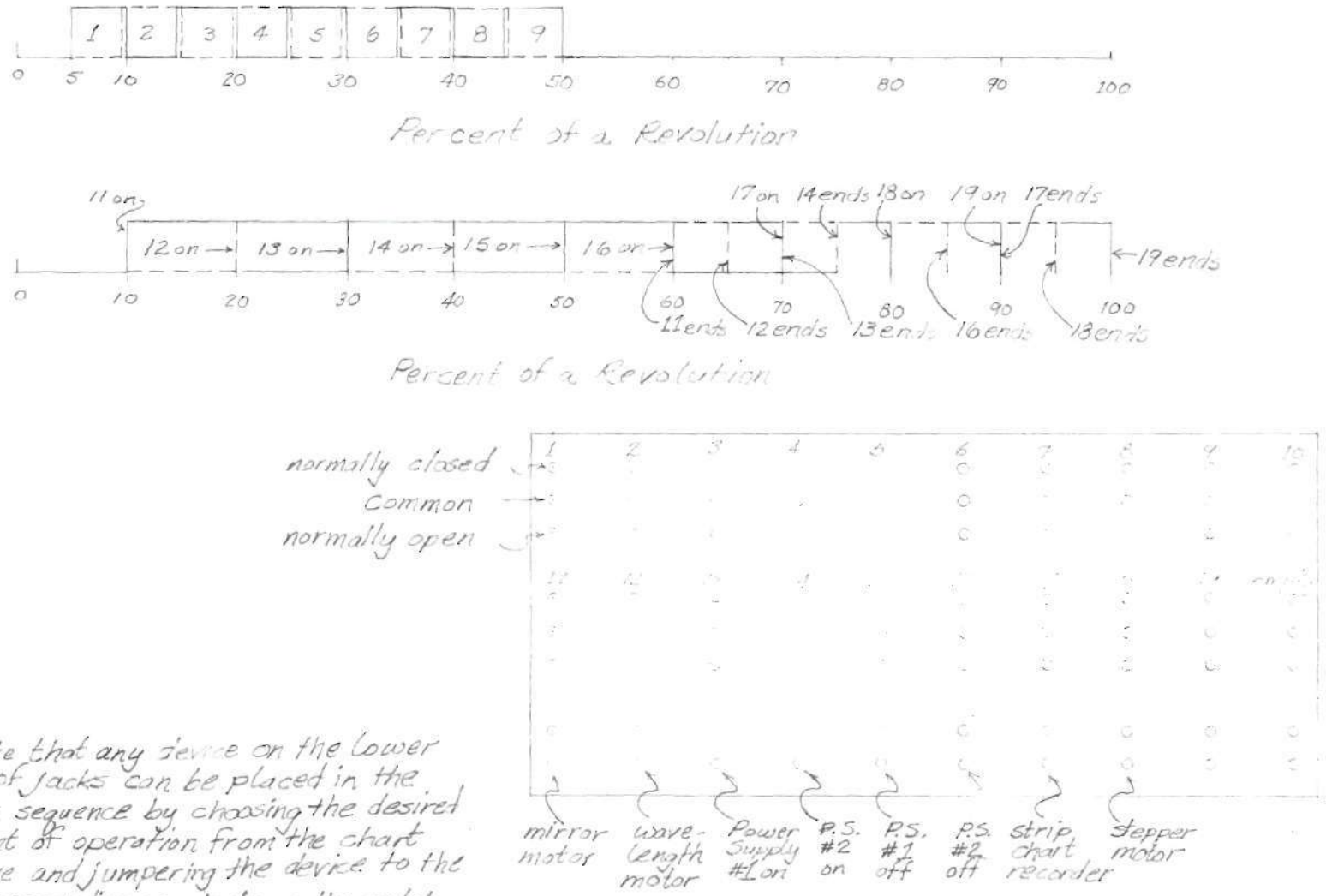

Note that any device on the lower set of jacks can be placed in the data sequence by choosing the desired point of operation from the chart above and jumpering the device to the corresponding cam jacks on the patch-board.

Figure 22. Cam Operator and Patchboard

the motor and timer when the appropriate cam switch closed. The timer was adjusted to shut the motor off when the proper wavelength was reached. The motor was reversible and a switching circuit allowed it to run the spectrometer back when the appropriate cam switch was closed. Again, the timer shut off the motor in time to allow the wavelength counter to reach its original setting. This procedure was repeatable and allowed rapid movement of the wavelength from 6965Å to 7000Å and back without human intervention.

The mirror motor was already remotely controlled, as was the stepper circuit, so leads were simply run to the patchboard. The strip chart recorder had a remote capability and this, too, was run to the patchboard.

In running many leads from the instruments to the patchboard, it was considered a good idea to include a second set of switches for everything previously mentioned (except power supplies) on the spectrometer stand. Having these switches at hand allowed an operator to move the mirror in either direction, move the wavelength counter on the spectrometer either way, and potentially do everything the cam operator did manually. This was a great convenience during a run since one person could handle all the optical components and see the direct result of his data without moving from his position, as was common in Run 1.

Included in the remote controls was a shutter motor which remotely raised or lowered a shutter between the chamber window and a thermopile which was used in Run 2. A control schematic appears in Figure 23.

By using the cam operator, it was envisioned that, with all components previously timed properly, a single button would activate the entire cycle for a data point. The only intervention necessary would be

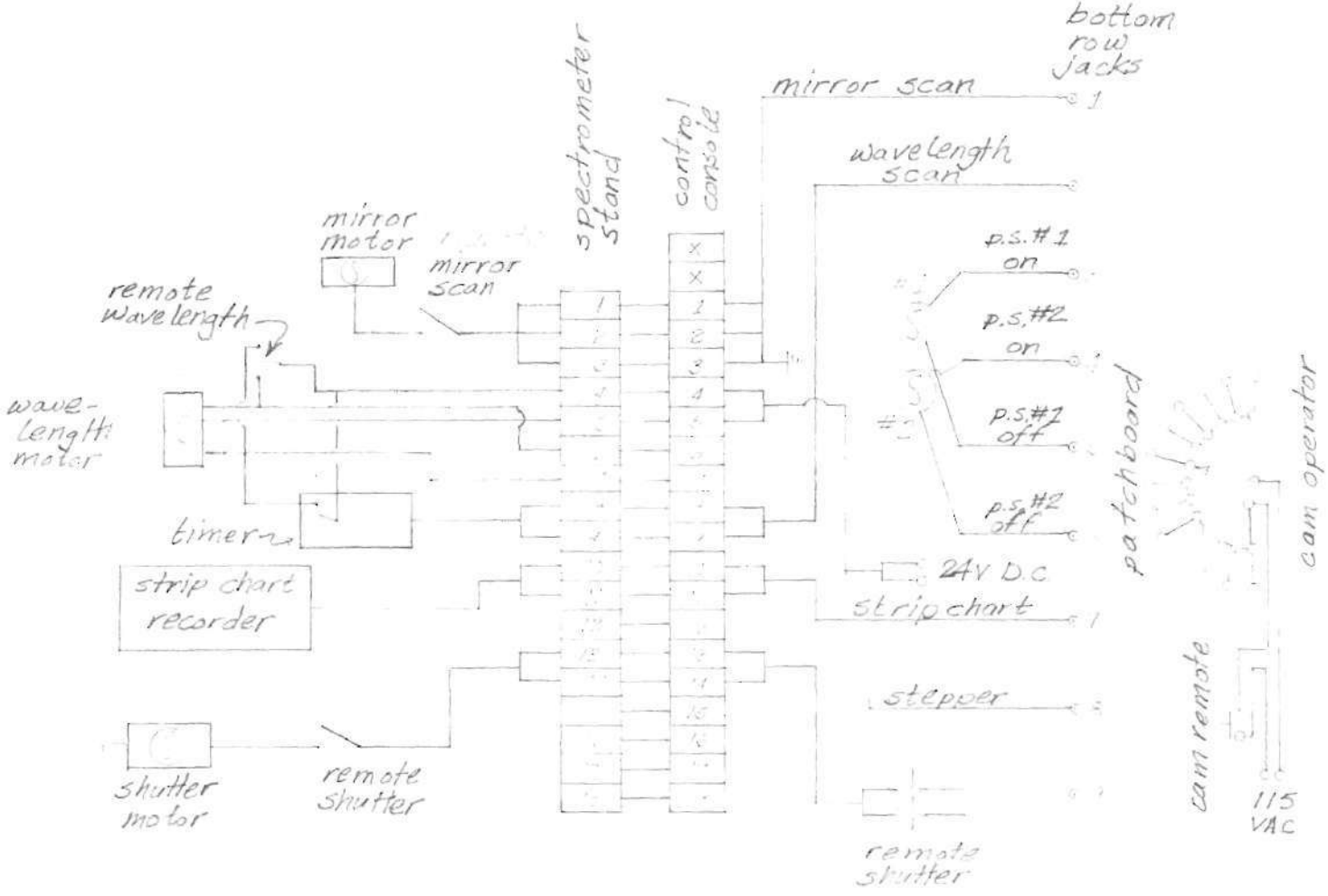

Figure 23. Control Schematic of 15,000 Psi System

to adjust the current and pressure manually. The digital recorder connected to the scanning DVM was incompatible with remote operation and had to be operated by hand.

The cam operator was never used to any extent in this study except to prove its feasibility, since the current-pressure range which was investigated was not in the regime of pulse-type operation. The inclusion of the control switches on the spectrograph stand, however, greatly increased data acquisition time from Run 1 to Run 2.

BIBLIOGRAPHY

1. R. S. Devoto, "Transport Coefficients of Ionized Argon", The Physics of Fluids, Vol. 16, No. 5, May 1973.

2. H. Maecker, Z Naturforsh, 110, 457, 1956.

3. U. H. Bauder and H. Maecker, "The Determination of Transport Properties From Arc Experiments: Methods and Results", Proc. IEEE, Vol. 59, No. 4, April 1971.

4. U. Bauder, R. S. Devoto, and D. Mukherjee, "Measurement of Electrical Conductivity of Argon at High Pressure", Physics of Fluids, Vol. 16, No. 12, pp. 2143-2148, December 1973.

5. J. Kopainsky, Z. Phys., 248, 417, 1971

6. J. C. Morris, R. P. Rudis, and J. M. Yos, "Measurement of Electrical and Thermal Conductivity of Hydrogen, Nitrogen, and Argon at High Temperatures", Physics of Fluids, Vol. 13, No. 3, March 1970.

7. U. H. Bauder and E. D. Stephens, "An Apparatus to Investigate Plasmas at Very High Pressure", Rev. Sci. Inst., 43, 9, 1972.

8. R. S. Devoto and D. Mukherjee, "Electrical Conductivity from Electric Arc Measurements", J. Plasma Physics, Vol. 9, Part 1, pp. 65-76, 1973.

9. H. W. Emmons, "Arc Measurement of High Temperature Gas Transport Properties", Physics of Fluids, Vol. 10, No. 6, June 1967.

10. H. W. Drawin and P. Felenbok, Data for Plasmas in Local Thermodynamic Equilibrium, Gauthier-Villars, ed., Paris, 1965.

11. National Standards Reference Data Series, NBS, No. 22, Vol. 2.

12. A. V. Larson and J. R. Williams, private communication.

13. Steven Thompson, "Radial Temperature Profiles in an RF Plasma Over a Wide Range of Applied Magnetic Flux Intensities; Theory and Experiment", Ph. D. Dissertation, School of Nuclear Engineering, Georgia Institute of Technology.

14. Computer program written by J. R. Williams, Mechanical Engineering Department, Georgia Institute of Technology.

15. U. H. Bauder and R. S. Devoto, "The Electrical Conductivity of Argon at High Pressure", Selected papers presented at the High Pressure

Arc Symposium (Sponsored by the American Physical Society), ARL Rep. 70-0135, pp. 115-128, August 1970.